AMERICAN MUSEUM
Novitates

PUBLISHED BY THE AMERICAN MUSEUM OF NATURAL HISTORY
CENTRAL PARK WEST AT 79TH STREET, NEW YORK, NY 10024
Number 3678, 60 pp., 23 figures, 2 tables March 4, 2010

First Crania and Assessment of Species Boundaries in *Nimbadon* (Marsupialia: Diprotodontidae) from the Middle Miocene of Australia

KAREN H. BLACK[1] AND SUZANNE J. HAND[2]

ABSTRACT

Abundant, exceptionally well-preserved cranial material of the zygomaturine diprotodontid *Nimbadon lavarackorum* is described from AL90 site, a middle Miocene deposit in the Riversleigh World Heritage Area, Queensland, Australia. The material has enabled a comprehensive assessment of the expected level of morphological variation within a fossil marsupial species from a single locality, thus forming a benchmark for determining species boundaries in extinct marsupials. Variation is assessed by quantitative and qualitative means. Univariate analyses of *N. lavarackorum* cranial and dental dimensions indicate low coefficients of variation consistent with expected values for single species populations. Conversely, qualitative analyses indicate high levels of morphological variation, particularly in structures previously deemed phylogenetically significant, such as the upper third premolar. Some cranial variation may be due to sexual dimorphism or ontogeny but there appears to be a high degree of intraspecific morphological variation. Features once regarded to distinguish *N. whitelawi* from the type species fall within the boundaries of that intraspecific variation and *N. whitelawi* is herein regarded as a junior synonym of *N. lavarackorum*. Comparison with morphological variation in the Miocene diprotodontid *Neohelos stirtoni* suggests that *N. lavarackorum* was a less variable species overall, reflecting differences between the taxa in body size, home range, and habitat preference and stability. *Nimbadon lavarackorum* was a relatively small (75–120 kg), possibly gregarious browsing species probably restricted to closed-forest habitats.

[1] School of Biological, Earth and Environmental Sciences, University of New South Wales, Sydney, 2052, New South Wales, Australia (k.black@unsw.edu.au).
[2] School of Biological, Earth and Environmental Sciences, University of New South Wales, Sydney, 2052, New South Wales, Australia; Division of Vertebrate Zoology (Mammalogy), American Museum of Natural History (s.hand@unsw.edu.au).

 ISSN 0003-0082

INTRODUCTION

Diprotodontids are extinct large-bodied, terrestrial browsing herbivores belonging to the marsupial infraorder Vombatomorphia. They are most closely related, among living taxa, to wombats and, more distantly, koalas (infraorder Phascolarctomorphia). Two diprotodontid subfamilies are currently recognized: Diprotodontinae (eight genera); and Zygomaturinae (11 genera). Both subfamilies are relatively common throughout Australian fossil deposits spanning the late Oligocene to the late Pleistocene, with Zygomaturinae also known from Plio-Pleistocene deposits in New Guinea (Plane, 1967; Flannery and Plane, 1986) and Irian Jaya (Flannery, 1992). Both families are characterized by simple bilophodont molars indicative of browsing.

The most diverse diprotodontid fauna recorded from any single region in Australia comes from Oligo-Miocene freshwater limestone deposits in the Riversleigh World Heritage Area, northwestern Queensland (19°S, 139°E). Five genera comprising 10 species are currently recognised (Black, 2008).

Until now the relatively small zygomaturine *Nimbadon lavarackorum* Hand et al. 1993, was known from a maxillary fragment, a partial dentary, and isolated teeth from the middle Miocene Henk's Hollow and Dwornamor local faunas of Riversleigh. Two additional species of *Nimbadon* were described by Hand et al. (1993), both on the basis of single specimens: *N. scottorrorum* from a maxillary fragment containing P3, M1–4 from the Fig Tree local fauna, Riversleigh; and *N. whitelawi* from a partial palate containing left P3, M1, partial M2 and right P3, M1–3, and partial M4 from the middle Miocene Bullock Creek local fauna, Northern Territory. Following a revision of *Neohelos* Stirton, 1967, material from Riversleigh, Black and Archer (1997) suggested *N. scottorrorum* is more appropriately assigned to *Neohelos*.

Since publication of Hand et al. (1993) a catastrophic accumulation of *Nimbadon lavarackorum* material has been discovered in AL90 site, a Miocene cave deposit also in the Riversleigh World Heritage Area, Queensland. This species is now known from at least 25 skulls and 18 lower jaws, hundreds of isolated teeth, and several articulated partial skeletons. Individuals ranging in age from suckling pouch young through to aged adults are represented in the sample. The Riversleigh specimens represent some of the most exceptionally preserved diprotodontid material known.

In this paper we describe the first cranial material referable to the zygomaturine *Nimbadon lavarackorum* and assess intraspecific cranial and dental morphological variation within the discrete AL90 *N. lavarackorum* fossil population. We compare our results with those of Murray et al. (2000b) for the middle Miocene diprotodontid population of *Neohelos stirtoni* from Blast Site, Bullock Creek, Northern Territory, the only other detailed study of this kind on diprotodontid marsupials.

Geological Setting

The diprotodontid material described here was recovered from a cave deposit known as AL90 site on the Gag Plateau in the Riversleigh World Heritage Area, Lawn Hill National Park, northwestern Queensland. The site represents the remains of a limestone cave whose roof is now missing but whose walls remain largely intact. The cave appears to have had a vertical entrance that acted as a natural pitfall trap. The completeness and associated (and at times articulated) nature of the fossil material in the deposit suggests fossilization occurred at or very near the point of accumulation with minimal postmortem disturbance (Arena, 2005).

Aside from abundant bat material, representing at least seven species, including the hipposiderid *Archerops annectens* (Hand and Kirsch, 2003), the AL90 fauna is dominated by medium-sized herbivores such as *Nimbadon lavarackorum* and balbarine and bulungamyine kangaroos. This limited diversity and homogeneity of the fossil marsupial sample suggests a catastrophic accumulation over a relatively short time frame. Smaller animals such as bandicoots and possums are underrepresented in the fauna and may have been able to escape the cave after entry.

Arena and Black (1997) and Arena (2005) have outlined the depositional history of the AL90 deposit which, in summary, can be divided into two stages: (1) the primary cave formation and infill characterised by deposition of flowstone and cave sediment. The closely associated and articulated remains of *Nimbadon lavarackorum* accumulated during this stage; and (2) secondary cave formation resulting from partial dissolution of the primary cave deposit and subsequent infill. This stage is characterized by a markedly different geology and fossil fauna.

On the basis of ongoing stratigraphic and faunal analyses, AL90 has been interpreted to be part of Riversleigh's Faunal Zone C deposits and as such middle Miocene in age (Archer et al., 1989, 1991, 1997; Black, 1997; Creaser, 1997; Travouillon et al., 2006).

Methods

Cusp nomenclature follows Archer (1984) and Rich et al. (1978) except that the hypocone of upper molars is now accepted to be the metaconule following Tedford and Woodburne (1987). Molar homology follows Luckett (1993) where the four permanent molars of the tooth row are numbered M1–4, and the deciduous anteriormost tooth in the cheek tooth row is dP3, which is eventually replaced by P3. General cranial terminology follows Stirton (1967), Murray (1990b), and Murray et al. (2000a, 2000b). Basicranial terminology follows Archer (1976) and Aplin (1987). Periotic terminology follows Wible (1990) and Crosby and Norris (1993). Higher-level systematic nomenclature follows Aplin and Archer (1987). Institutional abbreviations are as follows: NMV P, palaeontological collection of the National Museum of Victoria, Melbourne; QM F, palaeontological collection of the Queensland Museum, Brisbane.

Dental and craniomandibular measurements were made using CE electronic digital vernier callipers. All measurements are in millimeters and were made at least twice. Dental measurements are standard maximum anteroposterior lengths and buccolingual widths, taken at the base of the crown. For molars, maximum buccolingual anterior widths and posterior widths were taken across the anterior and posterior loph/lophids, respectively.

Variation was reviewed by means of univariate and qualitative analyses of adult cranial and dental material. In regard to dentitions, particular attention is focused on the phylogenetically significant (Stirton et al., 1967; Hand et al., 1993; Black and Archer, 1997; Murray et al., 2000a, 2000b) upper third premolar. Specimens used in the metric analysis consisted of nine adult skulls, five adult mandibles, several partial dentitions and hundreds of isolated teeth. Twenty-eight dental and 45 craniomandibular measurements (see fig. 11 and table 1 for definitions) were made and are listed in appendix 1A–B. Dental measurements from AL90 *Nimbadon lavarackorum* specimens are listed in appendix 1C–D. Because no further growth of diprotodontid cheek teeth occurs after they erupt, dental measurements were obtained from fully erupted teeth of both adult and juvenile dentitions. In regard to isolated specimens, only left teeth were scored so as not to bias results. When a specimen contained both left and right dentitions, the side containing the most complete tooth was scored.

The mean, standard deviation (SD), range, and coefficient of variation (CV) were calculated for the variables using the computer software PAST Version 1.51 (Hammer et al., 2006) and are listed in appendix 2A–B. The CV is a measure of dispersion around the mean. Coefficients of variation between 4 and 10 suggest a dataset is derived from a single population, while CV's less than 4 suggest an insufficient sample size (Simpson et al., 1960). Univariate statistics were also calculated (appendix 2C) for comparable dental and craniomandibular variables for the *Neohelos stirtoni* sample from Blast Site, Small Hills Locality, Camfield Beds, Bullock Creek, to enable comparison with the AL90 *Nimbadon lavarackorum* population. Measurements for *Neohelos stirtoni* are from Murray et al. (2000b: tables 2–5). Bivariate plots (figs. 12–13) were generated using Microsoft Excel. *Nimbadon lavarackorum* dental measurements from sites other than AL90 (appendix 1C–D)

TABLE 1
Definition of *Nimbadon lavarackorum* craniomandibular variables used in univariate analysis
Variable numbers refer to figure 11. Variables 33–45 are features of the dentary.

VARIABLE		DEFINITION
1	BB	braincase breadth between subsquamosal foramina
2	BL	basicranium length
3	DORB	diameter of orbit
4	DZAP	depth of zygomatic arch posteriorly
5	FCL	facial cranium length
6	FMH	foramen magnum height
7	FMW	foramen magnum width
8	FRL	frontal length (at midline)
9	HFP	height of cranium at frontoparietal suture
10	HROST	height of rostrum (above posterior margin of P3)
11	IPFW	interpterygoid fossa width
12	LDIA	upper diastema length
13	LFLC	length from lacrimal foramen to lambdoid crest
14	LMP	length of masseteric process
15	LROST	length of rostrum (from anterior tip of I1 to lacrimal tuberosity)
16	LSKULL	length of skull (from anterior tip of I1 to condyle)
17	LTR	length of tooth row
18	M4FO	distance between the M4 and the foramen ovale
19	MAXW	maximum width of skull
20	MXL	maxilla length (at midline)
21	NL	nasal length (at midline)
22	OCH	occiput height (from dorsal border of foramen magnum to lambdoid crest)
23	OCW	occiput width
24	PLL	palatine length (at midline)
25	PML	premaxilla length (at midline)
26	PRL	parietal length (at midline)
27	PRW	maximum parietal width (above braincase)
28	WLT	width between lacrimal tuberosities
29	WPALI3	width of palate between I3s
30	WPALM3	width of palate between M3s
31	WPALP3	width of palate between protocones of P3s
32	WROST	maximum width of rostrum
33	APWCO	anteroposterior width of articular condyle of dentary
34	ARCO	distance between the alveolar row and the articular condyle
35	ARL	alveolar row length (of dentary)
36	DL	lower diastema length
37	DM1	depth of dentary below m1
38	HCO	height of articular condyle above alveolar row
39	HRL	horizontal ramus length
40	LD	dentary length
41	MLWCO	mediolateral width of articular condyle
42	MWM	maximum width of mandible
43	SL	mandibular symphysis length
44	WM3	width of dentary at m3
45	WMEAP	maximum width across masseteric eminence and angular process

were also included in the bivariate plots for comparative purposes.

Anatomical Abbreviations

ac	aqueductus cochleae
aef	anterior entocarotid foramen
al	alisphenoid
ams	angle between dentaries at mandibular symphysis
ap	angular process
ar	ascending ramus
atp	alisphenoid tympanic process
av	aquaeductus vestibuli
bo	basioccipital
bs	basisphenoid
btp	basioccipital tympanic process
c1	canine alveolus
cf	condylar foramen
co	condyle
cp	coronoid process
dc	diastemal crest
dd	dorsal doming
dia	diastema
etf	epitympanic fenestra
exo	exoccipital
fc	fenestra cochleae
fm	foramen magnum
fnc	facial nerve canal
fns	frontonasal suture
fo	foramen ovale
fps	frontoparietal suture
fr	frontal
frc	frontal crest
fro	foramen rotundum
fss	frontosquamosal suture
fv	fenestra vestibuli
gf	glenoid fossa
hr	horizontal ramus
hts	hypotympanic swelling
hy	hypocone
hyl	hypolophid
iam	internal auditory meatus
ifr	inflated frontal
iif	interincisive foramen
ioc	infraorbital canal
iof	infraorbital foramen
ipf	interpterygoid fossa
itc	infratemporal crest
j	jugal
jss	jugosquamosal suture
lac	lacrimal
lc	lambdoid crest
lf	lacrimal foramen
lt	lacrimal tuberosity
mas	mastoid
me	masseteric eminence
mef	mental foramen
mf	masseteric fossa
mjs	maxillojugal suture
mlf	median lacerate foramen
mlj	masseteric line of jugal
mn	mandibular notch
mnf	mandibular foramen
mp	masseteric process
mx	maxilla
n	nasal
nf	nasal foramen
oc	occipital condyle
os	orbitosphenoid
pa	parietal
pal	palatine
pap	postalveolar process
pas	parastyle
pc	parietal constriction
pcd	paracristid
pe	petrosal
pef	posterior epitympanic fossa
per	periotic
pf	pterygoid fossa
pgp	postglenoid process
pgs	postglenoid sinus
phc	pharyngeal crest
plf	posterior lacerate foramen
pm	premaxilla
pmc	anterolingual parametacone crest
pmf	posterior mental foramen
pms	premaxilla-maxilla suture
poc	postorbital constriction
por	postorbital process
pr	protocone
prl	protolophid
prm	promontorium
ps	postalveolar shelf
pt	pterygoid
rcma	fossa for rectus capitus major muscle
rcmi	fossa for rectus capitus minor muscle
rttp	rostral tympanic process of the petrosal
saf	subarcuate fossa
saff	subarcuate fossa foramen
sas	squamoso-alisphenoid suture
sc	sagittal crest
sff	secondary facial foramen
slf	sublingual fossa
so	supraoccipital
sof	sphenorbital fissure
son	supraoccipital notch
spf	sphenopalatine foramen
sps	squamosoparietal suture
sq	squamosal

ssf	subsquamosal foramen
stf	stapedial fossa
syf	symphysis fused
syu	symphysis unfused
tb	tympanic bulla
tf	transverse foramen.
za	zygomatic arch

SYSTEMATIC PALEONTOLOGY

SUPERORDER MARSUPIALIA ILLIGER, 1811

ORDER DIPROTODONTIA OWEN, 1866

FAMILY DIPROTODONTIDAE GILL, 1872

SUBFAMILY ZYGOMATURINAE STIRTON, WOODBURNE AND PLANE, 1967

Nimbadon Hand et al., 1993

TYPE SPECIES: *Nimbadon lavarackorum* Hand et al., 1993.

ADDITIONAL SPECIES: *Nimbadon whitelawi* and *N. scottorrorum* Hand et al., 1993.

REVISED GENERIC DIAGNOSIS: *Nimbadon* species differ from all other zygomaturines in having: a broad, short rostrum; a dorsolaterally inflated premaxilla; a small lacrimal foramen; a slender, moderately elongate masseteric process; a sphenopalatine foramen that is well separated from the infraorbital canal; and a P3 with a small parastyle and (variably present) hypocone and undifferentiated parametacone.

Nimbadon spp. differ from all other zygomaturines except species of *Silvabestius* Black and Archer, 1997, in having: a weak suborbital shelf; a mildly inflated hypotympanic swelling; a grooved, winglike, short, ventral alisphenoid tympanic process; a large epitympanic fenestra; a delicate, short postglenoid process; a narrow, lanceolate i1; a distinct premetacristid on m1; and more anteriorly convex lophs on the upper molars.

Nimbadon spp. differ from all other zygomaturines except species of *Silvabestius* and *Raemeotherium yatkolai* Rich et al., 1978, in having a molar gradient that does not increase posteriorly along the molar row.

Nimbadon lavarackorum Hand et al., 1993

HOLOTYPE: QM F23141, a left maxillary fragment containing M2–3, and buccal half of P3.

TYPE LOCALITY AND AGE: Henk's Hollow Locality, Riversleigh World Heritage Area, Lawn Hill National Park, northwestern Queensland, Australia. Henk's Hollow is stratigraphically near the top of the Faunal Zone C sequence and is interpreted to be middle Miocene in age (Travouillon et al., 2006).

REFERRED SPECIMENS AND LOCALITIES: From the AL90 local fauna: QM F30552, mandible with complete left and right tooth rows; QM F30736, RM3; QM F30751, left partial dentary with m1 (broken), m2–4 and associated M3; QM F30775, juvenile skull with left and right I1–3, P3, M1–3, M4 encrypted; QM F30781, LP3; QM F30784, juvenile left dentary with i1, dp3, m1–3; QM F30793, right partial dentary with p3, m1–2; QM F30794, left partial maxilla with M1–2; QM F30795, right partial maxilla with P3–M2 (lacking buccal margins); QM F30834, Lm1; QM F30835, Rm4; QM F30856, right dentary fragment with p3–m4; QM F30903, LM2, LM3, RM3, Lm2, Lm3 + molar fragments; QM F30904, periotic; QM F30905, associated RM3–4, LM2, LM4, Rm1; QM F31498, dentary fragment with m2–4; QM F40337, mandible with L and R p3–m4; QM F40338, right dentary with m1–4; QM F40340, RM1, RM2, RM3; QM F40341, palate with L and R P3–M4; QM F40344, RI1, P3, M1, M2 fragment, M4 fragment; QM F40345, skull with LI1, P3–M4, RP3–M3; QM F41101, left partial maxilla with M1 + isolated dP3 + P3 fragment + ?M3; QM F41115, juvenile skull with left and right I1, LP3–M2,M4, RP3–M4, right periotic and basioccipital detached; QM F41122a–e, associated Li1, Ri1, Lm1, Rm1, Lm3; QM F41124, right dentary with i1, p3–m3, partial m4; QM F41190, RI1; QM F41191, juvenile RI1; QM F41192, juvenile right dentary with i1, m1–2; QM F41205, juvenile skull with LP3, M1–4, RM2–4; QM F41233, R i1; QM F41263, left juvenile partial maxilla with ?M4; QM F41280, right partial dentary with m2–4; QM F41282, right partial

dentary with p3, m1, partial m2–3; QM F41293, juvenile right partial dentary with m2–3 encrypted; QM F42677, subadult skull with left and right P3–M4; QM F42678, mandible with broken left and right i1, p3–m3, partial left and right m4; QM F42679, juvenile cranial fragments with RM1 and RM3 in maxilla and left basicranium; QM F50508, Lp3; QM F50509, Li1; QM F50548, left partial dentary with p3–m4; QM F50684a, right dentary with i1, p3, m1–4; QM F50684b, right premaxilla fragment with I1; QM F50694, RP3; QM F50695, RP3; QM F50696, RP3; QM F50697, LP3; QM F50698, RI1; QM F50699, RM1; QM F50700, RM2; QM F50701, RM4; QM F50702, LM2; QM F50703, Ri1; QM F50704, Lp3; QM F50705, Rp3; QM F50706, Lm1; QM F50707, Rm1; QM F50708, Lm2; QM F50709, Lm3; QM F50710, Rm2; QM F50745, LP3; QM F50746, RP3; QM F50747, Lm1; QM F53642, skull with LP3, M1–4, RP3; QM F53647, mandible with Lp3, m1–4, partial Rp3–m1, m2–4; QM F53648a, right juvenile premaxilla/maxilla with I1, dP3 (isolated), P3, M 1–3; QM F53648b, right dentary with i1, m1–3; QM F53648c, left squamosal; QM F53648d, right squamosal; QM F53648e, basisphenoid; QM F53649, mandible with Li1,p3, m1–3; Ri1, p3, m1–2; QM F53650, LP3; QM F53651, LP3; QM F53652, LP3; QM F53653, LP3; QM F53654, LP3; QM F53655, LP3–M1; QM F53656, RP3; QM F53657, LP3; QM F53658, LP3; QM F53659, RP3; QM F53660, LP3; QM F53784, RP3; QM F53785, RP3 missing lingual margin; QM F53786, right maxilla with P3, M1; QM F53787, RP3; QM F53788, left basicranium; QM F53789, juvenile right premaxilla with I1; QM F53791, juvenile left premaxilla with I1; QM F53792, juvenile partial skull with left and right dentaries, left and right I1–2, P3, M1–4, i1, p3, m1–4; QM F53793, articulated skull and mandible with left and right I1–3, P3, M1–4 and left and right i1, p3, m1–4; QM F53794, partial left dentary with p3,m1–4; QM F53795, partial right maxilla with M1–2; QM F53796, left maxilla with P3, M1–3; QM F53797, RM1; QM F53798, LM1; QM F53799, partial left dentary retaining ascending ramus and condyle; QM F53800, partial left maxilla with M1–2; QM F53801, partial left maxilla with P3, M1; QM F53802, Lp3; QM F53807, associated p3, m1, m2, m3; QM F53808, RM1; QM F53809, Lm1; QM F53810, Lm1; QM F53811, Lm1; QM F53812, Lp3; QM F53813, Lp3; QM F53814, Rm1; QM F53815, Rm1; QM F53816, Rp3; QM F53817, Rp3; QM F53818, Rp3; QM F53819, Rp3; QM F53820, Rp3; QM F53821, Rp3; QM F53822, partial left dentary with m1–2, m3 (isolated); QM F52823, Rp3, m1–2, m3 (isolated); QM F53824, mandible with left and right p3, m1–4; QM F53841, dp3; QM F53842, left periotic; QM F53844, right periotic; QM F53845, left periotic; QM F53846, left periotic; QM F53847, left periotic; QM F53848, left periotic; QM F53850, juvenile Ri1, dp3; QM F53851, left periotic; QM F53852, juvenile left periotic; QM F53866, right periotic; QM F53867, RM3. From Dome Site local fauna: QM F23308, left partial maxilla with P3, M1–2; QM F24049, right partial maxilla with P3, M1; QM F53843, mandible with Li1, Ri1, Lp3, Rp3, Rm1–4. From Gag Site Dwornamor local fauna: QM F23160, RM3–4; QM F53862, RM1; QM F53863, Rm4. From Henk's Hollow local fauna: QM F53855, LM4; QM F53856, LM2; QM F53857, Lm4; QM F53858, LM2; QM F53859, RM1. From Jim's Carousel local fauna: QM F16918, LM3; QM F20595, Rm1; QM F22777, LP3; QM F23423, fused mandibular symphyseal region with Li1, Ri1; QM F23895, LM4; QM F23896, LM4; QM F53860, right partial dentary with m3–4; QM F53861, partial right maxilla with M2–4. From Last Minute Site local fauna: QM F53854, Rm2. From Cleft of Ages local fauna: QM F30561, LM3; QM F53849, LM3; QM F53853, Rm2.

REFERRED LOCALITIES AND AGES: Gag Site and Last Minute Site occur on the northern section of the Gag Plateau and are stratigraphically near the base (188m) of the Faunal Zone C sequence (Creaser, 1997) and are interpreted to be middle Miocene in age. The AL90, Dome Site, Cleft, of Ages and Jim's Carousel local faunas are interpreted to be Faunal Zone C deposits (or middle Miocene)

based on biocorrelation of their fossil faunas (Black, 1997).

REVISED SPECIES DIAGNOSIS: The diagnosis for the species is that for the genus until other taxa are known.

SUPPLEMENT TO THE ORIGINAL DESCRIPTION

The following description of the adult cranium of *Nimbadon lavarackorum* is based on QM F31541 (fig. 2), unless otherwise stated. Previously unknown elements of the dentition are also described. Figure 1 is a stylized drawing of a *N. lavarackorum* cranium (based on QM F31541, QM F31377 and QM F53642) highlighting the major features of the skull.

GENERAL: QM F31541 (fig. 2) is a partially preserved cranium missing the right zygomatic arch, the central portion of the left zygomatic arch, the left pterygoid, the anterior of the parietals and the middorsal section of the frontals. Both mastoid-paroccipital processes are broken and the right petrosal is only partially preserved. Although not as complete as some other *Nimbadon lavarackorum* skulls available for description, QM F31541 is used as a basis for cranial description due to the excellent state of preservation of its features and the clearly discernable sutural relationships of the skull. The lack of preservation of the middorsal roof of the cranium allows investigation of the braincase and sinus development. In addition, closer analysis of the side wall of the braincase and orbital region is made possible by the absence of the right zygomatic arch.

QM F31541 is a relatively short broad skull, its maximum width occurring across the lateral glenoid eminences of the jugal. The highest point of the cranium is indeterminate because most of the dorsal surfaces of the frontals are not preserved; however, in QM F50470 (fig. 3) and QM F53642 the highest point of the skull occurs just anterior to the frontoparietal suture. In lateral profile, the skull is domelike and convex at this point. The basicranium of QM F31541 is elevated relative to the cheek tooth row but this feature was found to vary between skulls.

ROSTRUM: The rostrum is deep, broad, and short, comprising 33% of total skull length. It is constricted above the infraorbital foramen but flares laterally at the premaxilla resulting in an anteriorly bulbous snout. The nasals are inflated dorsal to the anterior orbital margin resulting in a convex rostrum in lateral profile, although the degree of convexity varies between skulls. The highest point of the rostrum is level with interproximal P3–M1.

The **nasals** are elongate and narrow, flaring both anteriorly and posteriorly resulting in an hourglass shape. They are bounded laterally by the premaxilla and maxilla and posteriorly by the frontals, and are generally confined to the dorsal surface of the rostrum with a slight ventral extension posterolaterally along the nasomaxillary suture. The nasals terminate posteriorly in line with the anterior margin of the orbit. Anteriorly, they terminate in a sharp point above I1. The frontonasal suture is W-shaped (when viewed posterodorsally) with the frontals forming a wedge between the nasals. In QM F50470, however, the frontonasal suture is semicircular and broadly concave. The ventral surfaces of the nasals are visible within the narial aperture and are dominated by a ridge of bone that runs parallel along either side of the nasal septum. On their dorsal surface the nasals are perforated by two small (~1 mm in diameter) foramina. The first lies 5 mm anterior to the frontonasal suture and 2 mm medial to the nasomaxillary suture. This foramen is confined wholly within the nasals in QM F31541, but its position varies in other skulls. The second foramen lies 7.7 mm anterior to the first, on or just medial to the nasomaxillary suture. The **narial aperture** is much wider (30.7 mm) than it is high (23.3 mm) due to the flaring premaxillary walls. The anterior palatal fenestrae (interincisive foramina) open into the floor of the narial aperture from the premaxillary palate. The floor of the narial aperture is deep and troughlike and is bordered laterally by thick premaxillary walls.

On the lateral face of the rostrum, the **premaxilla-maxilla suture** is nearly vertical except for a concave expansion posteriorly toward the infraorbital foramen. On the

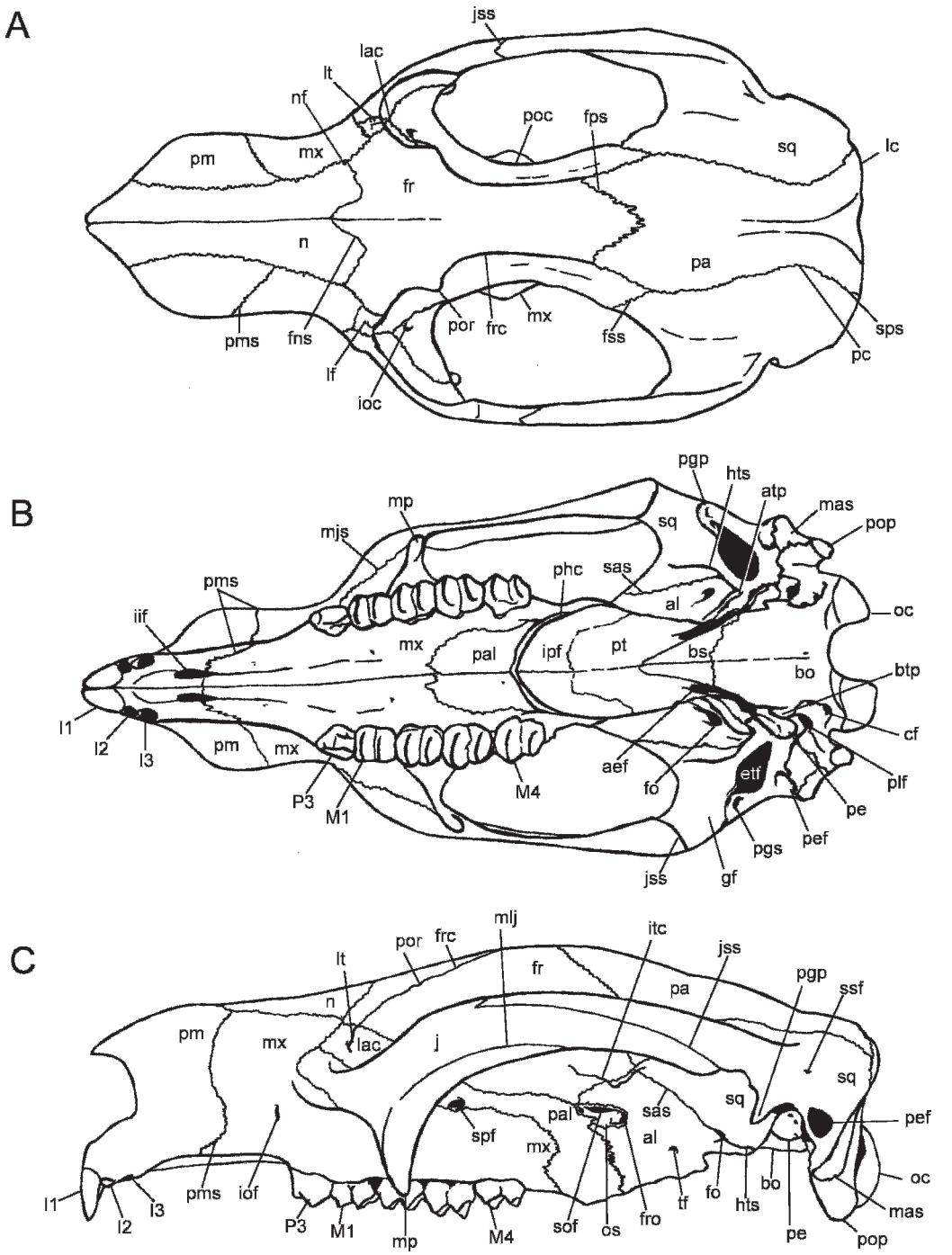

Fig. 1. Stylized drawing of *Nimbadon lavarackorum* cranium showing major features: **A**, dorsal view; **B**, occlusal view; **C**, lateral view.

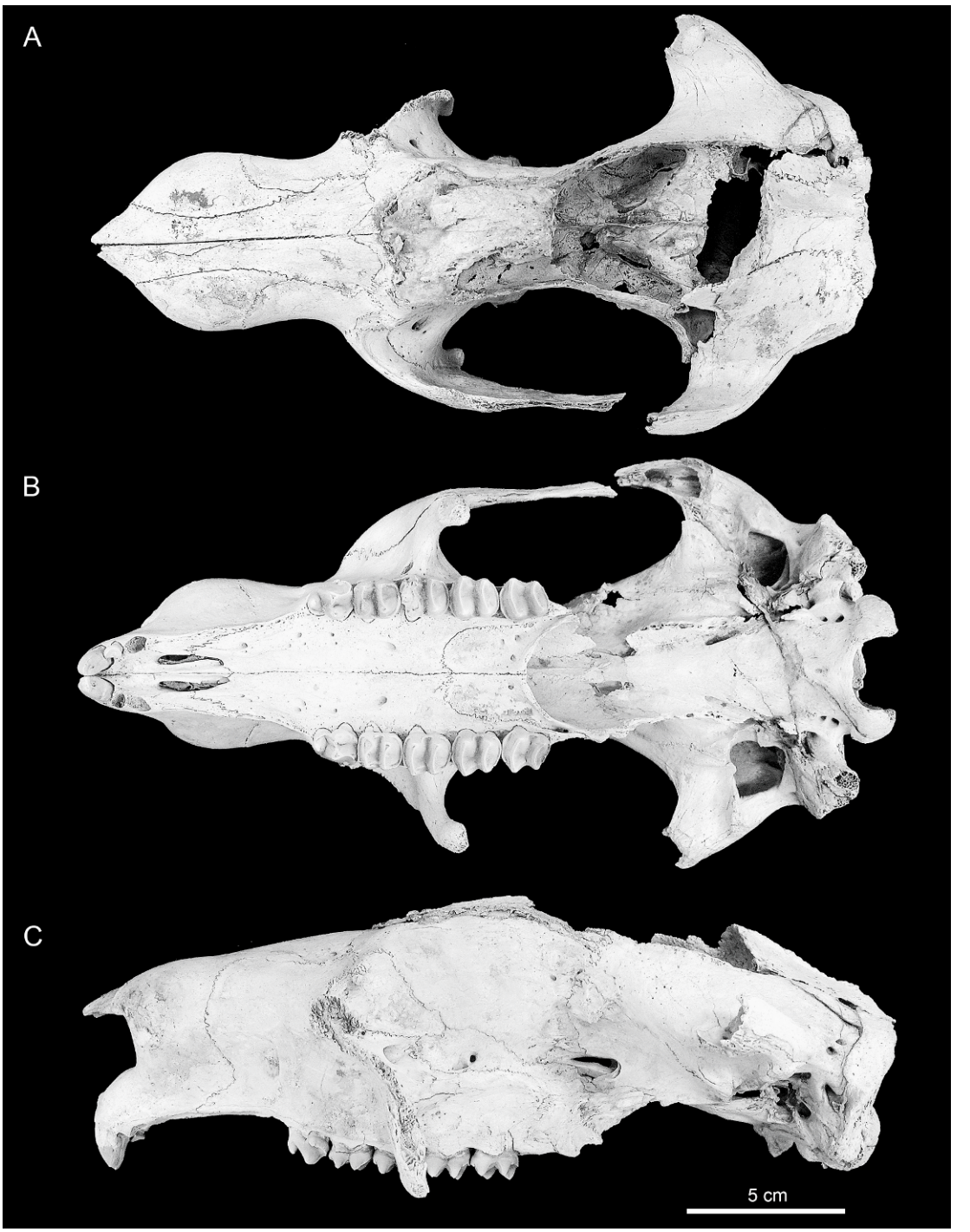

Fig. 2. *Nimbadon lavarackorum* cranium (QM F31541) in: **A,** dorsal; **B,** ventral; and **C,** lateral views.

dorsal surface of the rostrum, the suture extends posteriorly to meet the nasals at a point in line with the infraorbital foramen. Ventrally, the premaxilla-maxilla suture extends onto the occlusal surface of the palate 25.6 mm anterior to the root of P3. It then extends 9.6 mm posteriorly, following the lateral border of the palate to a small nutrient foramen. In QM F50470 a small canine was present at this point (but was broken during preparation). The premaxilla-maxilla suture then extends 16.8 mm anteromedially to a point approximately midway along the length of the lateral margin of the interincisive foramen.

The **maxillae** comprise just over 50% of the rostrum in lateral view. A narrow infraorbital foramen (5.9 mm high; 2.7 mm wide) lies 15.6 mm posterior to the premaxilla-maxilla suture, vertically in line with the anterior border of P3. The maxilla is best described in terms of its sutural relationships with adjacent bones. The maxillofrontal suture is short (right 5.6 mm; left 7.2 mm) and extends posteroventrally from the junction of the nasal, frontal, and maxilla. Contact between the maxilla and frontal is limited in all referred skulls and is at its maximum length in QM F53642 at 9.9 mm. The maxillolacrimal suture originates at the point of most lateral extension of the maxillofrontal suture and extends anteroventrally for 14.0 mm, terminating at the junction of the maxilla, lacrimal, and jugal bones at the anterior margin of the orbit. Within the orbit, the maxillolacrimal suture extends 17 mm posteriorly from the junction of the maxilla, lacrimal, and jugal bones.

The maxillopalatine suture originates from the midline of the palate at a point opposite the posterior root of M2. It curves posterolaterally, then posteriorly, running parallel with the tooth row, into the posterior palatine foramen. From here it ascends sharply for approximately 22 mm then continues anteriorly along the suborbital shelf for approximately 30 mm, curving dorsally once more and continues (for 8.5 mm) to meet the ventral border of the lacrimal. Within the orbit the maxillojugal suture curves laterally, following the curve of the anterior root of the zygomatic process then descends along the masseteric process to within 6 mm of its tip. It then curves around the lateral face of the masseteric process and continues anterodorsally, following the line of the maxillolabial fossa, eventually terminating at the anteromedial orbital margin at the maxilla-jugal-lacrimal suture.

PALATE: The **maxillary palate** is relatively shallow and open in QM F31541 but varies in depth among the referred skulls. It is perforated by numerous foramina, the largest of which lie 5.5 mm and 7.9 mm medial to the left and right M1, respectively, and 4.6 mm medial and 6.2 mm anteromedial to the left and right P3. The frequency and position of the many small foramina are highly variable between the referred skulls. There is also significant variation within the left and right sides of an individual with some foramina present on one side and not the other, or asymmetrically distributed. The foramina most consistently present are those medial to the M1 and anteromedial to P3. The tooth rows are relatively linear in QM F31541 running parallel to one another.

The medial palatal sulcus originates opposite the anterior root of M2 and becomes wider and deeper as it grades into the interincisival fossa anteriorly. The **premaxillary palate** is relatively narrow and 45.5 mm in length. The interincisival fossa is bordered anteriorly by the narrow U-shaped **incisor arcade** (19.6 mm long, 20.8 mm wide). The interincisive foramina are long and narrow (left 18.3 $\times$ 2.2 mm; right 19.7 $\times$ 2.3 mm) but their dimensions vary considerably within the skulls available for study. The diastema is 62.0 mm long and 37.6 mm wide across the anterior bases of the premolars and 25.6 mm wide across the most posterior extension of the premaxilla-maxilla suture. In lateral profile, the diastema is slightly arched.

The linear midline **palatine** suture is 20 mm long and dominated by a moderately developed ridge. This ridge is variably expressed in the referred skulls. The posterior border of the palate is defined by a moderately developed, arcuate, pharyngeal crest that forms the anterior border of the interpterygoid fossa. In QM F31541, the left palatine is perforated by three small foramina, and the right by a single foramen.

The posterior palatine foramen (or posterolateral palatine foramen sensu Archer, 1976) is found at the posterior end of a deep canal formed between the pharyngeal crest (medially) and the most posterior extension of the maxilla on the palate (laterally). It is much larger, deeper, and more trenchant in QM F50470. It opens on the lateral surface of the interpterygoid fossa on the maxillopalatine suture.

The large **interpterygoid fossa** (35 mm wide, 25 mm deep) is bordered anteriorly and anterolaterally by the palatine and posterolaterally by the pterygoid and alisphenoid. The relationship of the pterygoid is difficult to discern in all the adult crania. In the subadult skull QM F42677, however, the pterygoids are thin bony laminae that overlie the presphenoid and basisphenoid (on the roof of the interpterygoid fossa) and the palatine and alisphenoid (on the medial walls of the interpterygoid fossa). Elongate, tapering, winglike projections of the pterygoids extend posteriorly toward the tympanic processes of the basioccipital where they terminate. In more complete skulls (e.g., QM F53642) the pterygoids form a bony floor to the entocarotid canal.

ORBIT AND ZYGOMATIC ARCH: The **lacrimal** is roughly triangular in shape and forms a wedge between the frontals and maxillae posteriorly. The lacrimal is generally confined within the orbit, extending only 3 mm onto the rostrum. A moderately developed lacrimal tuberosity is situated at the anterodorsal border of the lacrimal and is perforated by small foramina on the left side of the skull. A very small ($<$ 1 mm diameter) lacrimal foramen is situated at the anteroventral base of the tuberosity. Within the orbit there is a broad (8 mm) connection between the lacrimal and palatine bones due to the deep extent of the lacrimal into the orbit.

Only a narrow wedge of the **orbitosphenoid** is visible in lateral profile. The fronto-orbitosphenoid suture extends 13 mm anteroventrally to meet the palatine at a point 10 mm directly anterior to the sphenorbital fissure. The orbitosphenoid-palatine suture extends posteriorly from this point to the sphenorbital fissure. A break in the bones surrounding the sphenorbital fissure reveals the lateral aspect of the presphenoid, which appears to form a bridge across the sphenorbital fissure.

The anteriorly oriented **orbit** has a semiovate opening in anterior view. The presence of a distinct postorbital process of the frontal cannot be determined for QM F31541 and is a variable feature in the referred skulls. It is absent in QM F53645 and QM F30833, but it is well developed in QM F50470 (fig. 3), QM F53642, QM F40345 and QM F53643a. The postorbital process is most prominent and winglike in QM F50470, lying at the posterior end of a 12.5 mm crest at the anterodorsal border of the orbit. The postorbital process of the jugal is a weak, roughened area for muscle attachment on the dorsal surface of the jugal at a point in line with the masseteric process. In QM F50470, the distance between the postorbital processes of the jugal and frontal is 27.8 mm.

The **suborbital shelf** is narrow and slopes steeply ventrally. A large (4.5 mm diameter), round infraorbital canal sits 4 mm ventral to the maxillolacrimal suture, 12 mm posterior to the anterior orbital margin. A smaller anteroposteriorly ovate sphenopalatine foramen lies approximately 16 mm posterior to the infraorbital canal and extends ventrally into the palatine. A number of smaller foramina perforate the suborbital shelf on either side of the skull, supplying vessels to the alveolar region.

Description of the zygomatic arch is based on QM F50470 (fig. 3) because this region is not preserved in QM F31541. The **zygomatic arch** is composed almost equally of jugal and squamosal. It is deepest through the masseteric processes. The elongate zygomatic process of the **jugal** tapers posteroventrally and terminates at the anterolateral border of the glenoid fossa. In ventral view, the jugal is ridgelike along its lateral border. The squamosal process of the zygomatic arch tapers anterodorsally and terminates 45 mm posterior to the anterior orbital margin. The lateral jugosquamosal suture extends anteroventrally for 10 mm, then curves in the opposite direction extending posteroventrally for 73 mm. Ventrally, the jugosquamosal suture is short (15 mm) and runs diagonally (posterolaterally) across the posterior base of the

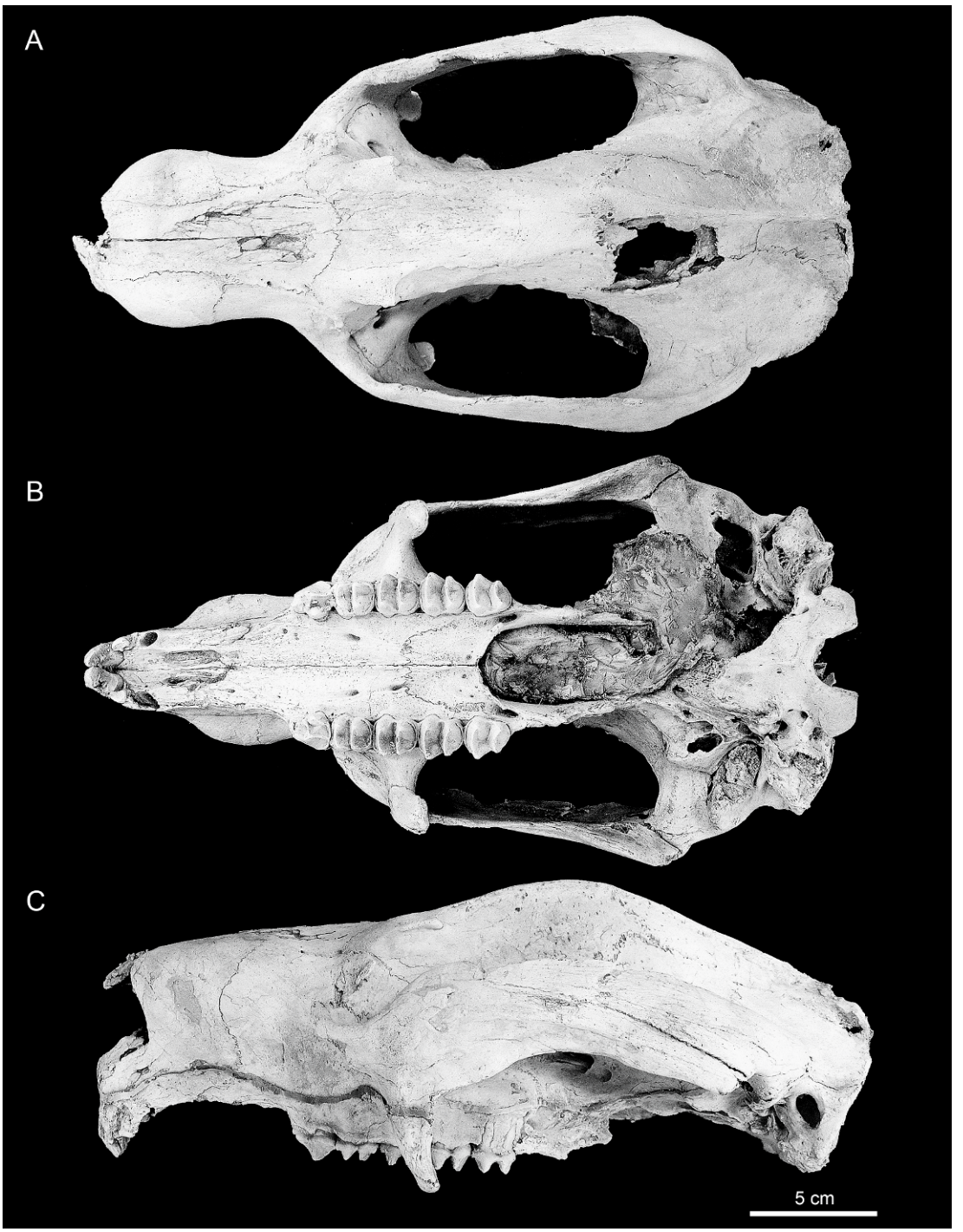

Fig. 3. *Nimbadon lavarackorum* cranium (QM F50470) in: **A,** dorsal; **B,** ventral; and **C,** lateral views.

zygomatic arch. The masseteric line of the jugal is a deep facet for the attachment of the masseter lateralis profundus muscle. It originates on the masseteric process and curves posterodorsally then posteroventrally, following the curve of the dorsal border of the zygomatic arch before attenuating along the inferior margin of the jugal. The **masseteric process** is well developed, elongate, slender, and rounded at its tip. In lateral view, the tip of the process curves posteriorly and terminates approximately 5 mm ventral to the occlusal surface of the molar row.

The dorsal surface of the **frontals** and the frontoparietal suture are not preserved in QM F31541 revealing the internal structure of the frontals (fig. 2). The frontals are dominated internally by two bilaterally symmetrical sinuses separated by a thin, transverse septum. They are confluent posteriorly with a network of sinuses within the alisphenoid, squamosal, and parietal bones. These sinuses separate the inner table of the braincase from the outer table of the skull both dorsally and laterally. The inner table of the braincase is a thin-walled bony capsule scarred by numerous nutrient channels and measures 50 mm (mediolaterally) at its widest point (fig. 2). Many of the septa separating the endocranial sinuses are missing from QM F31541, but analysis of partial crania (e.g., QM F53788) indicate the following sinuses are present: separate anterior and posterior parietal sinuses; an anterolateral parietal sinus that is confluent with a lateral squamosal/alisphenoid sinus; and lateral squamosal sinus that is confluent with a series of epitympanic sinuses surrounding the middle ear and invading the squamosal root of the zygomatic arch.

Description of the external relationships of the frontals is based on QM F53642. Dorsally, the frontals are broadly triangular and bounded by the nasals anteriorly and the parietals posteriorly. A shallow frontal depression occupies the anterior two-thirds of the frontals and is emarginated laterally by moderately developed frontal crests. They are 39 mm apart at their point of origin at the postorbital processes of the frontal, converging to within 17 mm of each other at a point in line with the anterior root of M4. From here they diverge, fading toward the highest point on the cranium at the anteriormost point of the frontoparietal suture. In QM F50470 (fig. 3), the frontal crests extend beyond the frontparietal suture, converging 35 mm behind this point, at the dorsal midline of the cranium where they become continuous with a well-developed sagittal crest.

The frontals measure 83 mm at their midline and are partially fused with only 34 mm of the midline suture evident anteriorly. The convoluted frontoparietal suture, however, remains highly visible. The frontals form a wedge between the parietals dorsally and the parietal and squamosal laterally. In QM F50470, however, the dorsal frontoparietal suture is relatively linear mediolaterally (such that the frontals do not form a wedge between the parietals), although a lateral frontal wedge is still evident.

In QM F31541, from the lateral junction of the frontal, parietal, and squamosal bones, the frontosquamosal suture descends anterolaterally along the wall of the orbit to its juncture with the **alisphenoid**. A rugose tuberosity, the infratemporal crest, lies at this point. The fronto-alisphenoid suture continues ventrally and slightly posteriorly from this point toward the sphenorbital fissure. Its junction with the orbitosphenoid occurs ~5 mm dorsal to the sphenorbital fissure.

The squamoso-alisphenoid suture extends posteroventrally from its contact with the frontal across the rugose infratemporal crests to the hypotympanic swelling, which is situated medial to the glenoid fossa. The squamoso-alisphenoid suture extends posteriorly across the lateral third of the bulla to its posterior margin then curves dorsomedially around the alisphenoid tympanic process, disappearing from view at the anterolateral tip (superior periotic process) of the petrosal. A full description of the basicranium is given below.

The **squamosal** comprises approximately two-thirds of the side wall of the braincase, which descends relatively steeply from the midline parietal suture. In QM F53642, the **parietals** are constricted to a minimum width of 12 mm, at a point 16 mm anterior to the lambdoid crest, expanding to their maximum width (52 mm) at the lambdoid crest. A

subsquamosal foramen is consistently present at the posterior base of the squamosal root of the zygomatic arch; however, in QM F31541 there is a secondary foramen 2 mm posteromedial to the primary subsquamosal foramen (but only on the right side of the skull).

CRANIAL BASE: The cranial base is elevated with respect to the alveolar row. Its maximum width (and indeed the maximum width of the skull) occurs through the glenoid process of the jugal at the posterior root of the zygomatic arch. The minimum width of the cranial base occurs across the postzygomatic constriction of the squamosal. The cranial base of QM F53642 is flat along the plane of the basioccipital and basisphenoid except for the shallow sulci lateral to the median crest of the basioccipital. In QM F31541, the **basioccipital** is inflated anteriorly where it contacts the basisphenoid (33 mm anterior to the foramen magnum). In QM F53642, a distinct median basioccipital crest extends anteriorly from the foramen magnum for 13 mm before fading out. The median basioccipital crest is unclear in QM F31541 and the basioccipital sulci are much shallower.

A short basioccipital tympanic process extends 3 mm ventral to the periotic. The maximum width of the basioccipital (37 mm) occurs at this point. Two condylar foramina occur posterior to the basioccipital tympanic process. The small (1 mm) anterior and larger (2.5 mm) posterior condylar foramina are confluent with the foramen magnum internally. The **basisphenoid** is 30 mm long and narrows anteriorly to 8 mm wide at its junction with the presphenoid. In more complete specimens, the presphenoid-basisphenoid suture is covered by the bony lamina of the pterygoid.

The **pterygoids** are broken posteriorly in QM F31541, thus exposing the groove for the entocarotid artery. This narrow (4 mm wide, 17 mm long) groove lies lateral to the basioccipital and basisphenoid bones and medial to the pterygoid crests. At its anterior margin lies the anterior entocarotid foramen, which enters the basisphenoid 8 mm anterior to the basisphenoid-basioccipital suture in QM F31541 (11 mm anterior in QM F53642). In QM F53642, the pterygoids are partially preserved and overlay the groove for the entocarotid artery lateral to the basioccipital. The groove remains open ventrally along its basisphenoid portion. In QM F42677 (in which the pterygoids are complete) the entocarotid groove and the anterior entocarotid foramen are not visible and only a small triangular wedge of the basisphenoid is exposed ventrally.

The **glenoid fossa** is broad and flat and composed entirely of squamosal. It is open laterally and terminates medially at the base of the hypotympanic swelling. The postglenoid sulcus (= mandibular fossa sensu Aplin, 1987) is an elongate, straight, mediolateral groove that runs the length of the glenoid fossa. It is bordered anteriorly by a relatively flat articular eminence. The postglenoid process is a slightly inflated, roughened nodule that lacks a postglenoid foramen; however, this feature varied markedly between skulls (see below).

AUDITORY REGION: The middle ear is open ventrally. The **ectotympanic** was unfused and is not preserved in any of the skulls under study. The hypotympanic swelling (''bulla'') is comprised mostly of the alisphenoid (fig. 4) with the squamosal contribution varying from 25%–33% in referred skulls. The degree of inflation of the hypotympanic swelling also varies from relatively flat (e.g., QM F40345) to more sinus inflated and ''bulla-like'' (e.g., QM F31541 and QM F50470). A rugose posterior extension or ''wing'' of the alisphenoid, the alisphenoid tympanic process, projects 5 mm from the floor of the hypotympanic swelling, in the direction of the paroccipital process. In QM F53642 (fig. 4), the alisphenoid tympanic process measures 5.2 mm at its maximum width and is composed of a central groove bordered by thin irregular ridges. The **squamoso-alisphenoid suture** follows the lateral border of the alisphenoid tympanic process, then curves dorsomedially around the posterior base of the hypotympanic swelling to meet the basisphenoid at the opening of the anterior entocarotid foramen. In QM F53788, however, the squamoso-alisphenoid suture extends more sharply posteromedially across the hypotympanic swelling resulting in a squamosal tympanic process (rather than an alisphenoid tympanic process). In QM F31541, the

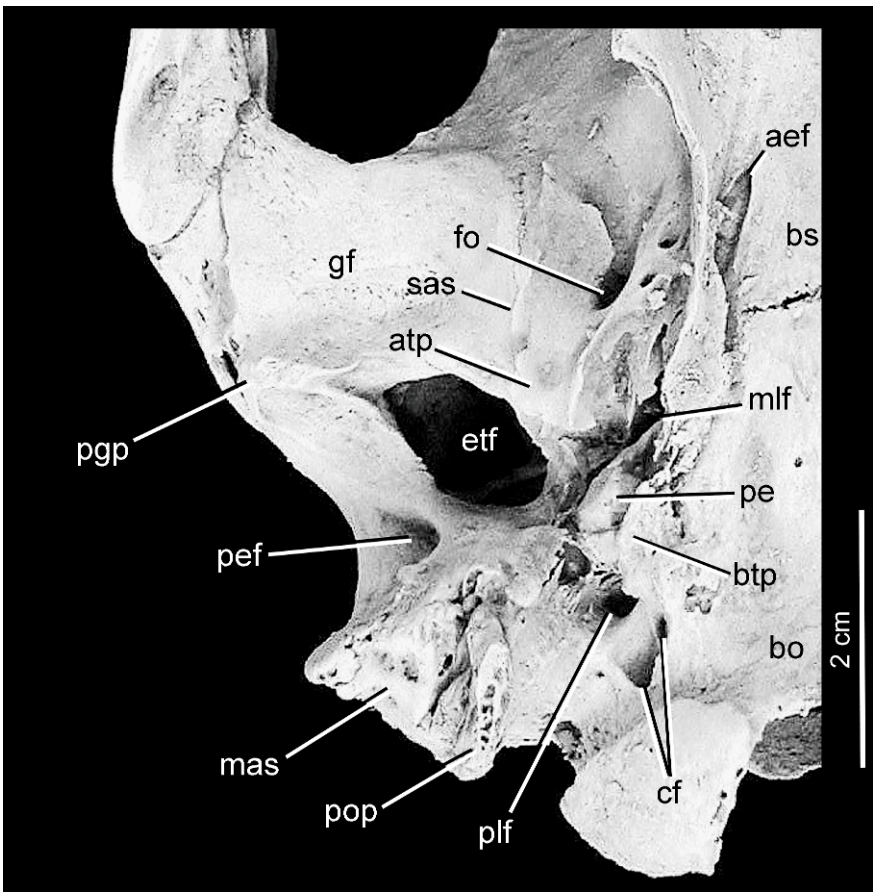

Fig. 4. Right basicranium of *Nimbadon lavarackorum* (QM F53642).

floor of the hypotympanic swelling is broken revealing the bilaminate internal structure wherein the alisphenoid overlays the squamosal medioventrally. The roof of the hypotympanic sinus is produced solely by the squamosal.

The size of the **epitympanic fenestra** varies between skulls. It is generally a moderate to large obliquely oriented fenestra. In QM F53642 (fig. 4), it measures 12 mm anteroposteriorly, 15 mm posteromedially and 12 mm mediolaterally. QM F31541 exhibits a proportionately larger, squarer epitympanic fenestra measuring 16 mm mediolaterally and anteroposteriorly. In all skulls, the epitympanic fenestra opens into a large epitympanic sinus, which is divided into smaller sinuses by a series of bony struts. A large posterior epitympanic fossa is positioned posterolaterally to the epitympanic fenestra and recessed within the squamosal in the roof of the paroccipital/mastoid process. It is clearly seen in lateral view as an oblique ovoid fossa behind the zygomatic arch. In QM F53642 it is 11 mm high and 5 mm wide. It is much smaller in QM F31541 (8 mm × 3 mm). It is not confluent with the large network of epitympanic sinuses.

The **foramen ovale** is located fully within the alisphenoid, but its structure is subject to considerable variation (fig. 17). In QM F53642 (fig. 4), the foramen ovale is 3 mm in diameter and opens into two shallow anteromedially and anterolaterally directed

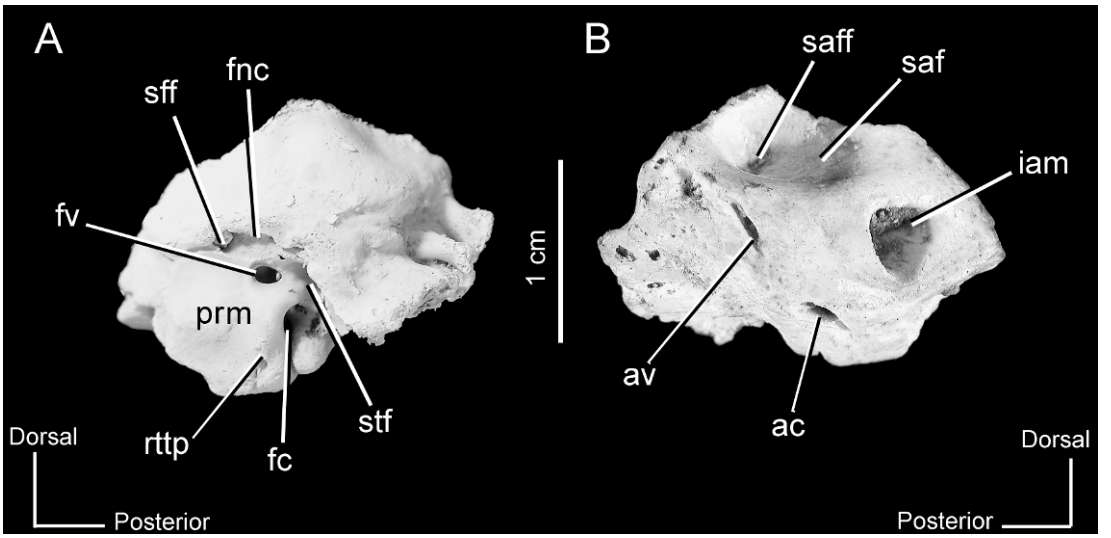

Fig. 5. *Nimbadon lavarackorum* left periotic (QM F53848): **A,** tympanic (lateral) face; **B,** cerebellar face.

channels. In QM F30833, these grooves are covered by a thin lamina of the alisphenoid resulting in two secondary foramina, anteromedial and anterolateral, to the primary foramen ovale.

The median lacerate foramen is most evident in QM F42677 and is positioned at the anteromedial tip of the petrosal, dorsal to the posterior opening of the entocarotid foramen. It is a short (3 mm), slitlike opening directed anterodorsally into the braincase. A larger, rounded posterior lacerate foramen lies posterior to the petrosal at the anteromedial base of the paroccipital/mastoid process.

The deep stylomastoid groove (for facial nerve VII) originates at the posterolateral corner of the petrosal, just lateral to the fenestra cochlearis, attenuating as it descends the anterior surface of the mastoid process. It is almost canallike in QM F53642 (fig. 4) wherein an anterior mastoid tympanic process overhangs the groove anteriorly. The lateral border of the stylomastoid groove is defined by the crista tympanica, which is a thin bony crest originating from the squamosal at the posteromedial corner of the epitympanic fenestra.

The tympanic recess that holds the periotic is roughly triangular in outline. It is bounded anteriorly by the hypotympanic swelling, posteriorly by the mastoid/paroccipital process and exoccipital, laterally by the epitympanic fenestra and medially by the basioccipital. The long axis of the petrosal is aligned anteromedially in ventral view and is partially floored by the basioccipital tympanic process. In QM F53642 the pars petrosus measures 13 mm long by 9 mm wide.

Petrosal: Description of the petrosal (fig. 5) is facilitated by isolated specimens QM F53844–QM F53848. The pars cochlearis is comprised of a smooth and flattened promontorium on its anterolateral face, and a roughened anteromedial flange. The promontorium can be either broad and rounded (e.g., QM F53642) or more flattened and pyramidial (e.g., QM F53844). In QM F53846 the promontorium is rugose rather than smooth.

The promontorium tapers anteromedially into an irregular, blunt anteromedial flange (or superior periotic process sensu Stirton, 1967). The anteromedial flange terminates anteriorly at the median lacerate foramen. The rostral tympanic process of the petrosal is a weak, blunt bulge at the posteroventral border of the promontorium that abuts the basioccipital tympanic process in some specimens (e.g., QM F53788).

A small 2 mm × 1.5 mm fenestra cochlearis (fenestra rotundum sensu Stirton, 1967) opens onto the posterolateral face of the petrosal. Anterodorsal to it lies the smaller (1.3 mm diameter) fenestra vestibularis (fenestra ovalis sensu Stirton, 1967). The fenestra cochlearis and fenestra vestibularis are separated by a 1.8 mm rounded crest (cristainterfenestralis). Dorsolateral to the fenestra vestibularis is a short (5.1 mm long), anteroposteriorly oriented groove that houses a slitlike secondary facial foramen that is confluent with the internal auditory meatus on the cerebellar face of the periotic. The secondary facial foramen carried the chorda tympani branch of the facial nerve. In QM F53844 it lies 2.9 mm anterior to the fenestra vestibularis. In QM F53845 the groove is covered by a thin bony lamina resulting in the development of a narrow 4.7 mm long canal.

Posterolateral and slightly dorsal to the fenestra cochlearis lies a deep pocket that is the stapedial fossa. In correct anatomical position, the facial nerve would travel posteriorly, lateral to the fenestra vestibularis, ventral to the stapedial fossa and onto the deep perpendicular stylomastoid groove in the anterior face of the mastoid.

The cerebellar (internal) side of the periotic is dominated by two large fossae: a dorsolateral subarcuate fossa and a deeper, ventromedial internal auditory meatus. The depth of the subarcuate fossa varies considerably between specimens and in some specimens (e.g., QM F53845, QM F53848) it is perforated by a foramen (fig. 21). The oval-shaped internal auditory meatus of QM F53844 has a maximum diameter of 3.9 mm. Two channels are evident within the internal auditory meatus: the more anterodorsal (foramen acousticum superius) carries the facial nerve and is confluent with the facial foramen on the tympanic face of the periotic, and the posteroventral channel (foramen acousticum inferious) that carries the acoustic (vestibulocochlear) nerve into the substance of the periotic.

Posteroventral to the subarcuate fossa in the rugose area of the sigmoid sinus lies the small, slitlike aqueductus vestibulae. A similarly small and slitlike aqueductus cochleae lies on the rugose basioccipital articular surface (posteromedial face) of the periotic, 6 mm dorsal to the rostral tympanic process.

OCCIPITAL REGION: The shape of the occiput in posterior view is highly variable in *Nimbadon* skulls (figs. 6, 19). In QM F31377, the occipital region is semicircular and relatively flat dorsoventrally except for the deep fossae on either side of the midline of the **supraoccipital** (for the attachment of the rectus capitus major muscle). The median crest of the supraoccipital is relatively indistinct, running dorsoventrally from the lambdoid to the foramen magnum. The distinct, semicircular **lambdoid crest** overhangs the occipital region, and is more pronounced on the median dorsal surface of the skull. The occipital region is inflated along the squamosal-mastoid suture, which, although irregular, generally parallels the lambdoid crest ventrally. The **mastoid** is a thin (4 mm) wedge of bone between the squamosal and the **exoccipital**. It extends 24 mm dorsally to a point in line with the dorsal margin of the occipital condyle. Lateral to the fossa for the rectus capitus major and dorsal to the occipital condyles lie the smaller, shallower, subtriangular fossae for the rectus capitus minor muscle. In QM F31377 (fig. 6) the **foramen magnum** has a distinct supraoccipital notch on its dorsal border, but in QM F53642 it is a broad (24 mm wide × 20 mm high; compared with 21 mm × 16 mm in QM F31541, which is a larger skull overall), laterally ovate structure bordered by large, subovate occipital condyles. The shape and dimensions of the foramen magnum and occipital condyles vary considerably between referred skulls. The intercondylar notch is broadly U-shaped.

The **mastoid-paroccipital processes** are large, rugose, sinus-inflated structures. The mastoid contribution generally terminates in line with the ventralmost point of the occipital condyles. The paroccipital process continues for approximately 10 mm ventral to this point and its structure varies between narrow, mediolaterally compressed processes (e.g., QM F53642) to blunt, rounded processes (e.g., QM F31377). Anteriorly, there is a rugose mastoid tympanic process that extends to within 1 mm of the periotic at its dorsal extreme. Laterally, this process underlies the

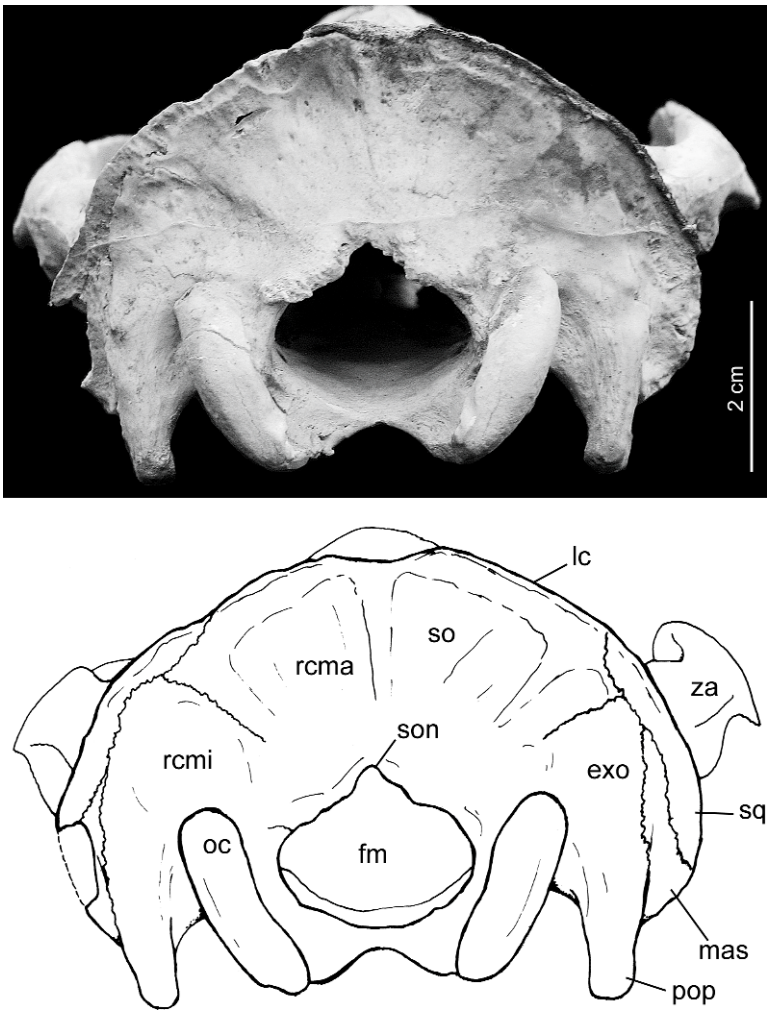

Fig. 6. *Nimbadon lavarackorum* occiput (QM F31377).

stylomastoid groove. In some more complete specimens, the mastoid tympanic process actually contacts the periotic (e.g., QM F53642).

In QM F31541 the **supraoccipital** (or possibly the interparietal) extends 8 mm onto the dorsal surface of the skull preventing contact between the parietals and the lambdoid crest. In dorsal view, the lambdoid crest has a distinct inverted U-shaped notch (9 mm deep) at its midline (fig. 19B) where it meets the sagittal crest. In most skulls, however, the lambdoid crest is generally arcuate.

MANDIBLE: Description of the mandible is based on QM F40337 (figs. 7–8), a mostly complete mandible with left and right i1, p3, m1–4. It is missing the coronoid processes, the right articular condyle, the floor of the right pterygoid fossa, and the posterior tip of the left angular process. Description is based on the left dentary. The dentaries of QM F40337 are fused at the mandibular symphysis limiting photographic access to their medial side. Instead, the unfused dentary QM F53792 is figured in medial view (fig. 9). The horizontal ramus is generally flat, bulging laterally below

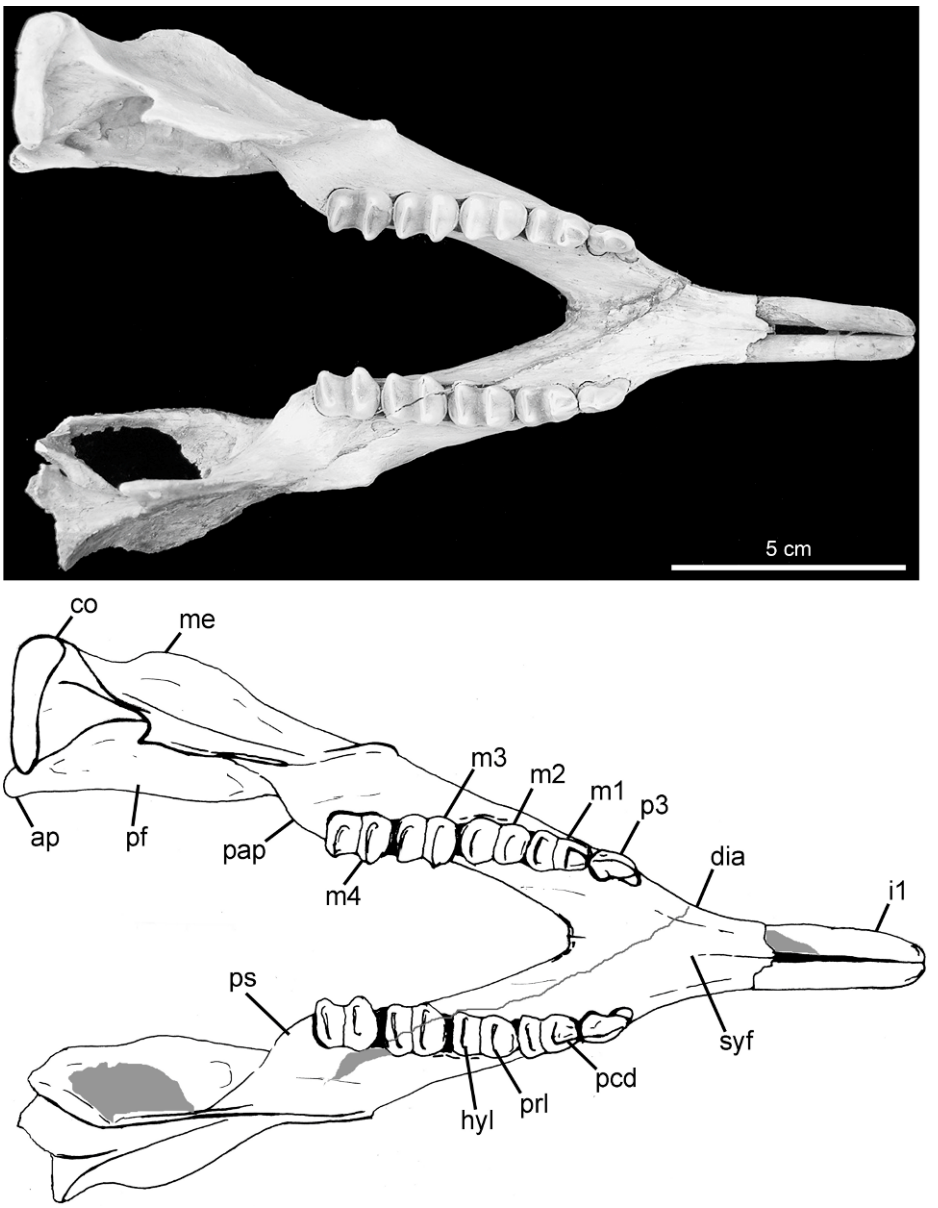

Fig. 7. *Nimbadon lavarackorum* mandible (QM F40337). Gray areas represent broken areas. Gray line represents epoxy resin join.

m2. The alveolar border of the dentary is straight, whereas the inferior border is convex. The greatest depth of the dentary occurs below the level of the protolophid of m3 and the horizontal ramus tapers anteriorly from this point. The diastemal crests are distinct and curve slightly laterally along their dorsal margin. The mandibular symphysis is well fused on its dorsal margin, the suture line only evident posterior to the posterior root of p3.

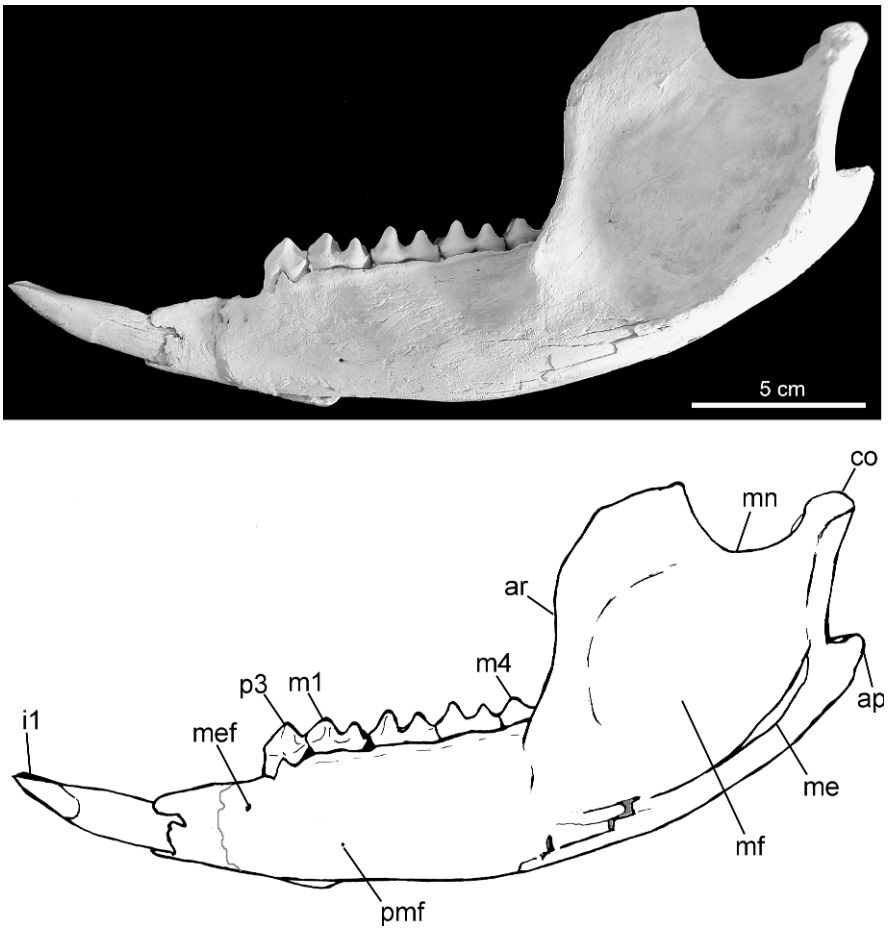

Fig. 8. *Nimbadon lavarackorum* mandible (QM F40337) in lateral view. Gray areas represent broken areas. Gray line represents epoxy resin join.

However, the suture is clearly evident on the ventral surface, becoming wider (i.e., more open) posteriorly along the transverse torus. Two distinct genial pits are found on the posteroventral border of the symphysis. The bone is rugose at this point. The sublingual fossa is relatively shallow (although much deeper in QM F53824) and slopes posteroventrally. A small mental foramen (2.5 mm diameter) lies 4.0 mm ventral to the occlusal surface of the diastema and 7.5 mm anterior to the anterior root of p3. A smaller, secondary mental foramen (< 1.0 mm diameter) lies 4.0 mm posterior to the first. An additional posterior mental foramen lies 19.0 mm ventral to the interloph valley of m1, but it is not present on the right dentary. The anterior border of the ascending ramus rises at an angle of 75° to the horizontal plane and is compressed mediolaterally such that it is very crestlike. It arises opposite the protolophid of m4 where it flares laterally at this point. The masseteric fossa is relatively shallow and fades out onto the horizontal ramus anteriorly. There is no masseteric foramen. The masseteric eminence (submasseteric crest) flares laterally almost to the lateral width of the articular condyle. The condyle is situated 37.0 mm above the level of the alveolar border of the cheek tooth row. The

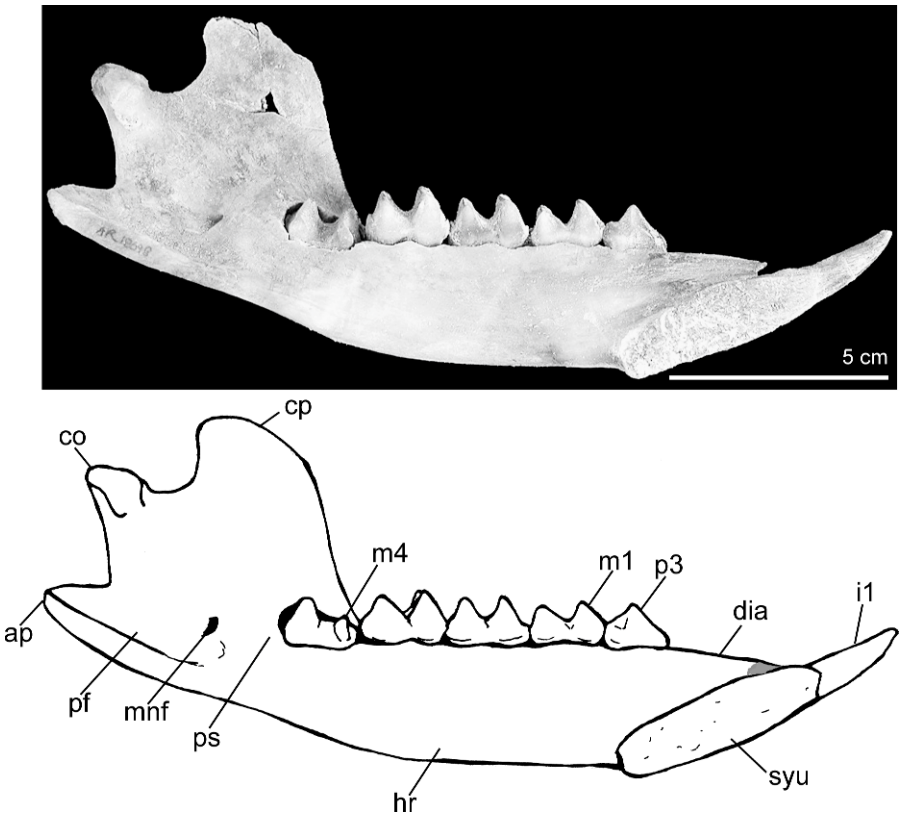

Fig. 9. *Nimbadon lavarackorum* subadult dentary (QM F53792) in medial view. Gray areas represent broken areas.

articular surface of the condyle is deepest (anteroposteriorly) laterally, tapering medially. It is flattened and anterolaterally inclined laterally, becoming convex medially, and tipping ventrally at its most medial point. The mediolateral width of the condyle is 27.8 mm. The mandibular notch is broad (21.1 mm) with relatively linear ventral and anterior borders. A deep and rugose pterygoid fossa is housed within a well-developed angular process of the dentary. A moderate (4.1 mm diameter) mandibular foramen opens posteriorly in line with the postalveolar shelf. A thin, shallow digastric fossa runs anteriorly from below the level of the postalveolar process, fading out below m3. A digastric process is not evident. The postalveolar shelf is short (10.2 mm) and terminates in a small but distinct postalveolar process. The cheektooth rows are relatively linear with a slight concavity opposite the protolophid of m2. The occlusal surfaces of m3–4 on each tooth row tilt lingually toward each other.

DENTITION: Description of the P3, M1–4 of *Nimbadon lavarackorum* can be found in Hand et al. (1993). What follows is a description of previously unknown teeth dP3, I1–3, i1, and dp3 (fig. 10).

I1: Large, curved, open-rooted tooth flattened mesially and concave laterally (fig. 10D–F). Enamel is restricted to the anterolateral surface. Tooth wear initially occurs only on the ventral tips, yet older individuals exhibit wear along the entire exposed posterior surface. In situ, the left and right incisors converge at their tips. In QM F31541 there is a 2.3 mm gap separating the incisors where they emerge from the

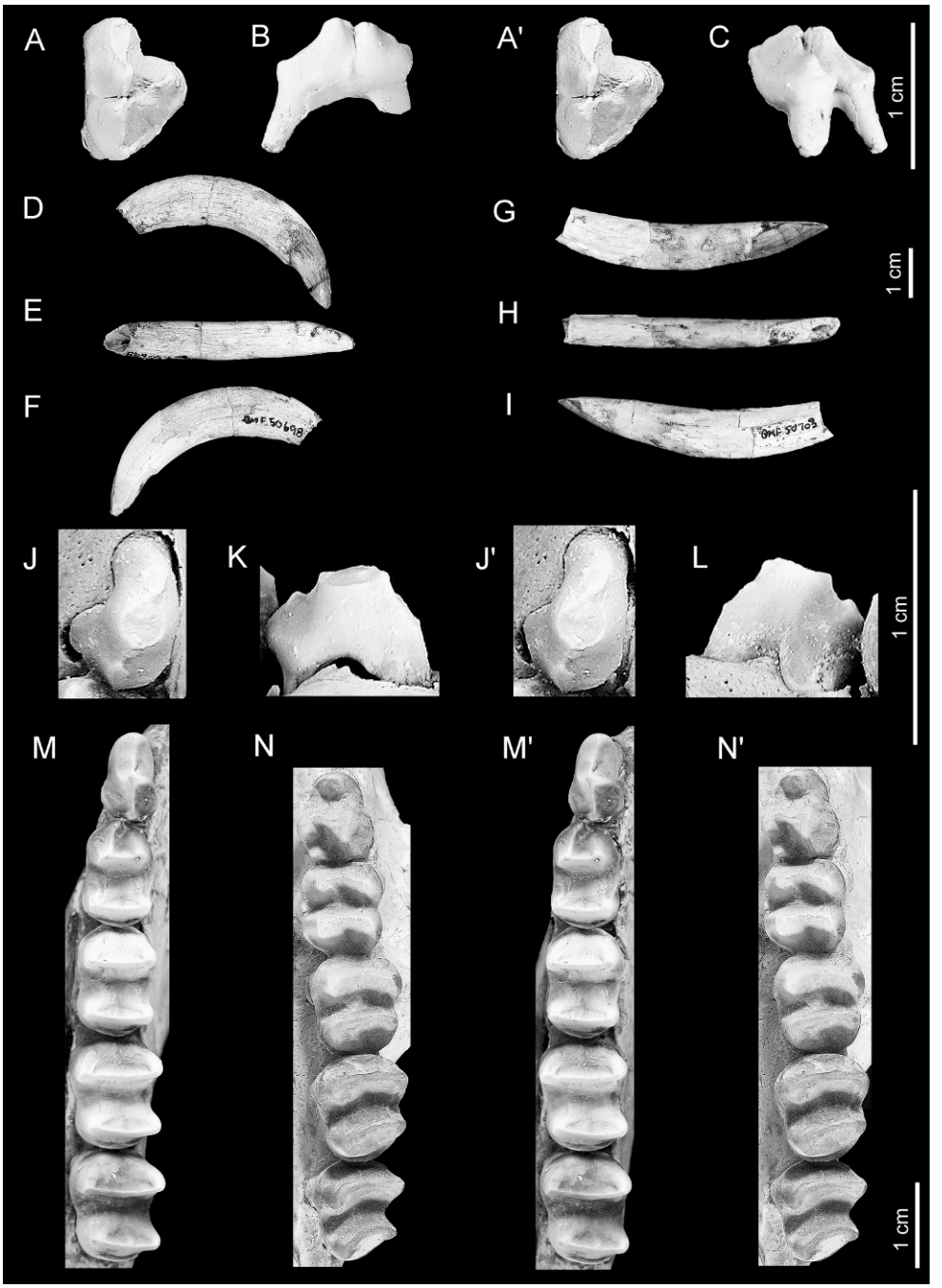

Fig. 10. *Nimbadon lavarackorum* dentition: **A–C,** dP3 (QM F53648a); **D–F,** right I1 (QM F50698); **G–I,** right i1 (QM F50703); **J–L,** dp3 (QM F30784). A–A′, occlusal stereopair; B, buccal view; C, lingual view; D, buccal view; E, occlusal view; F, lingual view; G, buccal view; H, occlusal view; I, lingual view; J–J′, occlusal stereopair; K, buccal view; L, lingual view; M–M′, occlusal stereopair left lower cheektooth row (QM F40337); N–N′, occlusal stereopair left upper cheektooth row (QM F31377).

premaxilla. The length of I1 from the alveolus to its tip is 15.5 mm. Of this, 10.3 mm is covered in enamel. An isolated I1 showing a similar degree of wear and enamel coverage to that in QM F31541 is 47.7 mm long (measured in a straight line from the distal tip to the proximal end of the root). Because the incisor is open rooted and continues to grow throughout the animals life, incisor length varies greatly between specimens.

I2: Small, subovate crowned tooth (4.9 mm long, 3.5 mm wide) that abuts I1 anteromedially. All surfaces are enamel covered, with tooth wear resulting in only an enamel outline around the occlusal surface. A shallow pocket is formed by wear in the dentine of the occlusal surface. I2 and I3 are rarely preserved in situ in both adult and juvenile skulls.

I3: Small, subtriangular tooth in occlusal outline. The apex of the triangle occurs at its anteromesial tip. Only one skull, QM F30833, preserves I3. The worn occlusal surface of I3 has an enamel perimeter and lies along the same plane as I2, which is 15.1 mm above the ventral tip of I1.

Deciduous P3: Description is based on QM F53648a (fig. 10A–C). The dP3 is a small, three-cusped (paracone, metacone, protocone), triangular tooth. It is aligned in an anterolingual direction with respect to M1. A weak longitudinal crest runs posterobuccally from a subcentral paracone (tallest cusp), through the metacone to the posterobuccal cingulum. A small posterolingually positioned protocone is the smallest cusp. There is a weak swelling in the anterior parastylar region of the tooth. A weak posterior cingulum runs lingually from its junction with the main longitudinal crest, to the posterior base of the protocone.

i1: Slender, elongate, lanceolate tooth flattened mesially and concave laterally (fig. 10G–I). Enamel is restricted to the ventral and lateral surfaces. In occlusal view, i1 is generally straight along its length with a medial curvature at its tip. In lateral view, the lower incisor projects at a slight angle to the generally horizontal plane of the dorsal diastemal surface as it follows the ventral curvature of the horizontal ramus anteriorly. In unworn specimens, the lateral occlusal enamel surface is ridgelike. Medial to the enamel ridge is a shallow sulcus in the dentine that runs the length of i1.

Deciduous p3: Description is based on QM F30784, a juvenile left dentary with i1, dp3, m1–3 (m3 encrypted). The dp3 (fig. 10J–L) is a small (4.8 mm long $\times$ 3.5 mm wide), two-rooted tooth, similar in most respects to p3 but on a smaller scale. The tooth is wider posteriorly and tapers anteriorly. In position in the dentary, dp3 is directed anteromedially, whereas m1 is positioned anterolaterally. The occlusal surface of dp3 is dominated by a central protoconid that shows a large degree of wear relative to its size. A small cuspate swelling lies at the posterior border of the tooth. A short crest originates from the protoconid apex and fades down its steep anterolingual face. The posterolateral corner of dp3 abuts the anterior terminus of the paracristid of m1.

QUANTITATIVE VARIATION

Univariate statistics for dental and craniomandibular measurements are listed in appendix 2A and B, respectively. Bivariate plots of select dental and cranial dimensions are given in figures 12 (A–H) and 13 (A–H), respectively. Graphical and statistical results for craniomandibular variables are interpreted with caution due to the small sample size ($N \leq 8$). In regard to the mandible, nine of the 13 variables have a sample size less than or equal to 4, and dentary length could be measured for only two specimens. Consequently, results for the mandible are not represented graphically.

Coefficients of variation (CVs) for dental variables range from 3.0 to 8.3 (appendix 2A), generally falling within the range expected (4–10) for a single mixed-sex population (Simpson et al., 1960). The upper third molar was the least variable tooth (in size) in the dentition with CVs ranging from 3.2–4.6. The lower third premolar was the most variable tooth (in size) with CVs ranging from 8.1–8.3.

Coefficients of variation for cranial measurements range from 3.8–17.1 with seven of the 32 variables expressing CVs greater than 10 (appendix 2B). These include: depth of the zygomatic arch posteriorly (17.1); foramen

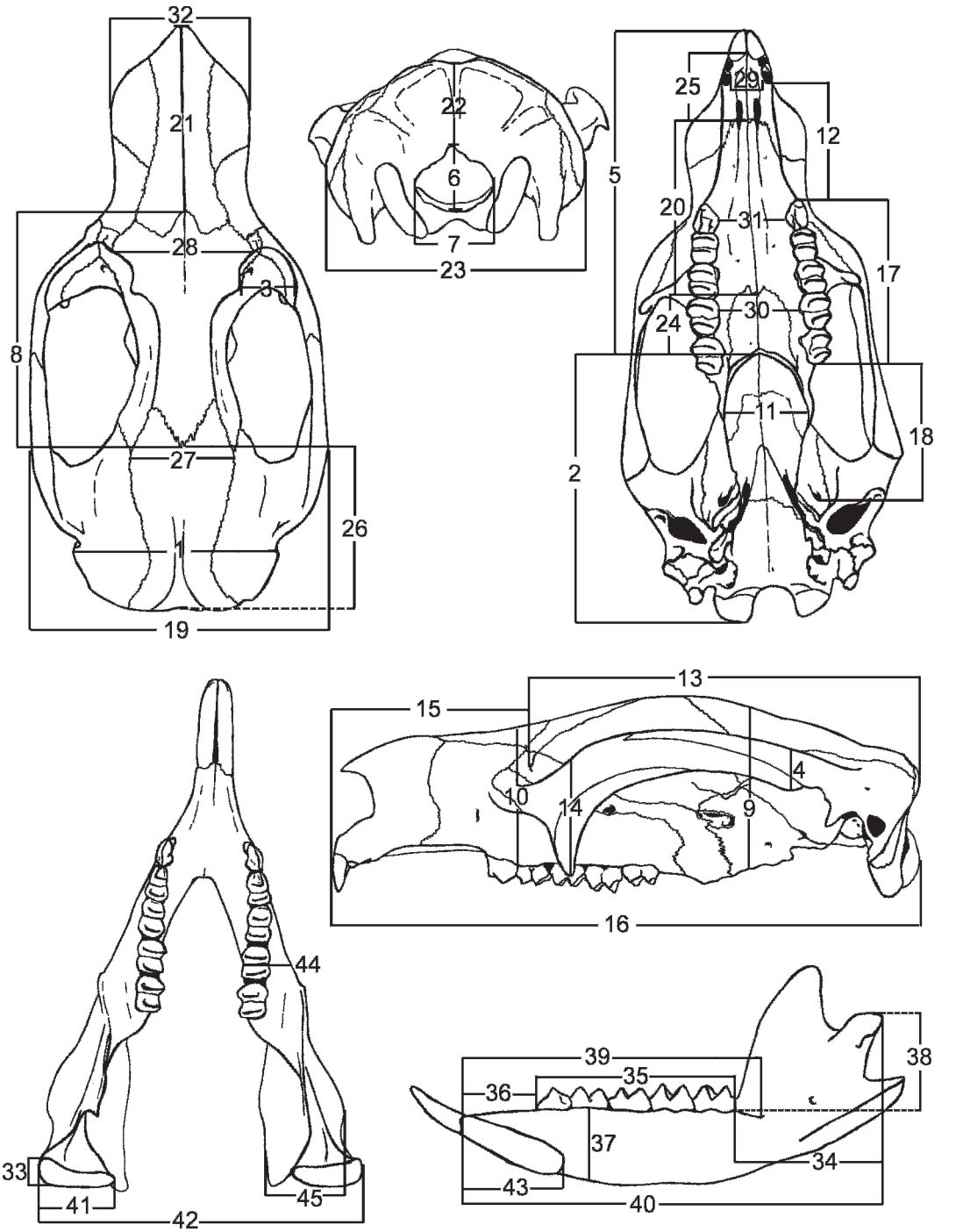

Fig. 11. Craniomandibular measurements for univariate analyses of *Nimbadon lavarackorum*. For definition of measurements, see table 1.

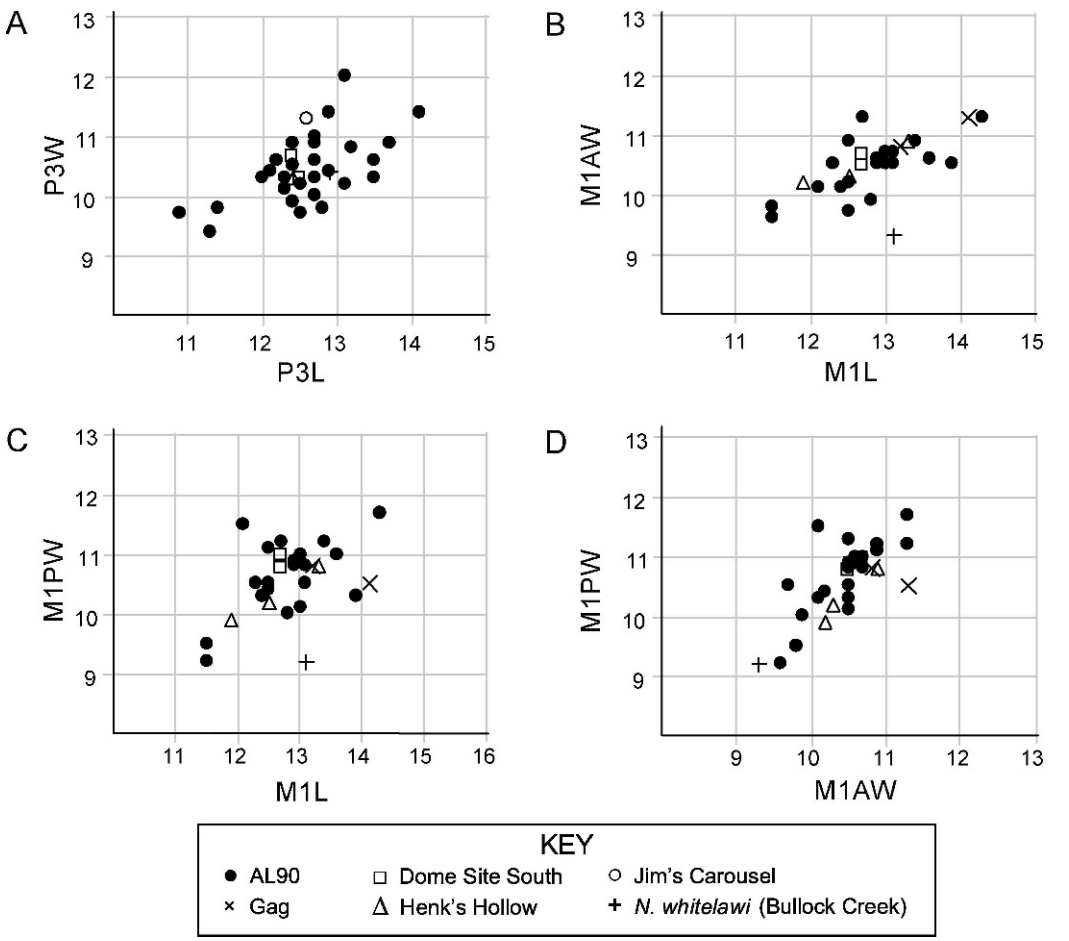

Fig. 12 (A–H). Bivariate plots of *Nimbadon lavarackorum* P3 and M1 dimensions (mm) by site.

magnum height (15.1) and width (10.6); interpterygoid fossa width (14.2); occiput height (10.7); parietal length (13.8); and parietal width (11.2). Low CVs were obtained for basicranium length (3.8), skull length (3.8), upper tooth row length (4.0), and facial cranium length (4.3). Coefficients of variation for mandibular measurements range from 2.9–13.2 with three of the 13 variables expressing CVs greater than 10 (appendix 2B). These include: symphysis length (13.2); the width of the dentary below m3 (10.6); and the maximum width from the masseteric eminence to the angular process (13.1).

Bivariate plots of dental variables (fig. 12A–H) show a strong clustering of the AL90 specimens. *Nimbadon lavarackorum* material from other System C sites at Riversleigh also groups well, generally falling within the range of dimensions for the AL90 population. The P3 and M1 dimensions of *Nimbadon whitelawi* from Bullock Creek, Northern Territory, are also included in fig. 12A–D for comparison. In terms of P3 dimensions (fig. 12A), *N. whitelawi* falls within the center of the *N. lavarackorum* cluster, although narrower molar widths (fig. 12B–D) slightly separate *N. whitelawi* from the Riversleigh sample.

Plots of select cranial variables against skull length (fig. 13A–H) suggest (on the basis of visual observation) that maximum cranial

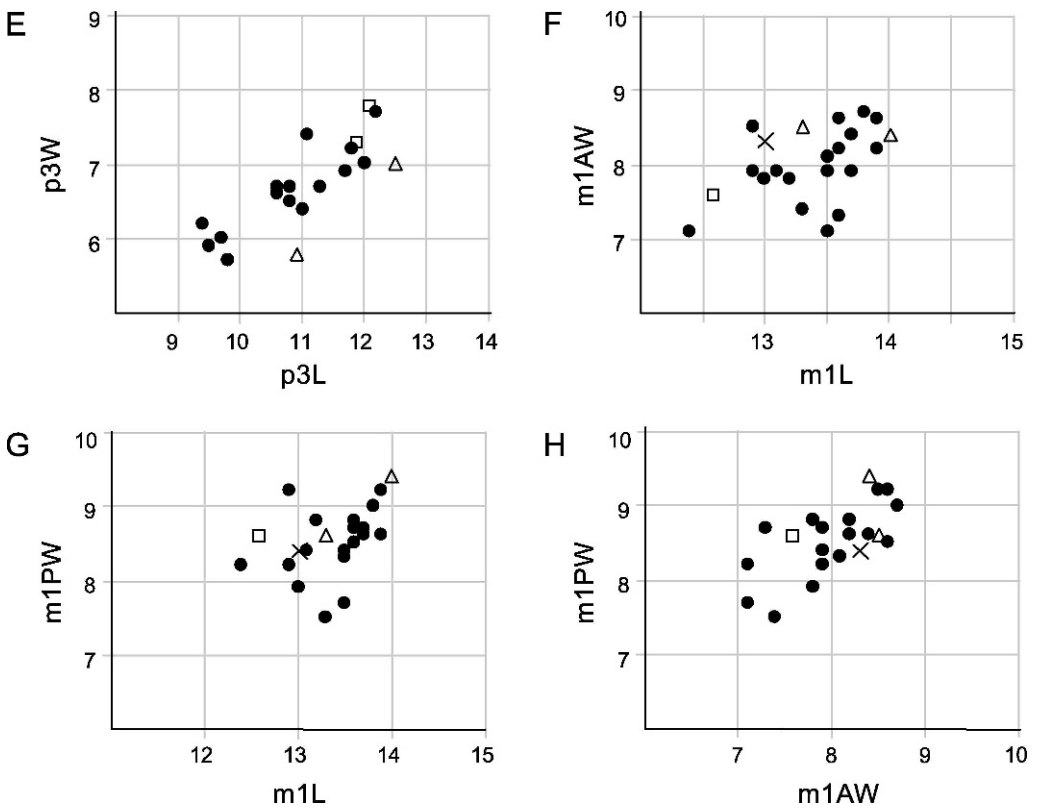

Fig. 12. *Continued.*

width, occiput width, rostrum length and upper tooth row length may be correlated with skull length, whereas rostrum width, rostrum height, cranial height, and occiput height (fig. 13E–H) appear poorly correlated with skull length. Further, figure 13A indicates a possible bimodal distribution for maximum skull width, although sample size ($N = 6$) is limited.

Univariate statistics for *Neohelos stirtoni* are given in appendix 2C. Of the 59 craniomandibular variables listed in Murray et al. (2000b: tables 4–5) only 22 were comparable with variables analyzed for *Nimbadon lavarackorum*. Thirteen of these had CVs greater than 10 for *Neohelos stirtoni* compared with only six variables for *N. lavarackorum*, suggesting *Neohelos stirtoni* is a more variable species overall. Four variables (FMH, FMW, OCH, SL) had high CVs in both taxa. Of the 28 dental variables analyzed, none had CVs greater than 10.

Morphological Variation

P3 Variation

Diprotodontid species, as a consequence of having somewhat uniform lophodont molars, have traditionally been distinguished on the basis of their upper premolar (P3) morphology. However, although P3 morphology has proven phylogenetically useful, it is subject to extreme intraspecific variation in both size and structure. What follows is a list of the most commonly variable features of the P3 of *Nimbadon lavarackorum*. A summary of this variation can be found in table 2 and a pictorial representation in figures 14 and 15. Letters in parentheses refer to figure 14 unless stated otherwise.

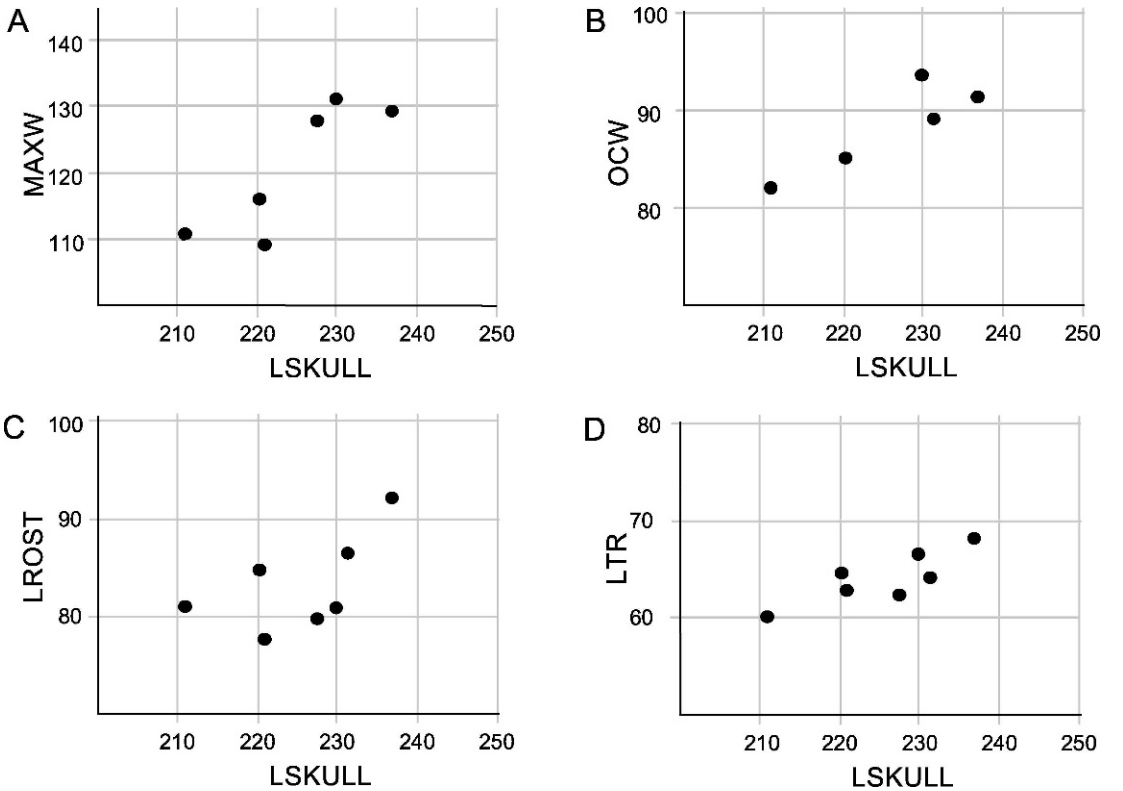

Fig. 13 (A–H). Bivariate plots of select cranial variables in *Nimbadon lavarackorum* from AL90 against skull length.

SIZE AND SHAPE: Premolar lengths range from 10.9–14.1 mm with a mean of 12.6 mm ± 0.7 mm and CV of 5.7, and widths range from 9.4–12.0 mm with a mean of 10.4 mm ± 0.6 mm and CV of 5.6. Figure 14 (A–L) shows that overall shape is extremely variable and is influenced by the relative development of the major cusps, buttresses and cingula of each individual tooth. For example, QM F50696 (B) has a short, round occlusal outline due to the combination of a short parastyle, weak anterolingual emargination between the parastyle and parametacone, and the absence of a buccal cingulum. In comparison, QM F50695 (C) is elongate and ovate due to the well-developed parastylar region and QM F30833 (E) is pyramidal in occlusal view, resulting from an underdeveloped parastylar region and minimal cingular development. QM F30781 (L) is broad posteriorly with a weak buccal emargination of its anterior and posterior tooth moieties, whereas QM F53643a (H) is narrow posteriorly but with a distinct buccal emargination. QM F53784 (D) exhibits a short parastylar region, whereas QM F50694 (G) has an elongate parastylar shelf. QM F53653 (A) has well-developed cingula all round, whereas QM F30833 (E) displays minimal cingular development.

HYPOCONE DEVELOPMENT: The development of the hypocone in the population sample (table 2) varies from absent in 32%, e.g., QM F53643a (H), to well developed in 4% of the sample, as in QM F53655. In 50% of specimens the hypocone appears as a small swelling (between 1.6–2.9 mm in height) on the posterolingual cingulum at the posterior base of the protocone (e.g., QM F50695; C). A

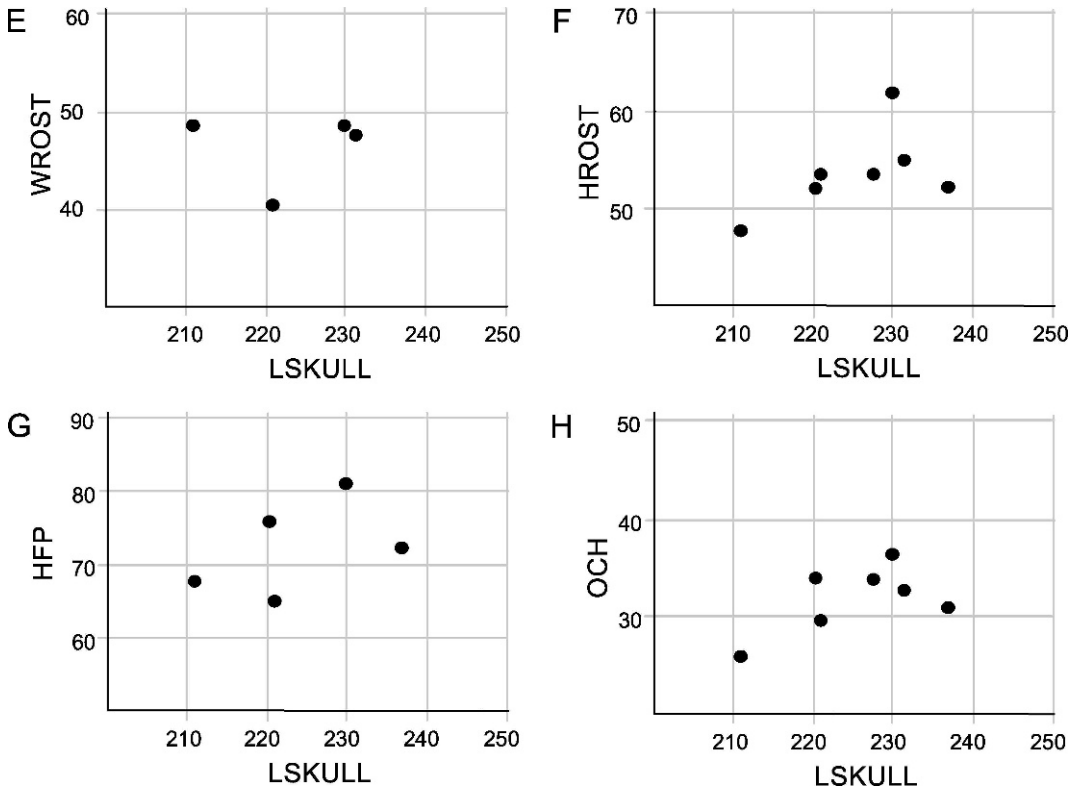

Fig. 13. *Continued.*

moderately developed hypocone (between 3.0–3.9 mm) is found in 14% of the sample population (e.g., QM F30781; L).

PROTOCONE DEVELOPMENT: The protocone varies from a bulbous, broad-based cusp to a smaller narrow cusp that is pushed to the lingual tooth margin. It is large and bulbous in QM F53784 (D) with a relatively gently sloping lingual face, but in QM F50695 (C) the lingual face of the protocone is steeply sloping and the apex is positioned more lingually. The protocone is very small (3.4 mm high) in QM F42677 (I) and QM F30833 (E). Protocone accessory crests are variably expressed: QM F30781 (L) and QM F50745 (J) possess a buccal protocone crest that meets the anterolingual parametacone crest.

PARASTYLE DEVELOPMENT: The parastyle varies from small (3.2 mm) as in QM F30833 (E) to well developed as in QM F53659 (F) wherein the parastyle (5.2 mm) is taller than the protocone (4.2 mm). The mean height of the parastyle is 4.9 mm. A ''hooked'' parastyle (i.e., the extent to which the parastyle apex curves posteriorly toward the parametacone) is found in 46% of the sample population but in varying degrees. It is not hooked in QM F30781 (L; fig. 15B), yet very hooked in QM F53653 (A; fig. 15D). The development of accessory crests from the parastyle apex is also variable. In QM F53651 (fig. 15A) a crescentic parastyle crest is continuous with the anterior parametacone crest. In QM F53784 (D), a deep transverse valley separates the parastyle and parametacone bases. This valley is shallow in QM F53654 (K; fig. 15C) and absent entirely in QM F30833 (E).

PARAMETACONE CREST DEVELOPMENT: The parametacone is consistently the largest cusp on P3 and is generally positioned slightly buccal of the longitudinal midline of the tooth.

TABLE 2

Comparative development of certain structures of the upper third premolar in *Nimbadon lavarackorum* material from AL90 site, Riversleigh

Abbreviations: A–L, extends anterolingually; cing, cingulum; H, height; Hyp, hypocone; L, length; mes, mesostyle; pa-me, parametacone; pas, parastyle; pr, protocone; P-B, posterobuccal; Transv, transverse; W, width; +, present; —, absent; ?, indeterminate. Measurements are in mm.

		Pr	Pas	Pas			Transv. pa-me crest			
QM F	Hyp	H	H	hooked	P-B cing	Mes	meets pr	A-L	P3 L	P3 W
30781	+	4.6	4.9	—	weak	—	+	—	12.7	10.0
30833	—	3.4	3.2	—	weak	—	—	+	11.4	9.8
31377	+	4.5	4.6	—	absent	—	+	—	11.0	9.8
31541	—	4.4	4.7	—	weak	+	+	—	12.7	10.3
36333	+	4.9	5.2	—	weak	—	—	+	12.1	10.4
40341	+	4.1	3.9	+	weak	—	—	+	12.7	10.4
40345	—	?	4.2	+	absent	—	—	+	12.2	10.6
41115	+	4.6	4.5	—	weak	—	—	+	11.3	9.4
41205	+	4.8	5.2	+	weak	—	—	+	12.7	11.0
42677	—	3.4	4.5	—	absent	—	—	+	12.8	9.8
50470	—	4.2	?	?	absent	—	—	+	14.1	11.2
50697	+	3.8	?	—	absent	—	—	+	12.5	9.7
50745	+	5.6	4.8	+	thick	—	+	—	13.1	12.0
53642	+	4.2	4.8	—	absent	—	—	+	12.3	10.0
53643	—	4.5	4.9	—	weak	—	—	+	12.8	10.4
53645	—	3.5	5.5	—	absent	—	+	—	12.7	10.9
53650	+	4.6	4.9	+	weak	—	+	—	12.4	10.5
53651	+	4.1	4.6	—	weak	+	—	+	12.4	10.9
53652	+	4.3	5.5	+	absent	—	—	+	13.7	?
53653	+	4.2	4.7	+	weak	—	—	+	12.9	10.4
53654	+	4.7	3.9	+	weak	—	—	+	13.1	10.2
53655	+	6.2	6.2	+	absent	—	—	+	14.1	11.4
53657	—	4.7	4.5	+	absent	—	—	+	12.7	10.6
53658	+	4.2	4.7	+	weak	—	—	+	12.0	10.3
53660	+	4.5	4.2	—	thick	—	—	+	13.5	10.3
53792	—	4.4	5.9	—	weak	—	—	+	13.0	10.7
53796	+	4.5	5.2	+	weak	+	+	—	12.9	11.4
53801	+	4.1	5.9	+	absent	—	+	—	12.4	9.9

In all specimens it is accompanied by an anterolingual parametacone crest, but the point of termination of this crest is subject to variation. In QM F53659 (F) and QM F53653 (A) it terminates at the anterior end of the longitudinal valley separating the protocone from the parametacone and is cusplike at its point of termination. In QM F50695 (C) and QM F53654 (K), the parametacone crest extends to the anterior lingual tooth border and is continuous with the lingual cingulum. In 29% of specimens (table 2), e.g., QM F30781 (L; fig. 15B) and QM F50745 (J), the anterolingual parametacone crest meets an anterobuccal protocone crest. A posterior parametacone crest is present in all specimens, yet it varies in the degree to which it extends posteriorly or posterobuccally. It extends more posteriorly in QM F53660 and more posterobuccally in QM F53796.

POSTEROBUCCAL CINGULUM: This varies from absent (B) to well developed (F). It may exist as a slight swelling, be cuspate, ridgelike, or shelflike. In QM F53653 (A), the posterobuccal cingulum is well developed, shelflike, and has a small cusp positioned opposite the parametacone apex. In QM F50745 (J) the posterobuccal cingulum is

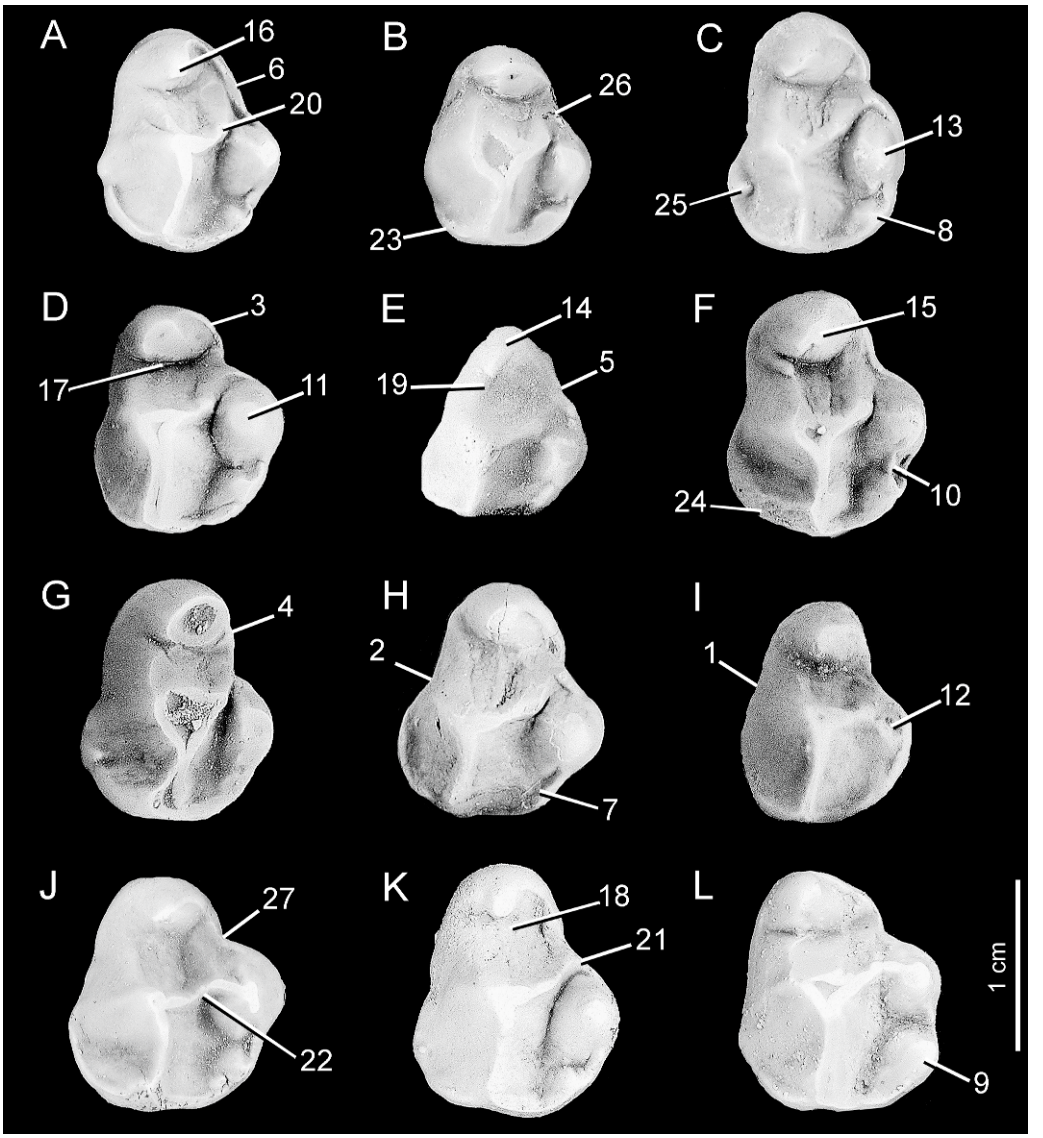

Fig. 14. Morphological variation in the RP3 of *Nimbadon lavarackorum* from AL90 site. Specimens used are as follows: **A,** QM F53653; **B,** QM F50696; **C,** QM F50695; **D,** QM F53784; **E,** QM F30833; **F,** QM F53659; **G,** QM F50694; **H,** QM F53643; **I,** QM F42677; **J,** QM F50745; **K,** QM F53654; **L,** QM F30781. Specimens A, E, J, K and L are mirror images of left P3's to facilitate comparison. 1, weak buccal emargination between anterior and posterior moieties compared with 2, strong emargination; 3, short parastylar shelf as opposed to 4, elongate; 5, weak anterolingual cingulum compared with 6, well developed; 7, hypocone absent compared to 8, small or 9, moderately developed; 10, anterior hypocone crest present; 11, protocone large and bulbous as opposed to 12, small, or 13, narrow and lingually compressed; 14, parastyle small compared with 15, well developed; 16, parastyle hooked; 17, deep transverse valley separating parastyle from parametacone base, compared with 18, shallow valley or 19, valley absent entirely; 20, anterolingual parametacone crest terminates at valley between protocone and parametacone bases as opposed to 21, meets the lingual cingulum or 22, meets a buccal protocone crest; 23, posterobuccal cingulum absent compared to 24, well developed; 25, mesostyle present; 26, weak anterolingual emargination between pas and protocone compared with 27, strong emargination.

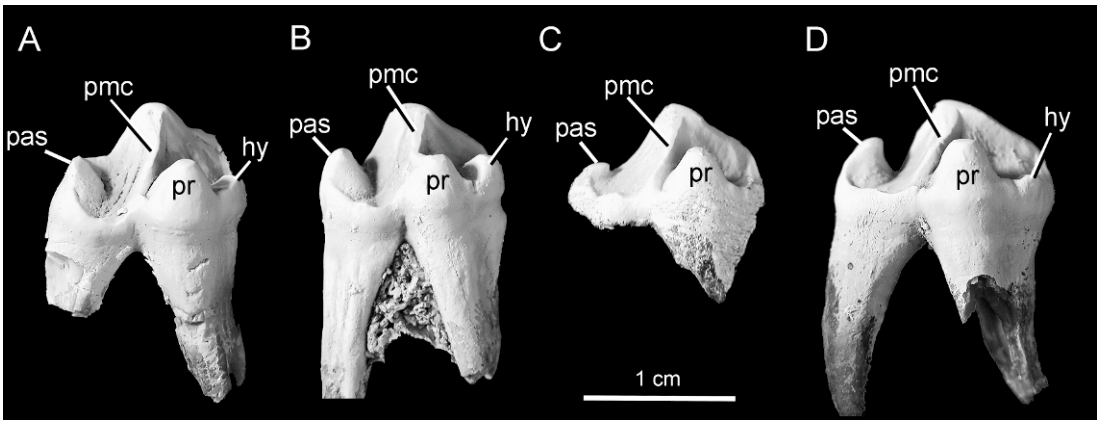

Fig. 15. Lingual view of select left P3's of *Nimbadon lavarackorum* showing variation in the size, structure, and development of accessory crests of the (unworn) parastyle. **A,** QM F53651; **B,** QM F30781 (mirror image); **C,** QM F53654; **D,** QM F53653.

moderately developed and crescentic. In QM F50695 (C) it is poorly developed, although a well-developed mesostyle lies on the posterobuccal face of the parametacone at the base of the crown. A distinct mesostyle is present in 11% of the sample population.

p3 Variation

SIZE AND GENERAL SHAPE: Coefficients of variation for p3 length and width (8.3 and 8.1) were the highest for any tooth in both the upper and lower tooth rows, although these values still fall within the expected range for a single population. Specimens vary between long and narrow (e.g., QM F41252), short and narrow (e.g., QM F53807), short and broad posteriorly (e.g., QM F50704) or long and broad (e.g., QM F53812). Length of p3 ranges from 9.4–12.2 mm with a mean of 10.8 mm ± 0.9 mm. Width of p3 ranges from 5.7–7.7 mm with a mean of 6.7 mm ± 0.6 mm.

HEIGHT OF PROTOCONID: The height of the central cuspid, the protoconid, appears to correlate to overall tooth size with large premolars possessing a taller protoconid (e.g., QM F41252).

DEVELOPMENT OF THE ANTEROLINGUAL CRISTID OF THE PROTOCONID: This structure shows varying degrees of expression from well developed (extending to the base of the crown) and distinct (e.g., QM F41252), to weak and relatively indistinct (e.g., QM F53812).

STEEPNESS OF THE POSTPROTOCRISTID: Regardless of the height of the protoconid, the steepness of the postprotocristid varies from steep and linear (e.g., QM F53816) to steep and arcuate (e.g., QM F53820), or it may gently grade into the posterior cuspid (e.g., QM F53818).

DEVELOPMENT OF THE BUCCAL CINGULUM: Most lower premolars exhibit a weak buccal cingulum, but some variation is evident. QM F53816 has a well-developed ridgelike buccal cingulum. In QM F53817 it is swollen but noncarinate. In QM F53819 the buccal cingulum is moderately developed and cuspate.

DEVELOPMENT OF THE LINGUAL CINGULUM: Most specimens exhibit a weak (e.g., QM F50704, QM F53817) to moderately strong (QM F41252, QM F50508) lingual cingulum.

M1 Variation

Molar morphology within *Nimbadon lavarackorum* is relatively conservative when compared with the degree of variation found in upper and lower premolars. Variation is generally restricted to the following:

SIZE: M1 length ranges from 11.5–14.3 mm with a mean of 12.8 mm ± 0.7 mm; anterior width ranges from 9.6–11.3 mm with a mean of 10.5 mm ± 0.5 mm; and posterior width ranges from 9.2–11.7 mm with a mean of 10.7 mm ± 0.6 mm. Coefficients of variation for M1 dimensions are consistently low, ranging between 4.4 and 5.8.

PARASTYLAR CORNER: The parastylar corner appears as a slight swelling of the anterior cingulum at its anterobuccal extreme. It may be more (QM F53801) or less cuspate (QM F40340), or dominated by a crescentic ridge (QM F53796). The height to which the parastylar corner ascends the anterior face of the protoloph varies from low-lying in QM F53801 to moderately tall in QM F40304.

LINGUAL CINGULUM: The lingual cingulum is generally a short crescentic ridge connecting the posterior base of the protocone with the anterior base of the metaconule, effectively sealing off the transverse valley lingually (e.g., QM F53795, QM F53797). In some specimens (e.g., QM F53801, QM F40341), it may be incomplete such that the transverse valley is open lingually. In QM F41205 and QM F53796 there is an additional small cusp on the lingual cingulum at the posterolingual base of the protocone. This cusp is also found in the M2 of these specimens, yet is absent in M3–4.

POSTMETACRISTA: The postmetacrista is usually moderately developed and continuous with the posterior cingulum through stylar cusp E at the posterobuccal tooth corner (e.g., QM F40341, QM F53801). However, in some specimens (e.g., QM F40340) the postmetacrista is poorly developed or discontinuous, attenuating before linking with stylar cusp E.

RELATIVE WIDTH OF ANTERIOR AND POSTERIOR MOIETIES: In some specimens the M1 is wider across the anterior tooth moiety than the posterior moiety (QM F53797, QM F31377, QM F31548, QM F50470) or vice versa (QM F53642, QM F53800, QM F31541), or they can be of equal width (QM F53796, QM F53795, QM F30833).

m1 Variation

SHAPE OF THE TRIGONID: The trigonid can be broad and subrectangular (QM F41122c), becoming more triangular in some specimens (QM F30834) due to a shortening of the protolophid and anterior border of m1 and/or greater development of the paracristid. This variation is not reflected significantly in the metric analysis with a coefficient of variation for anterior width of 6.3.

SHAPE OF THE PROTOLOPHID: The protolophid is generally linear (QM F53814), becoming more arcuate in some specimens (QM F53815, QM F50706).

CRANIUM

A selection of the most complete adult *Nimbadon lavarackorum* crania are represented in lateral and dorsal views in figure 16. Superficially, these skulls are similar in form, differing mainly in size, yet analysis of discrete areas (figs. 17–19) shows considerable morphological variation, particularly in the basicranial and occipital regions. Numbers in square parentheses refer to those in figure 16 unless stated otherwise.

OVERALL SIZE AND SHAPE: Adult *Nimbadon lavarackorum* skulls range in length from 211.1 mm to 237.0 mm with a mean length of 225.5 mm ± 8.6 mm. The maximum width of the skull (found across the zygomatic arches) ranges from 109.0 mm to 130.9 mm with a mean of 120.5 ± 9.8 mm. Figure 13A indicates a possible bimodal distribution for skull width but this may be an artifact of small sample size ($N = 6$). Clear differences in cranial shape are evident, however. QM F50470 (fig. 16E–E′) is a large, broad cranium with high dorsal doming [1] anterior to the frontoparietal suture, a well-developed sagittal crest [2], a laterally inflated rostrum [3], deep zygomatic arch [4], and well-developed masseteric process [5]. In contrast, QM F40345 (fig. 16B–B′) is a shorter, narrower skull with a slender rostrum [6], poor sagittal crest development, narrow zygomatic arch, slender masseteric process, and a narrow occiput. Of the skulls available for study, QM F40345 exhibits the most extensive wear of its dentition, possibly indicating an older individual. There are morphs in between these extremes, however. For example, QM F31377 (fig. 16D–D′) is a short narrow skull

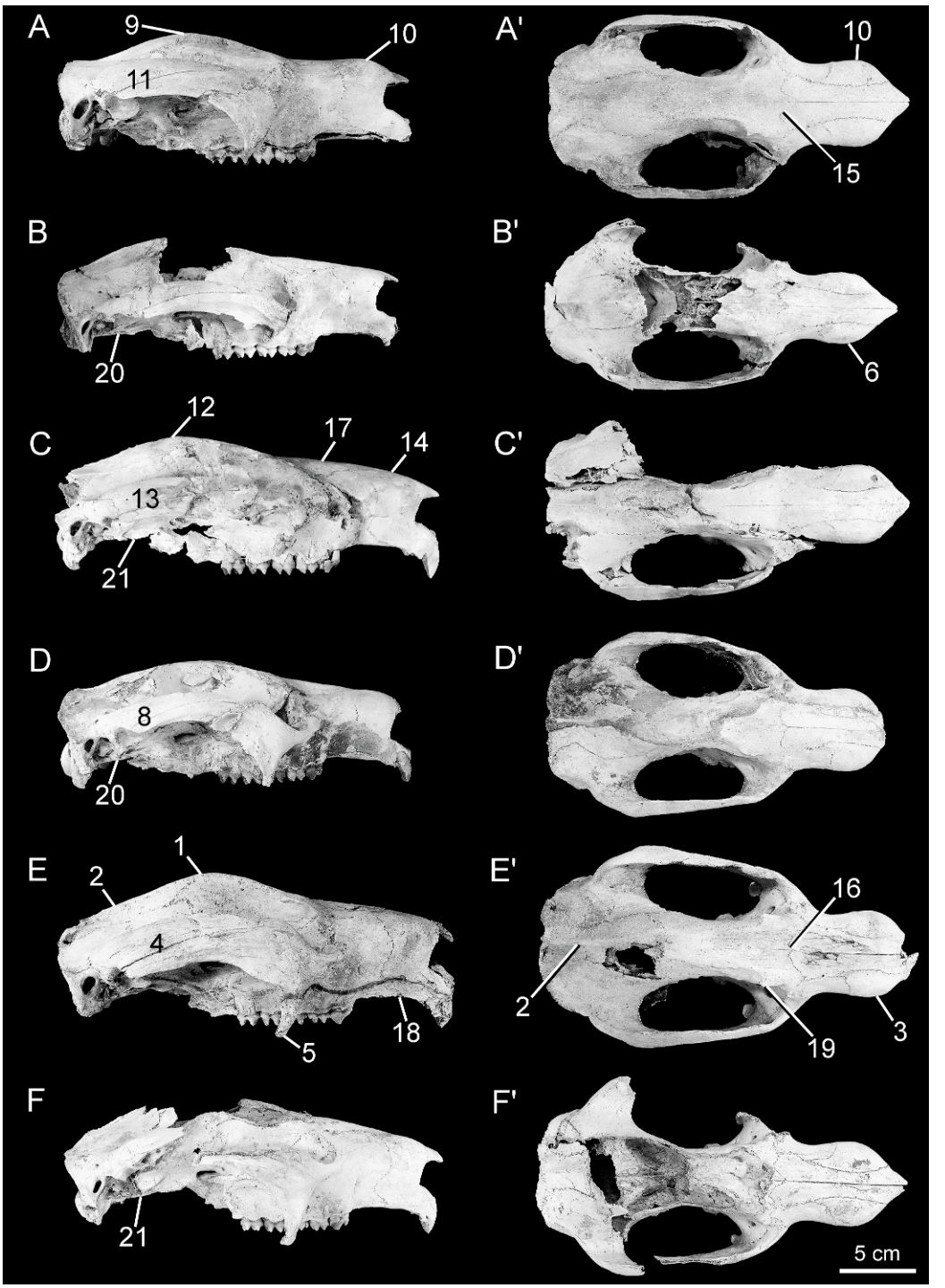

Fig. 16. Lateral (A–F) and dorsal (A′–F′) profiles of representative *Nimbadon lavarackorum* adult skulls from AL90 site. A– A′, QM F53642; B– B′, QM F40345; C– C′, QM F53645; D–D′, QM F31377; E–E′, QM F50470; F–F′, QM F31541. See text for explanation of numbers.

with a relatively broad rostrum but a shallow zygomatic arch [8]. Similarly, QM F53642 (fig. 16A–A′) is a short skull but displays moderate dorsal doming [9], a broad, dorsally inflated [10] rostrum, moderately deep zygomatic arches [11], and a narrow occiput. The longest and widest skull of the available sample, QM F53645 (fig. 16C–C′), displays only moderate dorsal doming [12] and a moderately deep zygomatic arch [13], although it does possess a broad, downturned [14] rostrum and wide occiput.

NASALS: The frontonasal suture is W-shaped in QM F31541 (fig. 16F–F′) with the frontals forming a wedge between the nasals posteriorly [15]. This is also the case in QM F53642 and QM F40345, but it is much reduced in QM F50470 [16] such that the suture is broadly concave. The nasals are inflated posteriorly in QM F53645, QM F50470 and QM F31541 [17] yet flattened in QM F53642. In the majority of skulls the nasals tend to flare anterolaterally before converging at their tip, although QM F40345 (fig. 16B–B′) has a somewhat reduced flare.

CANINE: Small canines were present in QM F50470 (although they were damaged during preparation). All other skulls lack canines except for a juvenile cranium (QM F53792).

LENGTH OF INTERINCISIVE FORAMINA: These vary between skulls and are bilaterally asymmetrical within individual skulls. They are long and narrow in QM F31541 (left 18.3 × 2.2 mm, right 19.7 × 2.3 mm) whereas in QM F53645 (a larger skull overall) they are shorter (left 14.1 × 1.8 mm, right 13.7 × 2.2 mm).

AUXILIARY (OR SECONDARY) INFRAORBITAL FORAMEN: This is absent in all skulls except QM F53643a (not figured) in which it exists as a 1.5 mm diameter foramen whose position on either side of the skull is variable. On the left side of the skull, the secondary infraorbital foramen lies 2 mm dorsal to the infraorbital foramen; on the right it lies 9 mm anterior to the primary infraorbital foramen.

SUPERNUMERARY SUTURE ON ROSTRUM: Found in QM F53642, wherein an additional bone lies between the lacrimal, jugal, and maxilla that prevents the maxillojugal suture from reaching the lacrimal. This bone comprises the anterior edge of the orbit and is bounded by the lacrimal medially, the maxilla posteriorly, the jugal laterally, and the jugal and maxilla anteriorly. It extends approximately 8 mm onto the rostrum and is present on both sides of the skull.

MASSETERIC PROCESS: Moderately developed in most skulls (fig. 16), with larger skulls tending to have a longer masseteric process that extends well below the tooth row (5).

MAXILLARY PALATE: This varies in depth among the referred skulls. It is deep and canallike (although not to the extent of the premaxillary palate) in QM F50470 and QM F31377, broad and deep in QM F53642, but relatively shallow and open in QM F31541.

TOOTHROW ALIGNMENT: The tooth rows are relatively linear in QM F50470 and QM F31541, running parallel to one another. However, in QM F53642 and QM F31377 they converge slightly anteriorly, whereas in QM F53645 they converge posteriorly.

PALATINE RIDGE AND PHARYNGEAL CREST: Generally, a moderately developed midline palatine ridge extends along the palatine suture and an arcuate pharyngeal crest forms the anterior border of the interpterygoid fossa. In QM F50470 they are both well developed and the posterior palatine foramen is larger, deeper, and more trenchant. In QM F53642 the palatine ridge is poorly developed and the posterior palatal foramen is elongate and moderately deep.

POSTORBITAL FRONTAL PROCESSES: A distinct postorbital process of the frontal is absent in QM F 53645 (fig. 16C–C′), but it is well developed in QM F53642, QM F40345, and QM F50470. This area is not preserved in QM F31541 (fig. 16F). It is most prominent and winglike in QM F50470 [19], lying at the posterior end of a 12.5 mm crest situated at the anterodorsal border of the orbit (or 24.4 mm posterior to the lacrimal-maxilla-frontal suture). This crest is reduced in QM F53642 and QM F40345 but well developed in QM F53643a.

CONFLUENT FRONTAL AND SAGITTAL CRESTS: In QM F53642 (fig. 16A′) the frontal crests run parallel to each other and fade out posteriorly at the anteriormost point of the frontal-parietal suture. In QM F50470

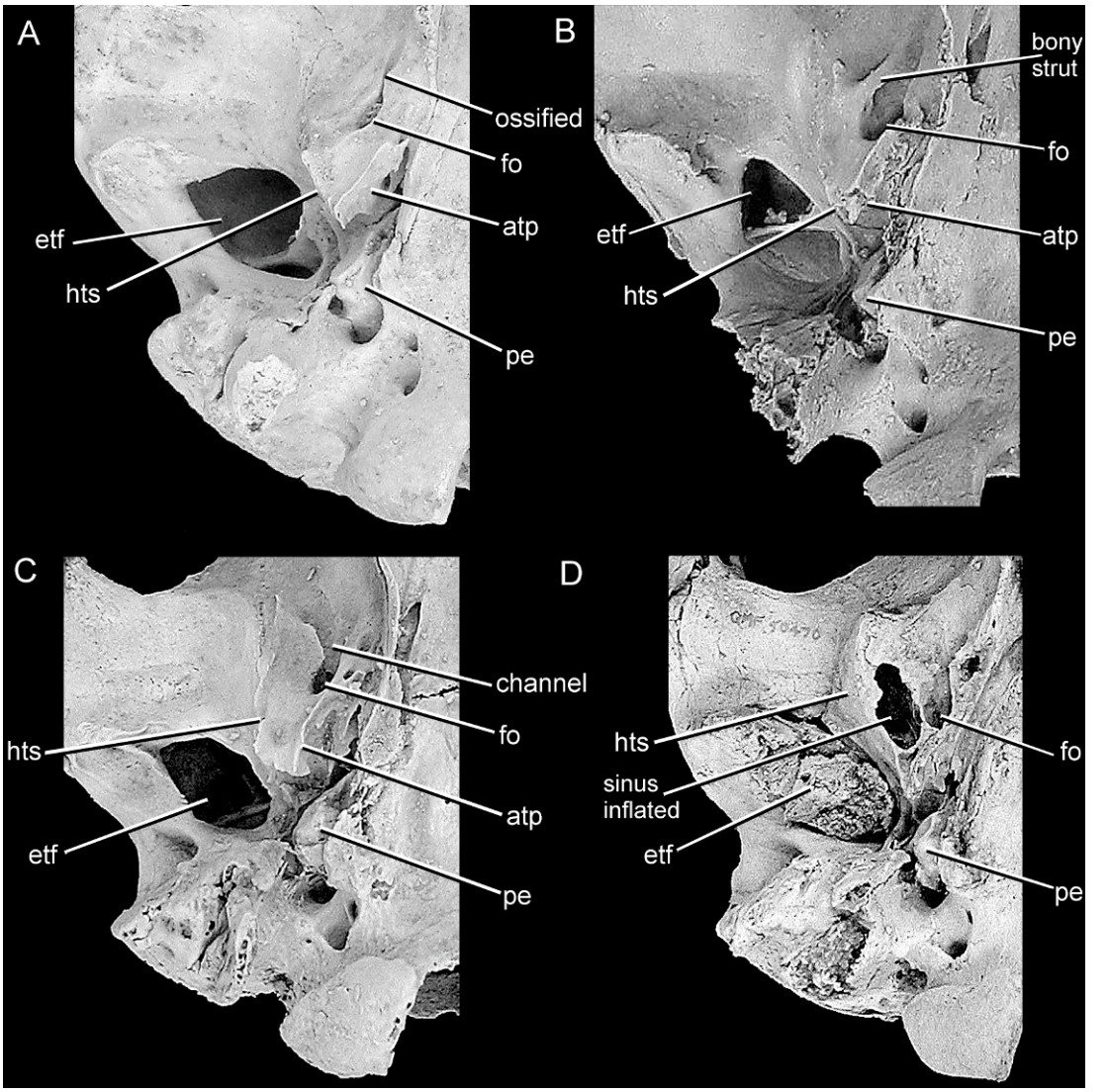

Fig. 17. Variation in *Nimbadon lavarackorum* basicranial structures. **A,** QM F42677; **B,** QM F40345; **C,** QM F53642; **D,** QM F50470. Not to scale.

(fig. 16E′), however, these crests extend beyond the frontoparietal suture, converging 35 mm beyond this point at the dorsal midline of the skull where they become continuous with a well-developed sagittal crest. The frontal/sagittal crests are also present in QM F53645 (fig. 16C′), although the sagittal crest is reduced.

Basicranium: The angle and position of the basicranium relative to the alveolar row is highly variable. QM F40345 and QM F31377 show the basicranium on a plane level [20] with the alveolar row. In QM F53645 and QM F31541, however, the basicranium is elevated [21] relative to the alveolar row. In QM F50470 and QM F31541, the basicranium is downturned relative to the horizontal plane of the skull.

Hypotympanic swelling: In QM F50470 (fig. 17D) and QM F30833 (not figured) the hypotympanic swelling is rounded and sinus

inflated (particularly laterally where it forms the medial border of the glenoid fossa) and hence is very ''bullalike.'' In QM F40345 (fig. 17B) the hypotympanic swelling is relatively flat, nonsinus inflated, but is formed by the thick rugose squamoso-alisphenoid suture and dominated by an alisphenoid tympanic process. The squamosal contribution to the hypotympanic swelling also varies between skulls from 25%–33%, as does the development of the alisphenoid tympanic process, which may be flattened (fig. 17B), channellike (fig. 17A, C), or absent, e.g., QM F53788, wherein the tympanic process is derived from the squamosal.

BASIOCCIPITAL: This is flat in QM F53642 but with a distinct median basioccipital crest, whereas the basioccipital is inflated anteriorly in QM F31541 where it contacts the basisphenoid, and the median basioccipital crest is poorly defined. The degree of development of the basioccipital tympanic process is also variable: in QM F31541, QM F50470, and QM F53645 this process is distinct, anterolaterally extensive, winglike, and rugose, whereas in QM F40345 and QM F42677 it is a less prominent, short, and rugose swelling.

GLENOID REGION: The structure of the postglenoid process varies considerably between skulls. In lateral view, it can be a delicate, elongate structure (fig. 18C) or broad, blunt process (fig. 18D). In QM F53642 (fig. 18A), it is a thin, sinus-inflated structure, which arches laterally, then posteriorly from the anterolateral corner of the epitympanic fenestra. On the left side of QM F53642, the postglenoid process is dominated by a deep, recessed pocket—the postglenoid foramen. On the right side of the skull, however, the postglenoid foramen is smaller and shallower. In QM F31541 (fig. 18B), the postglenoid process is a slightly inflated, roughened nodule that lacks a postglenoid foramen. QM F40345 similarly lacks a postglenoid foramen and the postglenoid process is not inflated or arched, but is dominated by a high, sharp, anterolateral crest. In QM F50470 and QM F30833 it is broadly sinus inflated but lacks any cavity or postglenoid foramen. The glenoid fossa varies between shallow in QM F31541 (fig. 18B) to relatively deep in QM F53642 (fig. 18A).

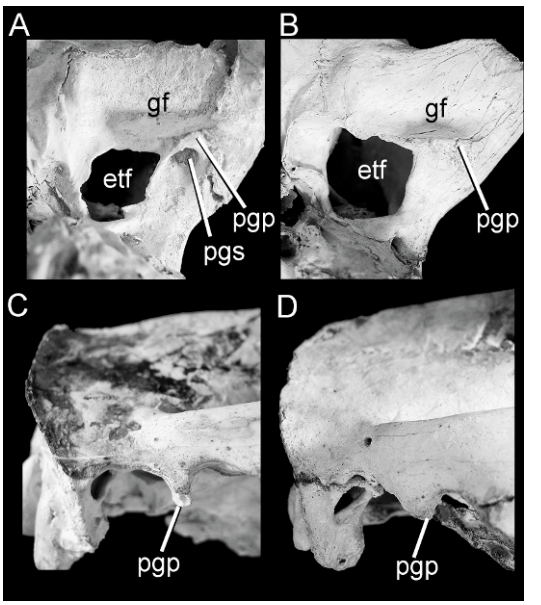

Fig. 18. Representative *Nimbadon lavarackorum* glenoid regions in occlusal (A–B) and lateral (C–D) views. **A,** QM F53642; **B,** QM F31541; **C,** QM F31377; **D,** QM F50470. Not to scale.

POSTERIOR EPITYMPANIC FOSSA: The posterior epitympanic fossa varies in size between skulls, from large and ovate (11 × 5 mm) in QM F53462 (fig. 16A) to moderate and round (6.5 mm diameter) in QM F31377 (fig. 16D) to narrow and slitlike (8 × 3 mm) in QM F31541 (fig. 16F). The size of the posterior epitympanic fossa does not correlate with skull length.

EPITYMPANIC FENESTRA: The epitympanic fenestra varies in size between skulls but is generally moderately large. In QM F31541 (fig. 18B) it is large and square, measuring 16 × 16 mm. In QM F53642 (figs. 17C, 18A), the epitympanic fenestra is obliquely oriented with a maximum width of 14 mm from the posteromedial to the anterolateral corner. In QM F40345 (fig. 17B) it is small, oblique and subovate with a maximum width of 13 mm.

FORAMEN OVALE: There is generally a single foramen ovale in the alisphenoid at the anteromedial base of the hypotympanic swelling. In QM F53642 (fig. 17C) the en-

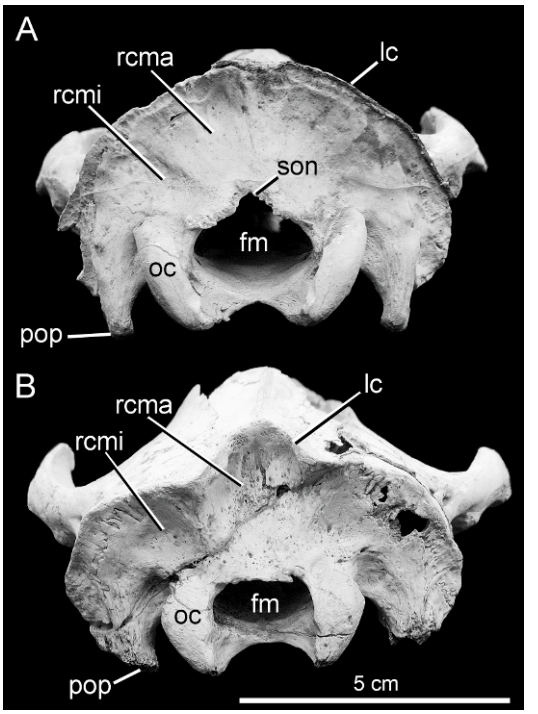

Fig. 19. Representative *Nimbadon lavarackorum* occipital regions. **A,** QM F31377; **B,** QM F31541.

trance to the foramen ovale is broken, but two distinct channels course across the alisphenoid entering the foramen ovale. In QM F30833 these channels are ossified such that two smaller foramina are situated anterolateral and anteromedial to the primary foramen ovale. In QM F42677 (fig. 17A) the area surrounding the foramen ovale is highly ossified. In QM F40345 (fig. 17B) a bony strut from the alisphenoid divides the channel to form what appears to be a secondary foramen ovale confluent with the primary foramen ovale. Wroe et al. (1998) noted similar variation in the position and development of the foramen ovale in pseudocheirid and petaurid possums.

PROMONTORIUM AND ROSTRAL TYMPANIC PROCESS OF THE PETROSAL: The promontorium can be broad and rounded (fig. 20C), more pointed and pyramidal (fig. 20B) or a weak, irregular bulge (fig. 20A). The surface of the promontorium may be either smooth or roughened. The rostral tympanic process (defined by Wible [1990: 188] in marsupials as ''a low crest… from the promontorial surface in front of the fenestra cochleae… [that] runs towards the midline'') varies from distinct (fig. 20C) to indefinite (fig. 20D).

SECONDARY FACIAL FORAMEN: The secondary facial foramen is generally housed within a short groove (the facial nerve canal) that carries the chorda tympani branch of the facial nerve. In some specimens (fig. 20A) the groove is covered by a thin bony lamina resulting in the development of a long canal. In others (fig. 20D) only a thin bony strut extends over the groove.

SUBARCUATE FOSSA: The subarcuate fossa is located on the cerebellar side of the periotic. Its depth and whether it is perforated by a foramen varies considerably between specimens. In QM F53866 (fig. 21D) the subarcuate fossa is perforated by a large foramen, whereas in QM F53848 (fig. 21A) it is shallow and perforated by a small foramen. In QM F53847a (fig. 21B), the subarcuate fossa is moderately deep and lacks a foramen.

OCCIPUT: Morphologically, the occiput is one of the most variable regions of the skull. Two extremes in morphology are represented in figure 19. The lambdoid crest varies between semicircular in dorsal profile in QM F31377 (fig. 19A) and highly convoluted in QM F31541 (fig. 19B), which has a distinct U-shaped notch (9 mm deep) at its midline where it meets the sagittal crest. The areas of muscle insertion vary greatly in depth. The supraoccipital fossa for the rectus capitus major is narrow and deep in QM F31541 (fig. 19B). In QM F50470, the lambdoid crest overhangs the occiput and the rectus capitus major fossa is deeply excavated and rugose.

FORAMEN MAGNUM: Size varies between skulls and does not appear to correlate with the overall size of the skull. For example, in QM F53642 the foramen magnum is broad and high (26 × 18 mm) compared with a shorter, narrower foramen (21 × 15 mm) in QM F53645, which is a larger skull overall. Most foramina magna are subovate in shape, yet in QM F31377 (fig. 19A) there is a distinct dorsal notch resulting in an inverted keyhole shape that appears to be related to the

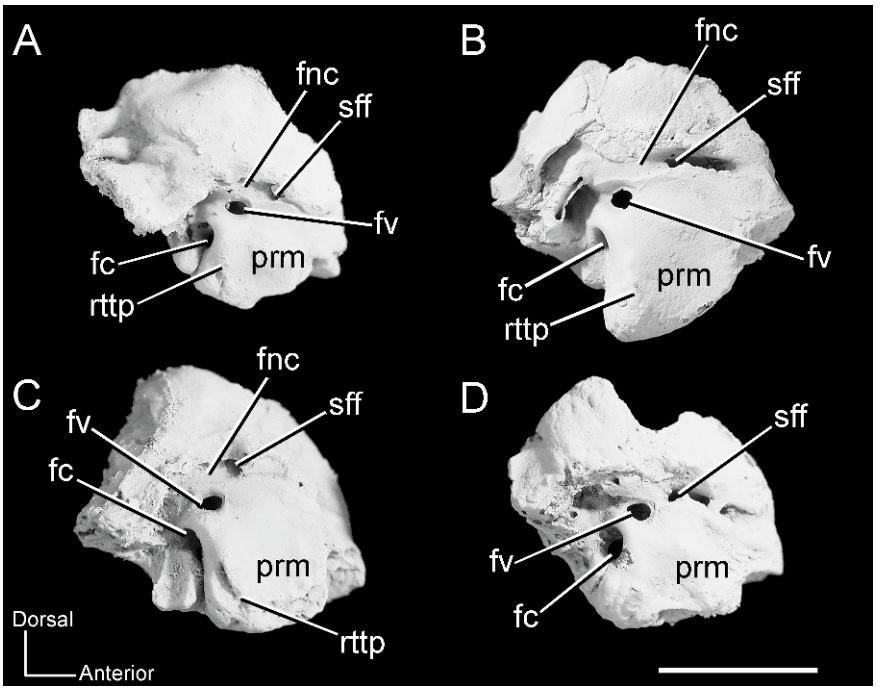

Fig. 20. Variation in the tympanic face of the right periotic of *Nimbadon lavarackorum*. **A,** QM F53848; **B,** QM F53844; **C,** QM F53842; **D,** QM F53846.

incomplete exclusion of the supraoccipital (by the exoccipital) from its dorsal border. This feature is commonly found in juvenile crania of both *Nimbadon lavarackorum* and extant marsupial taxa.

PAROCCIPITAL PROCESS: This may be delicate and mediolaterally compressed (e.g., QM F53642); short, rounded, and stublike (e.g., QM F31541; fig. 19B); or elongate, rounded, and blunt (e.g., QM F31377; fig. 19A).

MANDIBLE

Five adult mandibles were available for study, but few preserve the delicate regions of the ascending ramus, angular and coronoid processes, the articular condyle, and the incisors. Figure 22 shows two of the more complete mandibles available for comparison. Letters in parentheses refer to those in figure 22. The following variation is noted:

CURVATURE OF THE TOOTH ROW: The cheek-tooth row varies between slightly convex in QM F40337 (B) to linear and parallel in QM F53824 (A), where the left and right tooth rows remain 27.0 mm apart along their length, or anteriorly convergent as in QM F30552 (not figured).

DIASTEMAL CREST: The diastemal crest varies between well developed and arcuate (A′), less prominent and more linear (B′), to broadly rounded and noncarinate (QM F30552).

SUBLINGUAL FOSSA: This feature is correlated with the development of the diastemal crest. In specimens with well-developed diastemal crests (A) the sublingual fossa is deep, while specimens with weak diastemal crests exhibit shallow sublingual fossae (B).

DEPTH AND WIDTH OF HORIZONTAL RAMUS: This can vary between narrow and deep (B′), broad and shallow (A′), and broad and deep (QM F30552).

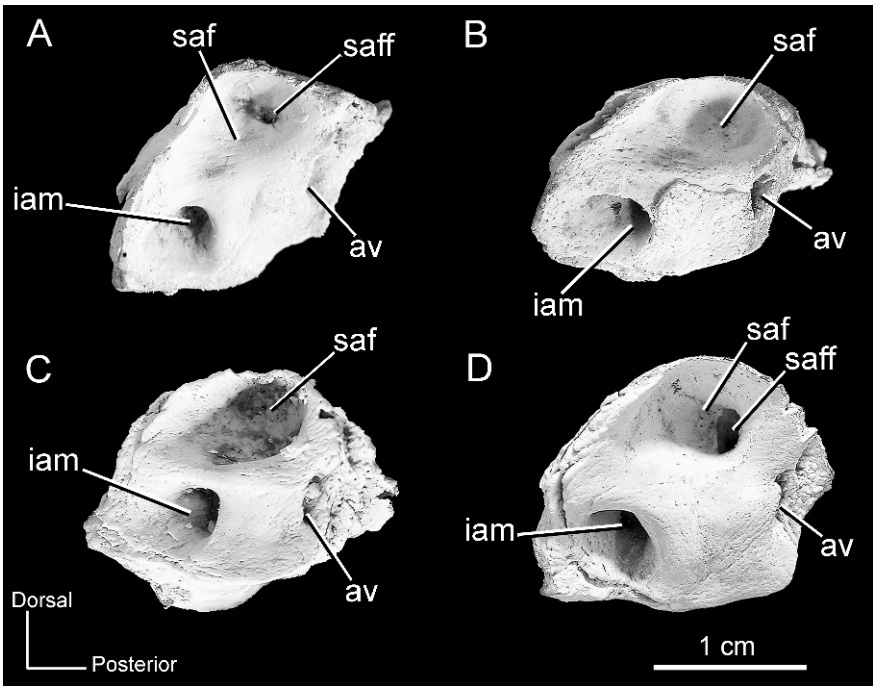

Fig. 21. Variation in the cerebellar face of the right periotic of *Nimbadon lavarackorum*. **A,** QM F53848; **B,** QM F53847; **C,** QM F30904; **D,** QM F53866.

ANGLE OF THE ANTERIOR BORDER OF THE ASCENDING RAMUS: Varies between 70° and 80°, e.g., 70° in QM F30552, 75° in B′, and 80° in A′.

GENIAL PITS: These vary between shallow (QM F53824) to well developed and deep (QM F40337, QM F30552).

HEIGHT OF THE CONDYLE ABOVE OCCLUSAL SURFACE OF TOOTH ROW: In A′ the condyle is positioned 24.5 mm above the occlusal surface of the molar row, whereas it is higher in B′ at 28.8 mm, which is a shorter jaw overall.

LATERAL EXTENT OF THE POSTERIOR MASSETERIC EMINENCE: Most *Nimbadon lavarackorum* dentaries exhibit a moderately flared posterior masseteric eminence that does not extend to the lateral extent of the condyle (B). In some more robust specimens the posterior masseteric eminence extends beyond the lateral extent of the condyle (A).

PTERYGOID FOSSA: The depth of the pterygoid fossa is variable between specimens and does not appear to be related to the overall robustness of the specimen. For example, QM F53824 (A), a relatively robust mandible, has broad, shallow pterygoid fossae, whereas QM F40337 (B), a more gracile mandible, has deeper, narrower, more rugose pterygoid fossae.

POSTALVEOLAR SHELF AND PROCESS: This feature varies between a very well-developed postalveolar shelf and a distinct postalveolar process (A), to a moderate posterolaterally tapering shelf and weaker process (B), but may also exhibit a well-developed, elongate shelf that tapers posterolaterally but possesses a weak postalveolar process (QM F30552).

MASSETERIC FOSSA: The depth of the masseteric fossa varies between specimens. In A′ and QM F40338, the massteric fossa is deep with distinct anterior and ventral borders. In B′ the fossa is shallower with less well-defined borders such that it attenuates anteriorly onto the horizontal ramus.

POSITION AND SIZE OF THE MENTAL FORAMEN: The mental foramen is large (4.3 mm diameter) in QM F53824 and small (2.5 mm

diameter) in QM F40337. The presence and position of the secondary mental foramen is highly variable. QM F30552 lacks a secondary mental foramen. In QM F40337 the secondary mental foramen is situated 4 mm posterior to the mental foramen. In QM F53824 the position of the secondary mental foramen varies on each dentary. On the left dentary it is within the medial wall of the primary mental foramen, whereas on the right dentary it is situated 1.0 mm posterodorsal to the primary mental foramen.

ANTEROPOSTERIOR WIDTH OF THE MANDIBULAR NOTCH: Width is 17.2 mm in QM F40338, 21.1 mm in B′, and 24.5 mm in A′.

MASSETERIC FORAMEN: This is present (albeit very small) in some specimens but absent in most. In QM F40337, a fused mandible, the left dentary lacks a masseteric foramen, but the right dentary has a small foramen.

DISCUSSION

The cranial material of *Nimbadon lavarackorum* described here is the most abundant, exceptionally preserved fossil material known for any marsupial species from the Oligo-Miocene sediments of the Riversleigh World Heritage Area, Australia. *Nimbadon lavarackorum* was originally described on the basis of a maxillary fragment, a partial dentary, and isolated teeth, but is now known from complete crania (representing pouch young through to aged adults) and all elements of its postcranial skeleton. The AL90 *N. lavarackorum* sample has enabled a comprehensive assessment of the level of cranial and dental variation that might be expected within a fossil marsupial species from a single locality, thus forming a benchmark for discriminating species boundaries in fossil marsupial taxa.

Nimbadon lavarackorum crania are characterized by: a broad, short rostrum; a dorsolaterally inflated premaxilla; a small lacrimal foramen; a slender, moderately elongate masseteric process; a sphenopalatine foramen that is greatly separated from the infraorbital canal; a low-crowned dentition; and P3 with a small parastyle and (variably present) hypocone and undifferentiated parametacone. The P3 features are considered plesiomorphic for Zygomaturinae (Stirton, 1967; Black and Archer, 1997; Murray et al., 2000a, 2000b). Features of the basicranium that further support a plesiomorphic position for *Nimbadon* within Zygomaturinae include: weakly developed postglenoid processes; large epitympanic fenestrae; and short alisphenoid tympanic processes. In combination, these features result in a ventrally open tympanic cavity. Murray et al. (2000a, 2000b) document a progressive structural change from the open tympanic cavity of plesiomorphic zygomaturines such as the late Oligocene *Silvabestius johnnilandi* Black and Archer, 1997, to the highly derived, completely floored tympanic cavity of the Pleistocene *Zygomaturus trilobus* Macleay, 1858, through expansion and fusion of the alisphenoid, postglenoid, and mastoid processes across the tympanic cavity and the subsequent reduction of the epitympanic fenestra.

Within Zygomaturinae, *Nimbadon lavarackorum* appears most similar to species of the plesiomorphic genus *Silvabestius* that are known to date only from the Riversleigh World Heritage Area. Black and Archer (1997) found a number of similarities in the dentitions of *Silvabestius* and *Nimbadon* species including: a P3 with an undifferentiated parametacone, small parastyle, and absent to small hypocone; a P3 that is shorter than M1; and rectangular molars in occlusal view. The subsequent discovery and study of skulls representing species of both genera has revealed a number of cranial similarities also, but most of these appear to be symplesiomorphic for Zygomaturinae (Black, 2008). These include: a mildly inflated hypotympanic swelling; a grooved, winglike ventral alisphenoid tympanic process; a weak suborbital shelf; a large epitympanic fenestra; an incomplete tympanic floor; nasals that are not retracted beyond the incisor arcade; a mediolaterally aligned glenoid fossa; short postglenoid processes; posteriorly shallow zygomatic arches; and I1s with convergent tips.

Previous authors (e.g., Murray, 1990b; Hand et al., 1993) suggested a close relationship between species of *Nimbadon* and the late

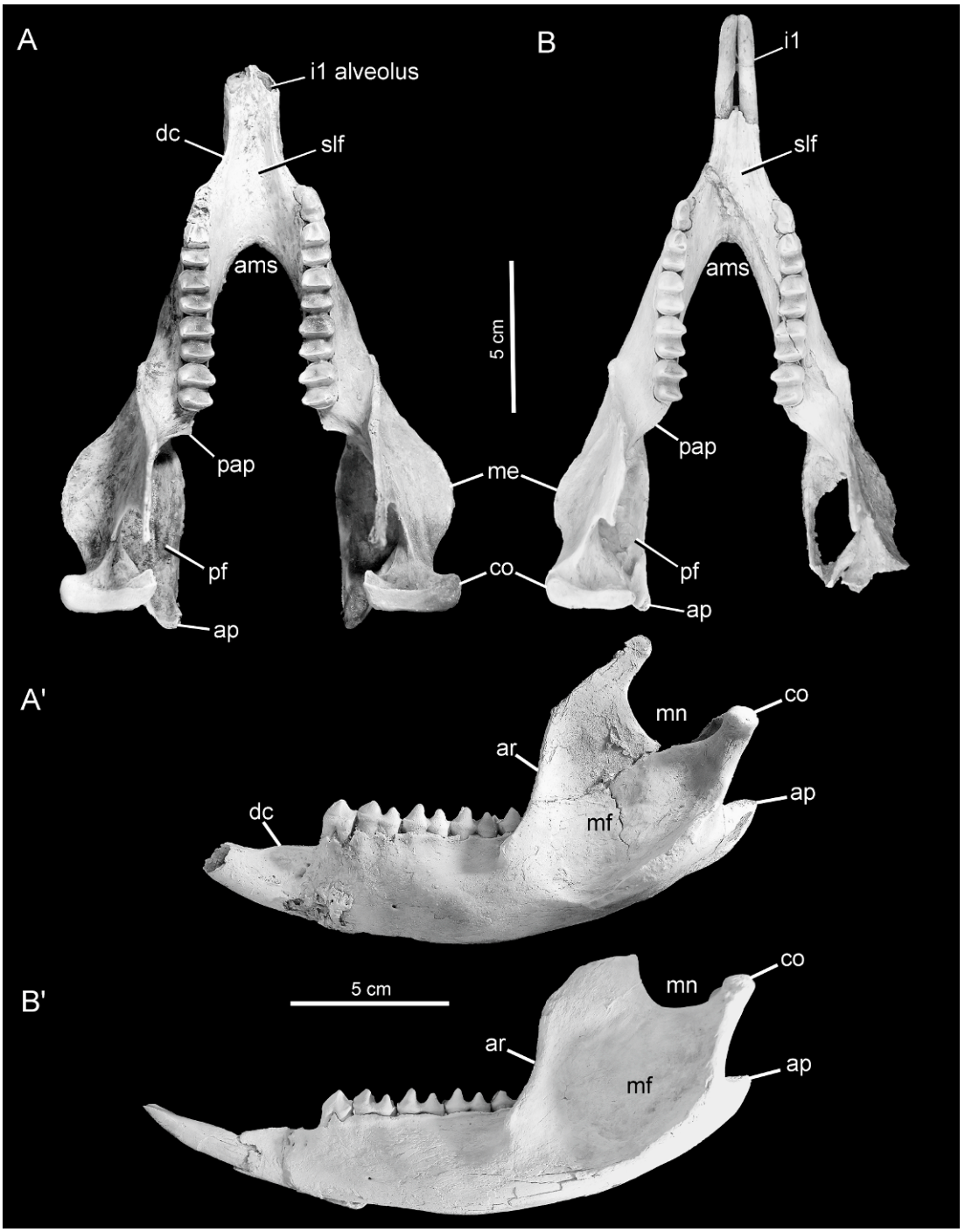

Fig. 22. Variation in the *Nimbadon lavarackorum* mandible. **A–A′,** QM F53824; **B–B′,** QM F40337.

Miocene *Plaisiodon centralis* Woodburne, 1967, known from abundant cranial and postcranial material from the Alcoota local fauna, Northern Territory (Murray, 1997). This apparent affinity was based on the shared presence of a hooked parastyle on P3. Here we have found that this feature is highly variable in *Nimbadon lavarackorum*, and sometimes expressed in species of *Neohelos*, making its phylogenetic utility questionable.

VARIABILITY, SPECIES BOUNDARIES, AND SEXUAL DIMORPHISM: Results of the metric analyses (appendix 2A–B; figs. 12–3) indicate that the *Nimbadon lavarackorum* craniodental material from AL90 represents a single, normally distributed population, with coefficients of variation for dental and craniomandibular dimensions generally falling within the expected range (i.e., 4–10) for a homogenous mixed-sex population (Simpson et al., 1960). In general, *N. lavarackorum* craniomandibular dimensions showed greater variation than dental dimensions with 10 of the 45 craniomandibular variables expressing coefficients of variation greater than 10 (appendix 2B), while none of the 28 dental variables exceeded 10 (appendix 2A). This result is consistent with other studies of marsupial craniodental variation (e.g., Archer and Dawson, 1982, *Thylacoleo carnifex*; Martin, 2005, *Lestodelphys halli*; Price, 2008, *Diprotodon optatum*) and may be attributed to sexual dimorphism and/or age-related variation in cranial morphology.

The lowest coefficients of variation for the *Nimbadon lavarackorum* cranium were obtained for basicranial length (3.8, $N = 6$), skull length (3.8, $N = 7$), upper tooth row length (4.0, $N = 8$), and facial cranium length (4.3, $N=6$). Ontogenetic study of the *N. lavarackorum* cranium indicate basicranium and facial cranium lengths grow isometrically with skull length, maintaining proportions of approximately 46% and 54%, respectively, of total skull length throughout ontogeny (Black et al., in press). It is therefore not surprising that such a consistent proportional relationship would be reflected in low coefficients of variation for these variables. Similarly, CVs for individual teeth are generally low, so CVs for toothrow lengths should also be low.

Morphologically, the occipital region was one of the most variable regions of the skull, which is reflected in the high CVs for foramen magnum height (15.1, $N = 7$), foramen magnum width (10.6, $N = 7$), and occiput height (10.7, $N = 7$). The general form of the lambdoid crest varies between semicircular in dorsal profile (fig. 19A) to highly convoluted (fig. 19B), which accounts for a proportion of the variation in occiput height. Similarly, a proportion of the variation in both foramen magnum height and occiput height can be explained by the presence in some specimens of a supraoccipital notch (fig. 19A). This appears to be retained from the juvenile condition in which the incomplete exclusion of the supraoccipital from the dorsal border of the foramen magnum by the exoccipital results in the development of a dorsal notch, giving the foramen magnum an inverted keyhole-shaped outline.

The dimensions of the parietals vary greatly between skulls, and are reflected in the high CVs for both length (13.8, $N = 4$) and width (11.2, $N = 6$). Parietal length could be measured for only four adult specimens, but there may be a general trend of increasing parietal length with increasing skull length. Parietal width, however, is not correlated with skull length but rather may be related to the degree of development of endocranial sinuses and the extent to which the squamosals overlap the parietals at their juncture (Black et al., in press).

Other areas of the cranium subject to a high degree of intraspecific variation include the development of the postglenoid, postorbital, masseteric, and paroccipital processes, and the frontal, pharyngeal, and sagittal crests. No doubt, by analogy with extant marsupial taxa, a proportion of this variation is both age and sex related, with older individuals and males exhibiting better-developed processes and crests (Jones, 1924). In the basicranium, the shape and dimensions of the epitympanic fenestra (figs. 17–18) and posterior epitympanic fossa (fig. 16) vary greatly and are unrelated to overall skull size. The structure of the foramen ovale (fig. 17) and petrosal (figs. 20–21), the relative contributions of the squamosal and alisphenoid to the tympanic

bulla, and the degree to which the bulla is sinus inflated, are all highly variable, as is the overall angle and position of the basicranium relative to the tooth row (fig. 16). In the glenoid region, the postglenoid processes vary between broad and blunt (fig. 18D) to more delicate and elongate structures (fig. 18C) that are variably sinus inflated and sometimes perforated by a postglenoid foramen (fig. 18A).

In the mandible, features variable in size with CVs greater than expected for a single population include: symphysis length (13.2, $N = 3$); the width of the dentary below m3 (10.6, $N = 8$); and the maximum width from the masseteric eminence to the angular process (13.1, $N = 5$). Variation within symphysis length appears to be age related with the mandibular symphysis continuing to ossify into adulthood (Black et al., in press). Extreme variation in the development of the masseteric eminence and angular process is evident in figure 22A–B and may be indicative of sexual dimorphism. Mandible A, which shows a broad lateral flare of the masseteric eminence and an angular process that extends posteriorly well beyond the level of the condyle in occlusal view, may represent a male of the species (see below). Mandible B, however, is more gracile overall, with a much-reduced masseteric eminence and a less posteriorly extensive angular process, and may represent a female of the species. The width of the dentary opposite m3 is related to the degree of convexity of its lateral border, with a more convex border resulting in a wider dentary. Mandible A (fig. 22) shows a bulge in the lateral border of the dentary opposite m3, whereas in mandible B the lateral border is relatively linear in occlusal profile, resulting in a narrower dentary overall.

In the dentition, dimensions of the M3 were found to vary least while dimensions of the p3 were found to vary most. In terms of morphological variation, however, the upper third premolar exhibited extreme differences in the relative development of cingula, cusps, and associated crests (figs. 14A–L, 15A–D). Surprisingly, this variation is not reflected in the results of the metric analysis, with CVs for P3 dimensions ranging between 5.6 ($N = 28$) and 5.7 ($N = 29$). In a similar study, Price (2008) morphometrically analyzed more than 1000 *Diprotodon optatum* teeth and noted considerable variation in P3 morphology yet, as in this study, the variation was not reflected in high coefficients of variation.

Bivariate plots (fig. 12A–H) of tooth dimensions show that *Nimbadon lavarackorum* specimens from other Riversleigh Faunal Zone C deposits fall within the range of variation displayed by the AL90 population and, for P3 dimensions in particular, tightly cluster with them.

The variability of the *Nimbadon lavarackorum* AL90 sample, both in size and morphology, raises doubt about the specific distinction of *N. whitelawi* from the Bullock Creek local fauna, Northern Territory. *Nimbadon whitelawi* is known from a single palate (NMV P186506) that preserves the left P3, M1 and partial M2, and the right P3, M1–3, and partial M4. As noted by Hand et al. (1993) in their original description of the holotype, all teeth (except for the left P3) are damaged and measurements of the width of the right P3, the anterior width of M1 (M2 their terminology), and the posterior width of M2 (M3 by their terminology) were estimated. Analysis of figure 12A shows that the *N. whitelawi* P3 falls within the centre of the AL90 *N. lavarackorum* cluster, its dimensions (12.9 mm $\times$ 10.4 mm) differing little from the *N. lavarackorum* mean values (12.6 mm $\times$ 10.4 mm) for premolar length and width. In fact, there are only two dimensions for *N. whitelawi*, M1 anterior width and M2 posterior width, that fall outside the range of measurements for *N. lavarackorum* from AL90, and both of these dimensions were estimated by Hand et al. (1993) because the specimen was incomplete. Figures 12B–D show *N. whitelawi* separate from the main cluster based on a narrower first upper molar. No doubt, a larger sample of *N. whitelawi* specimens from Bullock Creek would reflect a greater overlap of range in dimensions with *N. lavarackorum* material from Riversleigh. Hand et al. (1993) list one other diagnostic feature that distinguishes *N. whitelawi* from the similarly sized type species *N. lavarackorum*: a more anteriorly positioned swelling on the buccal margin of P3. It is

evident from figure 14 that the buccal margin of the *N. lavarackorum* P3 takes many forms depending on the degree of emargination between the anterior and posterior tooth moieties (characters 1, 2), the length of the anterior parastylar shelf relative to total premolar length (3, 4), and the degree of cingulum (23, 24) and mesostyle (25) development. The more anteriorly positioned swelling on the buccal P3 margin of *N. whitelawi* may have appeared as a significant specific difference from *N. lavarackorum* at the time of naming because only two premolars were known for *N. lavarackorum*. However, the AL90 *N. lavarackorum* sample suggests these differences fall within the bounds of intraspecific variation and, consequently, *N. whitelawi* should be regarded as a junior synonym of *N. lavarackorum*.

Black (1997) referred to a possible new, unnamed species of *Nimbadon* (*Nimbadon* sp.), also from AL90 site. Black (1997) noted that although it was similar to *N. lavarackorum* in size, molar morphology, and cranial profile, certain differences in upper premolar morphology suggested it was more plesiomorphic than *N. lavarackorum*. The single skull referred to by Black (1997) was the first of the AL90 skulls to be processed. It is now evident by comparison with subsequent crania that the specimen is undoubtedly *N. lavarackorum* and that the presumed plesiomorphic P3 (fig. 14E) is a result of a combination of commonly variable features such as a reduced parastyle, absent hypocone, and reduced posterobuccal cingulum.

Figures 13A–H show bivariate plots of select *Nimbadon lavarackorum* cranial dimensions plotted against skull length. Results are limited by the small sample size, but some trends are evident and tend to be allometric in nature. Larger skulls tend to be broader both across the zygomatic arch and the occiput, have longer masseteric processes, and a longer rostrum and tooth row (fig. 13A–D). There does not appear to be any correlation between skull length and rostrum width, rostrum height, cranial height (at frontoparietal suture), or occiput height (fig. 13E–H).

Comparison of coefficients of variation for *Neohelos stirtoni* and *N. lavarackorum* suggest *Neohelos stirtoni* is a more variable species in terms of craniomandibular dimensions. Thirteen of the 22 craniomandibular variables analyzed for *Neohelos stirtoni* had CVs greater than expected for a normal population (appendix 2C) compared with only six variables in *Nimbadon lavarackorum* (appendix 2B). Four variables (FMH, FMW, OCH, SL) had CVs greater than 10 in both taxa, a result that suggests these features are inherently variable across species and may be partially age related. Other dimensions found to be highly variable in *Neohelos stirtoni* include skull length and maximum width, nasal length, masseteric process length, upper and lower diastema lengths, the width of the orbit, the depth of the horizontal ramus below m1, and the anteroposterior width of the articular condyle. Murray et al. (2000b) found extreme variation in *Neohelos stirtoni* cranial shape, sagittal crest development, rostrum shape, zygomatic arch depth, the angle of the anterior border of the ascending ramus, and the morphology of P3. All of these features vary in *N. lavarackorum* also, although to a somewhat lesser extent with the exception of P3 morphology, which shows extreme variation in both taxa.

Determining the degree to which variation can be attributed to sexual dimorphism is difficult in fossil populations with a limited cranial sample and in the absence of gender and age data. Clarification requires a larger cranial sample. Bivariate plots of skull length plotted against maximum skull width may indicate a bimodal (fig. 13A) distribution. It is interesting to note, however, that the larger of the adult *Nimbadon lavarackorum* skulls available for study (QM F53645 and QM F50470) show the least amount of tooth wear and the smaller adult skulls (QM F53642 and QM F40345) show the most. This may suggest that age is not a factor in determining skull size and that perhaps sexual dimorphism plays a greater role. Figure 23 shows large (A–A′) and small (B–B′) *N. lavarackorum* cranial variants that may represent a male and female of the species, respectively. The larger skull (QM F50470) possesses a number of traits that are characteristic of male crania in sexually dimorphic extant marsupial species (Jones,

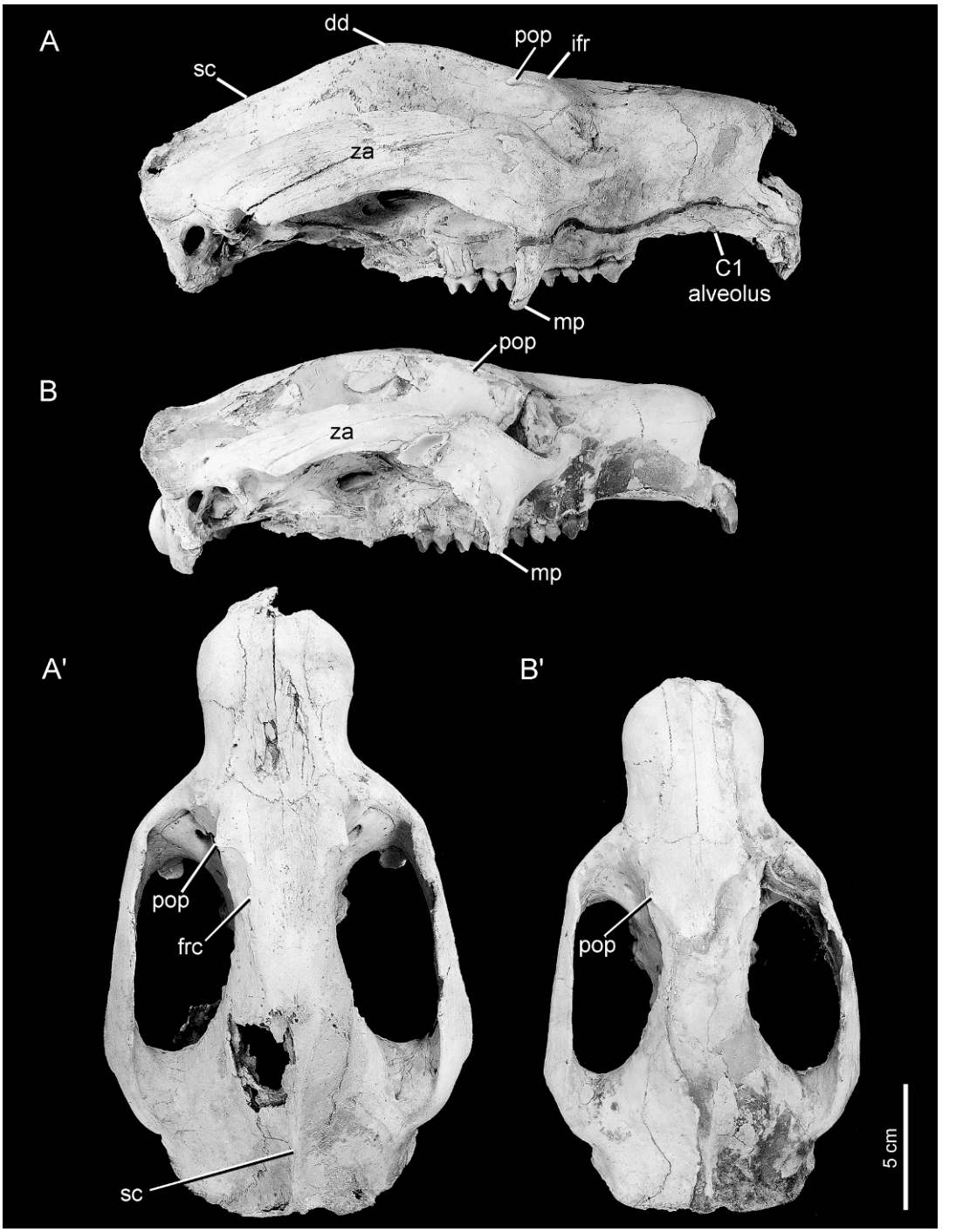

Fig. 23. Possible sexual dimorphism in *Nimbadon lavarackorum* crania: **A,** lateral and **A′,** dorsal views of ?male (QM F50470); and **B,** lateral and **B′,** dorsal views of ?female (QM F31377).

1924). These include: strong development of frontal and sagittal crests and the postorbital process; a deep cranium; inflated frontals; deep zygoma; elongate masseteric processes that extend well below the level of the tooth row; a bulbous flaring rostrum; and the presence of canines. In the mandible, variation that may be attributed to sexual dimorphism and consistent with a male of the species includes: a deeper, wider dentary; a large flaring masseteric eminence; and a wider angle at the posterior symphysis between the left and right dentaries of the mandible (fig. 22).

PALEOECOLOGY AND BIOCHRONOLOGY: If *Nimbadon lavarackorum* is sexually dimorphic, the relative difference in body size between males and females of this species is nowhere near that displayed by *Neohelos stirtoni*. Murray et al. (2000b) suggested that male *Ne. stirtoni* crania are 25%–50% larger than female crania. The largest *N. lavarackorum* skull is 12% longer and 20% wider than the smallest skull. That *N. lavarackorum* is a more homomorphic species than *Ne. stirtoni* is no doubt a consequence of a number of factors including relative body size, home range, and habitat preference and stability. Jarman (1989) found a strong correlation between body size and sexual dimorphism in extant kangaroos, with larger species tending to be more sexually dimorphic than smaller species. Hence, by analogy with extant taxa, we would expect the smaller zygomaturine species, *N. lavarackorum*, to be less dimorphic than its larger counterpart *Ne. stirtoni*. Species of the genus *Neohelos* have the largest geographic and temporal range of any Oligo-Miocene zygomaturine and are recorded from central Australia, the Northern Territory, and northwestern Queensland in deposits of late Oligocene through to early late Miocene age (Black, 1997; Murray et al., 2000a, 2000b). *Neohelos stirtoni* is known from a diverse range of paleohabitats including: the rainforest/closed forest Gag Site and open forest Henk's Hollow local faunas of Riversleigh (Archer et al., 1997; Travouillon et al., 2009); and the grassland and scrubland communities of Bullock Creek (Murray and Megirian, 1992). Murray et al. (2000b) suggest that this wide-ranging species, with limited niche constraints, correspondingly had minimal morphological constraints. The smaller *N. lavarackorum*, however, although contemporaneous with *Ne. stirtoni* at Bullock Creek and Riversleigh's Faunal Zone C Gag and Henk's Hollow sites, may have been restricted to more closed forest/open forest habitats within this range. Certainly at Bullock Creek it is a rare element in the fauna, currently known from a single specimen from the Horseshoe West Locality. This rarity does not appear to be an artifact of insufficient sampling (D. Megirian, personal commun.), but rather may suggest that this specimen is from a community distant to the depositional setting of the *Ne. stirtoni* population. This, in combination with its low-crowned browsing dentition, could suggest that *N. lavarackorum* belonged to a more distant open forest community than the Bullock Creek *Ne. stirtoni* population.

Based on the relative abundance of *Nimbadon lavarackorum* fossil material and a preliminary analysis of the postcranial skeleton, *N. lavarackorum* was most probably a gregarious, digitigrade, sheep-sized browser. Using Anderson et al.'s (1985) equation for predicting vertebrate body weight based on the circumference of the shaft of the humerus and femur, adult *N. lavarackorum* weighed between 75 kg and 120 kg. The postcranial skeleton of *N. lavarackorum* is similar in size and morphology to the late Oligocene diprotodontid *Ngapakaldia tedfordi* Stirton, 1967, currently known from the Ngapakaldi fauna of the Etadunna Formation, South Australia, which is one of the most generalized, plesiomorphic diprotodontids. *Nimbadon lavarackorum* differs from *Ngapakaldia tedfordi* in having a shorter tail and a larger manus and pes with more massive, laterally compressed unguals. Munson (1992) suggested *Ngapakaldia tedfordi* used its powerful forelimbs and large claws for stripping tree branches or uprooting bushes for tubers and roots. The postcranial skeleton of *N. lavarackorum* suggests a similar niche, although its relatively low-crowned dentition would rule out a diet of coarse vegetative material.

Nimbadon lavarackorum is known from several of Riversleigh's Faunal Zone C (mid-

dle Miocene) assemblages and, more recently, was recovered from the Cleft of Ages local fauna, which was previously regarded to be of uncertain age (Creaser, 1997; Archer et al., 1997). Travouillon et al. (2006) interpreted the Cleft of Ages local fauna to be a Faunal Zone C deposit because it consistently grouped with putative Faunal Zone C deposits such as Gag Site and Henk's Hollow Site on the basis of faunal composition. The presence of *N. lavarackorum* in the Cleft of Ages assemblage further supports a Faunal Zone C age for this deposit.

The faunal correlation between Riversleigh's low to mid Faunal Zone C assemblages and the middle Miocene Bullock Creek local fauna, Northern Territory (Archer et al., 1997; Black, 1997, 2006) is further strengthened by the presence of *Nimbadon lavarackorum* in both deposits. Additional shared diprotodontoid taxa include *Propalorchestes novaculacephalus* Murray, 1986 (Murray, 1990a; Black, 1997, 2006), and *Neohelos stirtoni* (Murray et al., 2000b).

Although *Nimbadon lavarackorum* is a useful marker species for Riversleigh's Faunal Zone C deposits, its presence in middle Miocene assemblages is somewhat of an anomaly. Considering its plesiomorphic position within Zygomaturinae a more basal position within the Riversleigh stratigraphic sequence might be expected. *Nimbadon lavarackorum* is unique among mid Miocene diprotodontids in its small stature, defying the general trend evident in other diprotodontid species of increasing body size over time. *Nimbadon lavarackorum* probably represents a relict species that diverged early from the zygomaturine radiation and may have been restricted to refugial closed-forest habitats.

ACKNOWLEDGMENTS

We thank M. Archer, H. Godthelp, P. Murray, B. Cooke, and E. Lundelius for their useful comments and A. Gillespie, R. Arena, K. Travouillon, G. Price, A. Camens, and R. Beck for information and assistance; and P. Creaser, Lizard (C. Cannell), B. Cooke, A. Rackham, and S. Williams for assistance in the field. Access to comparative specimens was kindly provided by D. Megirian and G. Dally from the Museum and Art Galleries of the Northern Territory, and D. Henry from the National Museum of Victoria. Financial support for Riversleigh research has been provided by the Australian Research Council grants to M. Archer and S.J. Hand, Queensland Parks and Wildlife Service, the Queensland Museum, the University of New South Wales, Xstrata Copper, and Phil Creaser and the CREATE Fund.

REFERENCES

Anderson, J.F., A. Hall-Martin, and D.A. Russell. 1985. Long-bone circumference and weight in mammals, birds and dinosaurs. Journal of Zoology (London) Series A 207: 53–61.

Aplin, K.P. 1987. Basicranial anatomy of the early Miocene diprotodontian *Wynyardia bassiana* (Marsupialia: Wynyardiidae) and its implications for wynyardiid phylogeny and classification. *In* M. Archer (editor), Possums and opossums: studies in evolution: 369–391. Sydney: Surrey Beatty.

Aplin, K.P., and M. Archer. 1987. Recent advances in marsupial systematics with a new syncretic classification. *In* M. Archer (editor), Possums and opossums: studies in evolution: xv–lxxii. Sydney: Surrey Beatty.

Archer, M. 1976. The basicranial region of marsupi-carnivores (Marsupialia), interrelationships of carnivorous marsupials, and affinities of the insectivorous peramelids. Zoological Journal of the Linnean Society 59: 217–322.

Archer, M. 1984. The Australian marsupial radiation. *In* M. Archer and G. Clayton (editors), Vertebrate zoogeography and evolution in Australasia: 634–808. Perth: Hesperian Press.

Archer, M., and L. Dawson. 1982. Revision of marsupial lions of the genus *Thylacoleo* Gervais (Thylacoleonidae, Marsupialia) and thylacoleonid evolution in the late Cainozoic. *In* M. Archer (editor), Carnivorous marsupials: 477–494. Sydney: Royal Zoological Society of New South Wales.

Archer, M., H. Godthelp, S.J. Hand, and D. Megirian. 1989. Fossil mammals of Riversleigh, northwestern Queensland: preliminary overview of biostratigraphy, correlation and environmental change. Australian Zoologist 25: 29–65.

Archer, M., S.J. Hand, and H. Godthelp. 1991. Riversleigh: the story of animals in ancient

rainforests of inland Australia. Sydney: Reed Books.

Archer, M., S.J. Hand, H. Godthelp, and P. Creaser. 1997. Correlation of the Cainozoic sediments of the Riversleigh World Heritage fossil property, Queensland, Australia. *In* J.-P. Aguilar, S. Legendre and J. Michaux (editors), Actes du Congrès BiochroM '97. Mémoirs et Travaux de l'École Pratique des Hautes Études, Institut de Montpellier 21: 131–152.

Arena, D. 2005. The geological history and development of the terrain at the Riversleigh World Heritage Area during the middle Tertiary. Ph.D. thesis, University of New South Wales.

Arena, D., and K. Black. 1997. An early-mid Miocene cave deposit at Riversleigh. Conference on Australian Vertebrate Evolution, Palaeontology and Systematics, July 2007, Sydney. Abstracts: 10–11.

Black, K. 1997. Diversity and biostratigraphy of the Diprotodontoidea of Riversleigh, northwestern Queensland. Memoirs of the Queensland Museum 41: 187–92.

Black, K. 2006. Description of new material for *Propalorchestes novaculacephalus* (Marsupialia: Palorchestidae) from the mid Miocene of Riversleigh, northwestern Queensland. Alcheringa 30: 351–361.

Black, K. 2008. Diversity, phylogeny, and biostratigraphy of diprotodontoids (Marsupialia: Diprotodontidae, Palorchestidae) from the Riversleigh World Heritage Area. Ph.D. thesis, University of New South Wales.

Black, K., and M. Archer. 1997. *Silvabestius* gen. nov., a primitive zygomaturine (Marsupialia, Diprotodontidae) from Riversleigh, northwestern Queensland. Memoirs of the Queensland Museum 41: 193–208.

Black, K., M. Archer, S.J. Hand, and H. Godthelp. In press. First comprehensive analysis of cranial ontogeny in a fossil marsupial – from a 15 million-year-old cave deposit in northern Australia. Journal of Vertebrate Paleontology

Creaser, P. 1997. Oligo-Miocene sediments of Riversleigh: the potential significance of topography. Memoirs of the Queensland Museum 41: 303–314.

Crosby, K., and C.A. Norris. 2003. Periotic morphology in the Trichosurin possums *Strigocuscus celebensis* and *Wyulda squamicaudata* (Diprotodontia, Phalangeridae) and a revised diagnosis of the tribe Trichosurini. American Museum Novitates 3414: 1–14.

Flannery, T.F. 1992. New Pleistocene marsupials (Macropodidae, Diprotodontidae) from subalpine habitats in Irian Jaya, Indonesia. Alcheringa 16: 321–331.

Flannery, T.F., and M. Plane. 1986. A new Late Pleistocene diprotodontid (Marsupialia) from Pureni, Southern Highlands Province, Papua New Guinea. Bulletin of the Bureau of Mineral Resources Geology and Geophysics (Australia) 10: 65–76.

Hammer, Ø., D.A.T. Harper, and P.D. Ryan. 2006. Palaeontological statistics (PAST). Version 1.51 (available at: http://folk.uio.no/ohammer/past/).

Hand, S.J., M. Archer, H. Godthelp, T.H. Rich, and N.S. Pledge. 1993. *Nimbadon*, a new genus and three new species of Tertiary zygomaturines (Marsupialia: Diprotodontidae) from northern Australia, with a reassessment of *Neohelos*. Memoirs of the Queensland Museum 33: 193–210.

Hand, S.J., and J.A.W. Kirsch. 2003. *Archerops*, a new annectent hipposiderid genus (Mammalia: Microchiroptera) from the Australian Miocene. Journal of Paleontology 77(6): 1139–1151.

Jarman, P.J. 1989. Sexual dimorphism in Macropodoidea. *In* G. Grigg, P. Jarman and I. Hume (editors), Kangaroos, wallabies and rat-kangaroos: 432–447. Sydney: Surrey Beatty.

Jones, F.W. 1924. The mammals of South Australia. Adelaide: Government Printer, 3 vols.

Luckett, W.P. 1993. An ontogenetic assessment of dental homologies in therian mammals. *In* F. Szalay, M.J. Novacek and M.C. McKenna (editors), Mammal phylogeny: Mesozoic differentiation, multituberculates, monotremes, early therians, and marsupials: 182–204. New York: Springer.

Martin, G.M. 2005. Intraspecific variation in *Lestodelphys halli* (Marsupialia: Didelphimorphia). Journal of Mammalogy 86: 793–802.

Munson, C.J. 1992. Postcranial descriptions of *Ilaria* and *Ngapakaldia* (Vombatiformes, Marsupialia) and the phylogeny of the Vombatiforms based on postcranial morphology. University of California Publications in Zoology 125: 1–99.

Murray, P. 1990a. Primitive marsupial tapirs (*Propalorchestes novaculacephalus* Murray and *P. ponticulus* sp. nov.) from the mid-Miocene of north Australia (Marsupialia: Palorchestidae). Beagle 7: 39–51.

Murray, P. 1990b. *Alkwertatherium webbi*, a new zygomaturine genus and species from the late Miocene Alcoota local fauna, Northern Territory (Marsupialia: Diprotodontidae). Beagle 7: 53–80.

Murray, P. 1997. Alcoota: a snapshot of the Australian late Miocene. Riversleigh Notes 35: 2–7.

Murray, P., and D. Megirian. 1992. Continuity and contrast in Middle and Late Miocene vertebrate communities from the Northern Territory. Beagle 9: 195–218.

Murray, P., D. Megirian, T. Rich, M. Plane, K. Black, M. Archer, S. Hand, and P. Vickers-Rich. 2000a. Morphology, systematics and evolution of the marsupial genus *Neohelos* Stirton (Diprotodontidae, Zygomaturinae). Museums and Art Galleries of the Northern Territory Research Report 6: 1–141.

Murray, P., D. Megirian, T. Rich, M. Plane, and P. Vickers-Rich. 2000b. *Neohelos stirtoni*, a new species of Zygomaturinae (Diprotodonta: Marsupialia) from the mid-Tertiary of the Northern Territory, Australia. Records of the Queen Victoria Museum 105: 1–47.

Plane, M. 1967. Two new diprotodontids from the Pliocene Otibanda Formation, New Guinea. *In* R. Stirton, M. Woodburne and M. Plane (editors), Tertiary Diprotodontidae from Australia and New Guinea. Bulletin of the Bureau of Mineral Resources Geology and Geophysics (Australia) 85: 107–228.

Price, G.J. 2008. Taxonomy and paleobiology of the largest-ever marsupial, *Diprotodon* Owen, 1838 (Diprotodontidae, Marsupialia). Zoological Journal of the Linnean Society 153: 389–417.

Rich, T.H., M. Archer, and R.H. Tedford. 1978. *Raemeotherium yatkolai* gen. et sp. nov., a primitive diprotodontid from the medial Miocene of South Australia. Memoirs of the National Museum of Victoria 39: 85–91.

Simpson, G.G., A. Roe, and R.C. Lewontin. 1960. Quantitative zoology. Revised ed. New York: Harcourt Brace.

Stirton, R.A. 1967. The Diprotodontidae from the Ngapakaldi fauna, South Australia. *In* R. Stirton, M. Woodburne and M. Plane (editors), Tertiary Diprotodontidae from Australia and New Guinea. Bulletin of the Bureau of Mineral Resources Geology and Geophysics (Australia) 85: 1–44.

Stirton, R.A., M.O. Woodburne, and M.D. Plane. 1967. A phylogeny of the Tertiary Diprotodontidae and its significance. *In* R. Stirton, M. Woodburne and M. Plane (editors), Tertiary Diprotodontidae from Australia and New Guinea. Bulletin of the Bureau of Mineral Resources Geology and Geophysics (Australia) 85: 149–160.

Tedford, R.H., and M.O. Woodburne. 1987. The Ilariidae, a new family of vombatiform marsupials from Miocene strata of South Australia and an evaluation of the homology of molar cusps in the Diprotodontidae. *In* M. Archer (editor), Possums and opossums: studies in evolution: 401–418. Sydney: Surrey Beatty.

Travouillon, K.J., M. Archer, S.J. Hand, and H. Godthelp. 2006. Multivariate analyses of Cenozoic mammalian faunas from Riversleigh, northwestern Queensland. Alcheringa Special Issue 1: 323–349.

Travouillon, K.J., S. Legendre, M. Archer, and S.J. Hand. 2009. Paleoecological analyses of Riversleigh's Oligo-Miocene sites: Implications for Oligo-Miocene climate change in Australia. Paleogeography, Paleoclimatology, Paleoecology 276: 24–37.

Wible, J.R. 1990. Petrosals of Late Cretaceous marsupials from North America and a cladistic analysis of the petrosal in therian mammals. Journal of Vertebrate Paleontology 10: 13–205.

Wroe, S., J. Brammall, and B.N. Cooke. 1998. The skull of *Ekaltadeta ima* (Marsupialia, Hypsiprymnodontidae?): an analysis of some marsupial cranial features and a re-investigation of propleopine phylogeny, with notes on the inference of carnivory in mammals. Journal of Paleontology 72: 738–751.

APPENDIX 1

Nimbadon lavarackorum craniodental measurements:
A. _Nimbadon lavarackorum_ adult cranial measurements (mm) from AL90 site, Riversleigh World Heritage Area, Australia

See table 1 and Abbreviations for definition of abbreviations. Additional abbreviations: APFL, anterior palatal foramen length; BOL, basioccipital length; GFL, glenoid fossa length; GFW, glenoid fossa width; LPAL, palatine length; NAPH, narial aperture height; NAPW, narial aperture width; * estimate; Ψ measurement made from one side of skull and doubled; ^ variable used in univariate analysis.

	QM F 30833	QM F 31377	QM F 31541	QM F 40345	QM F 50470	QM F 53642	QM F 53643	QM F 53645
APFL		13.8	19.6	16.3	19.4	18.0	18.0	14.5
BB^	86.0	73.3	82.0	76.3	84.6	71.8		78.5
BL^	102.9	98.1	103.5	99.7	109.3	101.7		
BOL		30.0	32.7	28.7		30.6		30.3
DORB^	24.7	21.1	22.9	23.2	25.7	25.3	21.1	
DZAP^	21.5	17.7		18.4	27.8	24.2		21.6
FCL^	124.7	113.0	128.0	121.3	119.4	118.8		
FMH^	19.1	20.5	18.4	13.7	21.5	18.2		15.4
FMW^	24.8	23.7	21.7	19.6	25.4	26.0		20.9
FRL^		76.5			73.1	84.4		79.0
GFL		14.0	16.6	13.6	16.6	17.1		13.2
GFW		23.3	25.9	21.3	24.2	24.0		
HFP^		67.6		64.7	80.8	75.6		72.0
HROST^	53.3	47.5	54.8	53.3	61.6	51.8		52.0
IPFW^		28.2		22.4	27.0	31.8		
LDIA^	44.1	42.5	44.7	39.9	44.6	45.7	37.8	46.2
LFLC^	145.1	134.3	155.0	144.2	153.6	136.3		
LMP^	55.8		53.3		57.2	49.6	45.9	
LPAL	58.0	54.0	62.3	57.8	60.6	55.7	61.8	
LROST^	79.7	80.9	86.3	77.5	80.7	84.6		92.0
LSKULL^	227.6	211.1	231.5	221.0	230.1	220.5		237.0
LTR^	62.2	60.0	64.0	62.7	66.4	64.5	66.0	67.9
M4FO^	53.6	52.2	57.5	52.2	61.7	50.3		59.0
MAXW^	127.6	110.7		109.0	130.9	115.9		128.9
MWMP			95.2		96.8	95.6		
MXL^		51.4	61.1	59.2	57.4		59.3	59.0
NAPH			23.2	22.9	20.2	22.6	21.1	21.5
NAPW	30.4	28.5	31.3	28.4	30.5	32.0		30.9
NL^			89.4	78.9	90.1	80.7	80.7	89.4
OCH^	33.6	25.8	32.5	29.5	36.2	33.8		30.8
OCW^		81.9	89.0		93.5	84.9		91.1
PLL^	24.4	22.7	20.2	20.8	22.6		20.2	
PML^		40.1	40.5	35.9	39.8		39.1	42.8
PRL^		59.2			80.0	61.8		69.6
PRW^	40.6	43.9		32.9	36.8	38.1		33.4
WLT^	61.2		54.1	48.5	57.4	56.7	56.0	
WPALI3^	14.3	11.5	10.9	13.4	13.4		13.1	13.9
WPALM3^	30.1	28.0	29.9	26.4	28.8	31.3	30.0	
WPALP3^		25.7	28.5	23.7	28.1	29.6	27.1	31.7
WROST^		48.4	47.5	40.2	48.5		51.5	

B. *Nimbadon lavarackorum* adult dentary measurements (mm) from AL90 site, Riversleigh
Abbreviations: *, estimate; ^ variable used in univariate analysis. See figure 11 and table 1 for definition of abbreviations.

	QM F 30552	QM F 30856	QM F 40337	QM F 40338	QM F 41282	QM F 50548	QM F 53645	QM F 53647	QM F 53824
APWCO^			9.0				10.3		10.6
ARCO^			66.8	66.9			70.3		62.1
ARL^	67.4	63.4	65.9			66.9		63.4	67.4
DL^	29.2*		31.4						29.5
DM1^	36.2		35.5	28.9	29.9	37.5		32.5	32.2
DM3	32.2	29.4	33.8	30.5	30.1		34.3	31.3	31.2
DMF	5.6		3.7		5.2			4.4	6.4
DP3	41.5		34.7	31.8		39.8		32.8	36.2
HCP			46.2						
HCO^			37.0	42.9			38.9		42.3
HRL^	118.8		107.1						112.4
I1L									
LD^			150.5						162.4
MFP3	7.2		8.9		5.1	7.3		8.0	4.2
MLWCO^			27.8				29.7		27.8
MWM^	131.5*		114.9						121.8
SL^	62.7		48.1						57.2
WM3^	20.9	16.9	16.4	20.5		16.5	16.2	19.2	17.6
WMEAP^	44.6*		33.1				33.1	37.3	40.4

C. *Nimbadon* upper cheek teeth measurements (mm)

Abbreviations: AW, anterior width; BCk, Bullock Creek; COA, Cleft of Ages Site; DSS, Dome Site South; HH, Henk's Hollow Site; JC, Jim's Carousel Site; L, length; PW, posterior width; W, width. * Dentition measurements used in univariate analysis.

		P3		M1			M2			M3			M4		
QM F	Site	L	W	L	AW	PW	L	AW	PW	L	AW	PW	L	AW	PW
N. lavarackorum															
30736	AL90												14.4	11.8	9.9
30751*	AL90									13.7	10.9	9.4			
30775*	AL90	13.7	10.9	12.5	10.9	11.1	15.1	12.4	11.0	13.8	11.7	10.0			
30775*	AL90	13.4					13.1		11.0	13.9	11.7	10.3	13.2	11.3	8.3
30776*	AL90						13.7	11.8	11.0						
30781*	AL90	12.7	10.0												
30794*	AL90			13.4	10.9	11.2	14.5	12.3	11.6						
30795	AL90	12.9		13.1											
30833*	AL90	11.4	9.8	12.3	10.5	10.5	12.9	11.8	10.5	12.8	11.7	9.4	12.5	11.3	8.2
30833	AL90			12.8	10.7	10.8	12.8	12.0	10.8	12.8	12.2	9.7	12.1	11.0	8.7
31377*	AL90	10.9	9.7	11.5	9.8	9.5	12.5	10.9	9.7	13.2	11.0	9.5	13.0	10.5	8.5
31377	AL90	11.0	9.8	11.6	9.8	9.5	12.9	10.8	9.9	13.2	11.1	10.2	12.9	10.8	8.6
31432	AL90	11.7	9.3	12.6	10.2	10.6	13.1	11.7	10.8	14.6	11.7	10.1			
31541	AL90	12.6	10.7	12.2	10.3	10.6	13.3		11.0	13.6	11.6	10.4	12.8	11.6	9.3
31541*	AL90	12.7	10.3	12.5	10.2	10.4	12.8	11.1	10.9	13.6	11.6	10.2	12.9	11.1	9.4
31548	AL90	12.7	11.1	13.7	11.5	11.0	14.2	12.4	10.9	14.6	12.4	10.1	14.0	11.6	9.5
36333	AL90			11.9			13.8	12.0	11.3	14.0	11.9	10.4	13.7	11.1	9.5
36333*	AL90	12.1	10.4	12.1	10.1	11.5	13.3							12.2	10.5
36360	AL90	12.8	10.7												
36360*	AL90	12.3	10.3	12.4	10.1	10.3	12.8	11.2	10.4	13.1	11.2	9.8	12.3	10.8	8.8
40340	AL90			13.1	10.2	9.9	13.3	11.2	10.4	13.2	11.3	9.5			
40341	AL90	12.7	10.4	12.7	10.0	9.9	12.9	11.0	10.4	14.4	11.6	10.6	13.8		9.0
40341*	AL90	12.5	10.2	12.5	9.7	10.5	13.9	11.2	10.3	13.0	11.0	9.8	13.5	10.9	9.1
40344	AL90	12.6	10.1	13.2	10.3	10.3									
40345*	AL90	12.2	10.6	11.5	9.6	9.2	13.0	10.7	9.7	13.8	11.0	9.5	13.1	10.9	
40345	AL90	12.0	10.5	12.2	9.6	9.2	13.0	10.8	9.9	13.3	11.1	9.7			
41101*	AL90			14.3	11.3	11.7									
41115	AL90	11.0	9.8	12.2	10.2	10.9	13.1	11.5	11.1				13.6		
41115*	AL90	11.3	9.4	12.9	10.6	10.9	13.3	11.7	11.2	13.3	11.6	10.5	13.3		
41205*	AL90	12.7	11.0	13.1	10.7	10.8	13.7	12.1	11.1	13.6	12.1	10.7	14.3	11.8	9.7
41205	AL90						14.1	12.2	10.9	13.7	12.3	11.1	13.7		9.6
42677*	AL90	12.8	9.8	12.9	10.5	10.8	13.8	11.6	11.1	13.8	11.6	10.0	13.0	11.4	9.3

APPENDIX 1
(Continued)

		P3		M1			M2			M3			M4		
QM F	Site	L	W	L	AW	PW	L	AW	PW	L	AW	PW	L	AW	PW
42677	AL90	12.6	9.6	13.0	10.4	11.0	13.8	11.6	11.1	13.6	11.7	10.1	13.4	1.7	9.3
42679	AL90			13.7	11.5	11.7				14.6	12.4	10.6			
50470*	AL90	13.5	10.6	13.0	10.5	10.1	13.5	11.7	10.6	14.0	12.1	10.4	13.5	11.0	9.0
50470	AL90	14.1	11.2	13.0	10.3	10.0	13.6	11.7	10.3	13.4	11.9	10.1	13.5	11.1	8.8
50694	AL90	12.7	9.8												
50695	AL90	14.1	10.0												
50696	AL90	12.0	9.6												
50697*	AL90	12.5	9.7												
50699	AL90			13.7	10.9	11.0									
50700	AL90						14.3	12.7	11.2						
50701	AL90												14.2	13.1	10.8
50702*	AL90						13.8	11.6	10.7						
50745*	AL90	13.1	12.0												
50746	AL90	13.6	10.4												
53642*	AL90	12.3	10.1	13.6	10.6	11.0	13.5	11.9	11.3	14.4	12.0	10.3	13.2	11.6	9.7
53642	AL90	12.3	10.0												
53643a*	AL90			13.0	10.5	10.9									
53645*	AL90	12.7	10.9	12.7	11.3	11.2	13.9			14.1	12.2		14.4	11.9	10.2
53648a	AL90			13.9	11.3	11.7	13.8	12.0	11.4	13.3	11.7	10.6			
53650*	AL90	12.4	10.5												
53651*	AL90	12.4	10.9												
53652*	AL90	13.7													
53653*	AL90	12.9	10.4												
53654*	AL90	13.1	10.2												
53655*	AL90	14.1	11.4												
53656	AL90	13.6	11.3												
53657*	AL90	12.7	10.6												
53658*	AL90	12.0	10.3												
53659	AL90	13.5	10.7												
53660*	AL90	13.5	10.3												
53784	AL90	12.1	9.8												
53785	AL90	12.2													
53786	AL90	12.4	11.3	13.1	11.1	11.0									
53792	AL90	13.0	10.7	13.3		10.4	13.5	11.3	10.2	14.4	11.3	10.6			

APPENDIX 1
(Continued)

		P3		M1			M2			M3			M4		
QM F	Site	L	W	L	AW	PW	L	AW	PW	L	AW	PW	L	AW	PW
53792*	AL90	13.2	10.8	13.9	10.5	10.3	13.2	11.4	9.7	14.1	11.3	10.3			
53795	AL90			11.1	9.2	9.2	12.4	11.3	9.5						
53796*	AL90	12.9	11.4	13.1	10.5	10.5	13.7	11.7	10.9	13.4	11.3	9.2			
53797	AL90			12.8	10.6	10.4									
53798*	AL90			12.8	9.9	10.0									
53800*	AL90				10.5	11.3	13.4	11.7	11.2						
53801*	AL90	12.4	9.9	13.0	10.7	11.0									
53808	AL90			15.3	11.7	11.9									
53867	AL90									14.2	12.1	10.5			
30561	COA									14.6	12.6	10.3			
23308	DSS	12.5	10.3	12.7	10.7	11.0	13.7	12.0	11.1						
24049	DSS	12.4	10.7	12.7	10.5	10.8									
23160	Gag						13.9	11.2	10.2	14.6	11.6	10.3			
53862	Gag			13.2	10.8	10.8									
23141	HH	12.7		11.9	10.2	9.9	12.3	11.3	10.1						
23143	HH	14.1													
23144	HH	12.4	10.3												
23145	HH			13.3	10.9	10.8									
23146	HH						13.7		10.9						
23147	HH									13.8	11.5	10.7			
23148	HH											12.5			
23149	HH									14.3	12.2	10.4			
23150	HH												13.5	11.3	9.8
53856	HH						13.8	12.1	11.0						
53858	HH						13.4	11.5	10.6						
53859	HH			12.5	10.3	10.2									
16918	JC						13.9	12.1	11.3						
22777	JC	12.6	11.3												
23895	JC									14.3	12.0	10.5			
23896	JC												14.2	12.2	9.9
Nimbadon	BCk	12.9	10.4	13.1	9.3	9.2	13.1	10.9	9.5	13.5	11.1	9.7			
whitelawi	BCk	13.0	10.9	13.2											

D. *Nimbadon lavarackorum* lower cheekteeth measurements (mm)

Abbreviations: AW, anterior width; COA, Cleft of Ages Site; DSS, Dome Site South; HH, Henk's Hollow Site; L, length; LM, Last Minute Site; PW, posterior width; W, width. * Dentition measurements used in univariate analysis.

		p3		m1			m2			m3			m4		
QM F	Site	L	W	L	AW	PW	L	AW	PW	L	AW	PW	L	AW	PW
30552*	AL90	11.8	7.2	13.7	8.4	8.6	13.7	9.8	9.3	14.8	11.1	10.2	14.8	11.5	9.8
30552	AL90	11.4	7.6	13.8	9.4		14.1	9.9	9.4	14.8	11.0	9.7	15.0	11.4	9.5
30586	AL90	10.9	6.5	12.5	8.1	8.3	13.6	9.8	9.3	13.7	10.8	9.7	13.7	11.1	9.7
30751*	AL90						12.0		9.7	12.9	9.3	9.1	13.1	9.5	9.1
30784*	AL90			12.9	8.5	9.2	14.1	10.1	10.1						
30793*	AL90	9.8	5.7	12.4	7.1	8.2	13.7	8.9	9.3						
36333*	AL90	11.0	6.4	12.9	7.9	8.2	14.7	9.9	9.2	14.6	11.1	10.0	14.0	11.0	9.9
36333	AL90	10.2	6.7	12.6	8.0		13.6						14.0	11.1	9.9
40337*	AL90	9.5	5.9	13.2	7.8	8.8	14.5	9.2	9.6	14.9	10.2	9.3	14.4	9.9	9.4
40337	AL90	9.5	5.9	13.6	7.9	8.7	14.8	9.2	10.4	15.0	10.7	10.3	14.1	10.3	9.6
40338	AL90			13.0	8.2	8.8	14.0	9.6	9.2	14.5	10.9	10.0	14.1	10.9	9.6
41122c*	AL90			13.9	8.6	9.2									
41122d	AL90			13.8	8.9	9.1									
41122e*	AL90									14.5	11.4	9.2			
41124	AL90	9.9	5.9	13.2	7.9	9.1	14.5	9.7	9.6	14.5	10.7	10.3			
41252*	AL90	12.0	7.0												
41280	AL90						14.0		9.1	14.6	10.2	9.8	13.9	9.9	9.4
41282	AL90	9.9	6.2	12.3	7.4	7.9		8.7							
42678*	AL90	9.7	6.0	13.0	7.8	7.9	13.7	9.1	8.8	14.3	10.0	9.5		10.3	
42678	AL90	10.3		12.6	7.7	8.1	13.8	9.1	9.0	13.8	9.8	9.4		10.2	
50508*	AL90	10.8	6.7												
50548*	AL90	11.7	6.9	13.5	8.1	8.3	13.6	9.4	9.2	14.1	10.2	9.5	14.7	10.3	9.6
50684a	AL90	10.1	6.3	12.7	7.7	8.2	13.6	9.4	9.0	14.0	10.6	9.4			
50704*	AL90	10.6	6.7												
50705	AL90	10.4	6.0												
50706*	AL90			13.5	7.9	8.4									
50707	AL90			12.9	7.6	8.2									
50708*	AL90						13.8	10.4	9.9						
50709*	AL90									13.8	11.1	9.8			
50710	AL90						13.5	9.4	8.8						
50747*	AL90			13.6	8.2	8.8									
53645b*	AL90						14.9	10.1	9.8	13.8	10.5	10.3			
53647*	AL90	9.4	6.2	13.6	8.6	8.5	13.9	10.0	8.9	13.9	10.7	9.1	14.3	10.9	9.4

APPENDIX 1
(Continued)

		p3		m1			m2			m3			m4		
QM F	Site	L	W	L	AW	PW	L	AW	PW	L	AW	PW	L	AW	PW
53647	AL90	9.2	6.0	13.7	8.2	8.8	14.1	9.8	9.3	13.8	10.6	9.6	13.5	10.5	9.2
53648b	AL90			13.4	8.6	9.2	13.9	10.2	10.3						
53649*	AL90	10.6	6.6	13.5	7.1	7.7	14.0	9.0	8.6	13.7	9.8	9.4			
53649	AL90	10.5	6.5	12.5	7.3	7.5	13.6	9.0	8.8						
53661e*	AL90	11.3	6.7	13.9	8.2	8.6	13.7	10.0	9.6	13.9	10.7	9.7		10.9	
53792*	AL90	10.8	6.5	13.3	7.4	7.5	13.6	8.7	8.6	13.9	9.5	9.2			
53792	AL90	10.4	6.8	12.7	7.6	7.5	13.6	8.5	8.7	13.8	9.5	9.0			
53807	AL90	9.9	5.8	13.0	8.6	9.0	14.6				10.3				
53808*	AL90			13.6	7.3	8.7									
53810*	AL90			13.1	7.9	8.4									
53811*	AL90			13.7	7.9	8.7									
53812*	AL90	12.2	7.7												
53813*	AL90	11.2	7.2												
53814	AL90			13.8	8.3	8.7									
53815	AL90			13.7	8.4	9.1									
53816	AL90	11.3	6.9												
53817	AL90	11.0	6.7												
53818	AL90	10.1	5.7												
53819	AL90	12.2	7.5												
53820	AL90	10.9	6.3												
53821	AL90	10.8	6.6												
53824*	AL90	11.1	7.4	13.8	8.7	9.0	15.0	9.8	9.5	15.0	10.4	9.9	14.8	11.3	10.4
53824	AL90	11.3	7.1	14.2	8.6	9.0	14.6	10.0	9.2	14.6	10.6	10.1	14.4	11.4	10.0
53853	COA						13.9	9.2	9.2						
30793	DSS	11.9	7.3												
30793	DSS	12.1	7.8	12.6	7.6	8.6	14.2	10.6	9.2	14.8		10.3	15.3	11.3	10.6
23155	Gag			13.0	8.3	8.4									
23142	HH	12.5	7.0	14.0	8.4	9.4	15.4	10.1	10.0	15.5	11.0	10.2	15.9	11.1	10.0
23153	HH	10.9	5.8												
23154	HH			13.3	8.5	8.6									
23158	HH									14.0	10.6	9.8			
23159	HH												14.3	11.2	9.9
53857	HH												14.1	10.1	9.8
53854	LM						16.1	10.6	10.3						

E. *Nimbadon lavarackorum* upper incisor measurements (mm)
Abbreviations: A-P, anteroposterior length; H, height of crown (from base of enamel); W, width.

		I1			I2			I3		
QM F	Side	H	A-P	W	H	A-P	W	H	A-P	W
30833	L	19.1	9.9	7.0	3.7	4.7	4.2	3.3	3.8	5.2
30833	R	18.1		6.2	3.7	4.8	4.2			
31377	L	14.6	6.7	5.2						
31377	R	15.6	7.3	5.3						
31541	L	10.2	7.1	5.8	2.8	4.9	3.6			
31541	R	9.4	7.8	5.7						
50470	L	13.7	8.9	7.4	3.7	5.8	4.1			
50470	R	12.3	8.9		2.6	5.3	4.0			

APPENDIX 2

Univariate statistics

A. Univariate statistics for *Nimbadon lavarackorum* dentitions from AL90 site, Riversleigh
Abbreviations: AW, anterior width; CV, coefficient of variation; L, length; N, sample size; PW, posterior width; SD, standard deviation; SE, standard error of the mean. "U" and "L" in front of variables denote upper and lower dentition respectively.

Variable	*N*	Min	Max	Mean	SE	SD	CV
UP3L	29	10.9	14.1	12.6	0.1	0.7	5.7
UP3W	28	9.4	12.0	10.4	0.1	0.6	5.6
UM1L	21	11.5	14.3	12.8	0.1	0.7	5.3
UM1AW	22	9.6	11.3	10.5	0.1	0.5	4.4
UM1PW	22	9.2	11.7	10.7	0.1	0.6	5.8
UM2L	20	12.5	15.1	13.5	0.1	0.6	4.5
UM2AW	19	10.7	12.4	11.6	0.1	0.5	3.9
UM2PW	19	9.7	11.6	10.7	0.1	0.6	5.3
UM3L	17	12.8	14.4	13.6	0.1	0.4	3.2
UM3AW	17	10.9	12.2	11.5	0.1	0.4	3.7
UM3PW	16	9.2	10.7	10.0	0.1	0.5	4.6
UM4L	13	12.3	14.4	13.3	0.1	0.6	4.6
UM4AW	12	10.5	11.9	11.2	0.1	0.4	3.8
UM4PW	11	8.2	10.2	9.2	0.1	0.6	6.3
LP3W	16	9.4	12.2	10.8	0.2	0.9	8.1
LP3L	16	5.7	7.7	6.7	0.1	0.6	8.3
LM1L	18	12.4	13.9	13.4	0.1	0.4	3.0
LM1AW	18	7.1	8.7	8.0	0.1	0.5	6.3
LM1PW	18	7.5	9.2	8.5	0.1	0.5	5.5
LM2L	15	12.0	15.0	13.9	0.1	0.7	5.2
LM2AW	14	8.7	10.4	9.6	0.1	0.5	5.6
LM2PW	15	8.6	10.1	9.3	0.1	0.5	5.0
LM3L	14	12.9	15.0	14.2	0.1	0.6	4.0
LM3AW	14	9.3	11.4	10.4	0.1	0.6	6.1
LM3PW	14	9.1	10.3	9.6	0.1	0.4	4.2
LM4L	7	13.1	14.8	14.3	0.1	0.6	4.2
LM4AW	9	9.5	11.5	10.6	0.1	0.7	6.2
LM4PW	7	9.1	10.4	9.7	0.1	0.4	4.4

B. Univariate statistics for *Nimbadon lavarackorum* adult craniomandibular variables from AL90 site, Riversleigh

Abbreviations: CV, coefficient of variation; SD, standard deviation; SE, standard error of the mean; ?, indeterminate. Variable numbers correspond to figure 11. See table 1 for definitions.

	Variable	*N*	Min	Max	Mean	SE	SD	CV
1.	BB	7	71.8	86.0	78.9	1.9	5.5	7.0
2.	BL	6	98.1	109.3	102.5	1.3	3.9	3.8
3.	DORB	7	21.1	25.7	23.4	0.7	1.9	8.1
4.	DZAP	6	17.7	27.8	21.9	1.3	3.7	17.1
5.	FCL	6	113.0	128.0	120.9	1.8	5.2	4.3
6.	FMH	7	13.7	21.5	18.1	0.9	2.7	15.1
7.	FMW	7	19.6	26.0	23.2	0.8	2.4	10.6
8.	FRL	4	73.0	84.4	77.2	1.6	4.7	6.1
9.	HFP	5	64.7	80.8	72.1	2.3	6.4	8.8
10.	HROST	7	47.5	61.6	53.5	1.5	4.3	8.0
11.	IPFW	4	22.4	31.8	27.4	1.4	3.9	14.2
12.	LDIA	8	37.8	46.2	43.2	1.0	2.9	6.8
13.	LFLC	6	134.3	155.0	144.8	2.8	8.5	5.9
14.	LMP	5	45.9	57.2	52.4	1.6	4.6	8.8
15.	LROST	7	77.5	92.0	83.1	1.7	4.9	5.9
16.	LSKULL	7	211.1	237.0	225.5	2.9	8.6	3.8
17.	LTR	8	60.0	67.9	64.2	0.9	2.6	4.0
18.	M4FO	7	50.3	61.7	55.2	1.4	4.2	7.6
19.	MAXW	6	109.0	130.9	120.5	3.3	9.8	8.1
20.	MXL	6	51.4	61.1	57.9	1.1	3.4	5.9
21.	NL	6	78.9	90.1	84.9	1.8	5.3	6.2
22.	OCH	7	25.8	36.2	31.7	1.1	3.4	10.7
23.	OCW	5	81.9	93.5	88.1	1.6	4.7	5.3
24.	PLL	6	20.2	24.4	21.8	0.6	1.7	7.8
25.	PML	6	35.9	42.8	39.7	0.7	2.2	5.7
26.	PRL	4	59.2	80.0	67.7	3.1	9.3	13.8
27.	PRW	6	32.9	43.9	37.6	1.5	4.2	11.2
28.	WLT	6	48.5	61.2	55.7	1.5	4.2	7.6
29.	WPALI3	7	10.9	14.3	12.9	0.4	1.3	9.7
30.	WPALM3	7	26.4	31.3	29.2	0.5	1.6	5.6
31.	WPALP3	7	23.7	31.7	27.8	0.9	2.6	9.4
32.	WROST	5	40.2	51.5	47.2	1.5	4.2	8.9
33.	APWCO	3	9.0	10.6	10.0	0.3	0.9	8.5
34.	ARCO	4	62.1	70.3	66.5	1.1	3.4	5.1
35.	ARL	6	63.4	67.4	65.7	0.6	1.9	2.9
36.	DL	3	29.2	31.4	30.0	0.4	1.2	4.0
37.	DM1	7	28.9	37.5	33.2	1.1	3.3	9.8
38.	HCO	4	37.0	42.9	40.3	0.9	2.8	7.0
39.	HRL	3	107.1	118.8	112.8	2.0	5.9	5.2
40.	LD	2	150.5	162.4	156.5	2.8	8.4	5.4
41.	MLWCO	3	27.8	29.7	28.4	0.4	1.1	3.9
42.	MWM	3	114.9	131.5	122.7	2.8	8.3	6.8
43.	SL	3	48.1	62.7	56.0	2.5	7.4	13.2
44.	WM3	8	16.2	20.9	18.0	0.6	1.9	10.6
45.	WMEAP	5	33.1	44.6	37.7	1.6	4.9	13.1

C. Univariate statistics for *Neohelos stirtoni* from Blast Site, Bullock Creek, Northern Territory
Generated using data from table 4 and table 5 in Murray et al. (2000b). Right upper dentition and left lower dentition used only. See figure 11 and table 1 for cranial variable definitions.

	N	Min	Max	Mean	SE	Var	SD	CV
BL	8	147.0	186.0	165.5	4.6	214.9	14.7	8.9
DORB	5	26.0	35.0	30.6	1.0	10.3	3.2	10.5
FMH	6	19.0	26.0	22.5	0.8	6.7	2.6	11.5
FMW	8	31.0	52.0	38.0	2.2	50.0	7.1	18.6
IPFW	6	46.0	58.0	53.7	1.5	21.9	4.7	8.7
LDIA	7	60.0	84.0	67.9	2.6	66.5	8.2	12.0
LMP	9	51.0	81.0	65.7	3.0	87.3	9.3	14.2
LSKULL	4	338.0	436.0	381.5	13.6	1857.0	43.1	11.3
LTR	6	102.0	110.0	106.3	1.0	9.9	3.1	3.0
MAXW	6	175.0	224.0	191.3	6.2	386.3	19.7	10.3
NL	5	118.0	152.0	130.4	4.2	173.3	13.2	10.1
OCH	3	56.0	93.0	75.7	5.9	346.3	18.6	24.6
OCW	7	127.0	156.0	138.7	3.8	141.2	11.9	8.6
APWCO	4	13.0	17.0	15.3	0.6	2.9	1.7	11.2
ARL	9	98.0	111.0	103.9	1.3	14.6	3.8	3.7
DL	6	37.0	59.0	45.2	2.7	64.6	8.0	17.8
DM1	9	45.0	63.0	50.8	2.1	39.7	6.3	12.4
HRL	6	155.0	186.0	171.0	4.9	212.8	14.6	8.5
LD	5	225.0	280.0	255.4	7.8	545.8	23.4	9.1
MLWCO	3	40.0	44.0	42.0	0.7	4.0	2.0	4.8
SL	3	70.0	95.0	79.3	4.6	186.3	13.7	17.2
WM3	9	24.0	33.0	27.4	0.8	6.0	2.5	8.9
UP3L	21	16.0	20.2	18.4	0.2	1.3	1.1	6.2
UP3W	19	15.0	17.6	16.0	0.1	0.5	0.7	4.5
UM1L	20	17.2	21.7	19.6	0.2	1.0	1.0	5.0
UM1AW	18	16.1	19.1	17.7	0.2	0.9	1.0	5.4
UM1PW	17	16.4	20.2	18.2	0.2	0.9	0.9	5.2
UM2L	20	19.6	22.9	21.6	0.2	0.6	0.8	3.7
UM2AW	16	18.0	21.3	20.0	0.2	0.8	0.9	4.5
UM2PW	18	18.1	21.4	19.4	0.2	0.9	0.9	4.8
UM3L	12	21.0	24.2	23.0	0.2	1.1	1.1	4.6
UM3AW	12	19.3	22.4	21.0	0.2	0.9	1.0	4.6
UM3PW	11	17.9	21.0	19.1	0.2	1.2	1.1	5.8
UM4L	10	21.8	25.0	23.2	0.2	1.4	1.2	5.1
UM4AW	9	18.2	22.0	19.9	0.2	1.4	1.2	5.9
UM4PW	7	14.4	16.9	15.7	0.2	0.9	1.0	6.2
LP3L	11	11.5	16.3	14.4	0.3	1.4	1.2	8.2
LP3W	9	9.7	11.9	10.8	0.2	0.6	0.8	7.2
LM1L	15	17.3	22.7	19.6	0.3	2.1	1.4	7.4
LM1AW	13	12.4	16.7	13.8	0.2	1.2	1.1	7.9
LM1PW	14	13.2	18.7	15.3	0.3	1.9	1.4	9.0
LM2L	14	19.1	23.9	21.8	0.3	2.1	1.4	6.6
LM2AW	11	15.6	18.3	17.3	0.2	0.7	0.9	5.0
LM2PW	14	15.0	19.5	17.0	0.3	1.9	1.4	8.2
LM3L	16	22.7	25.9	24.1	0.2	0.8	0.9	3.7
LM3AW	15	17.0	21.4	18.6	0.2	1.3	1.1	6.1
LM3PW	14	16.1	19.7	17.7	0.2	1.0	1.0	5.7
LM4L	11	20.0	25.2	23.4	0.4	3.0	1.7	7.4
LM4AW	9	17.2	18.9	18.1	0.1	0.3	0.6	3.3
LM4PW	8	15.9	18.3	17.0	0.2	0.8	0.9	5.4